ESPOO 2008 VTT PUBLICATIONS 688

Mervi Hirvonen

Performance enhancement of small antennas and applications in RFID

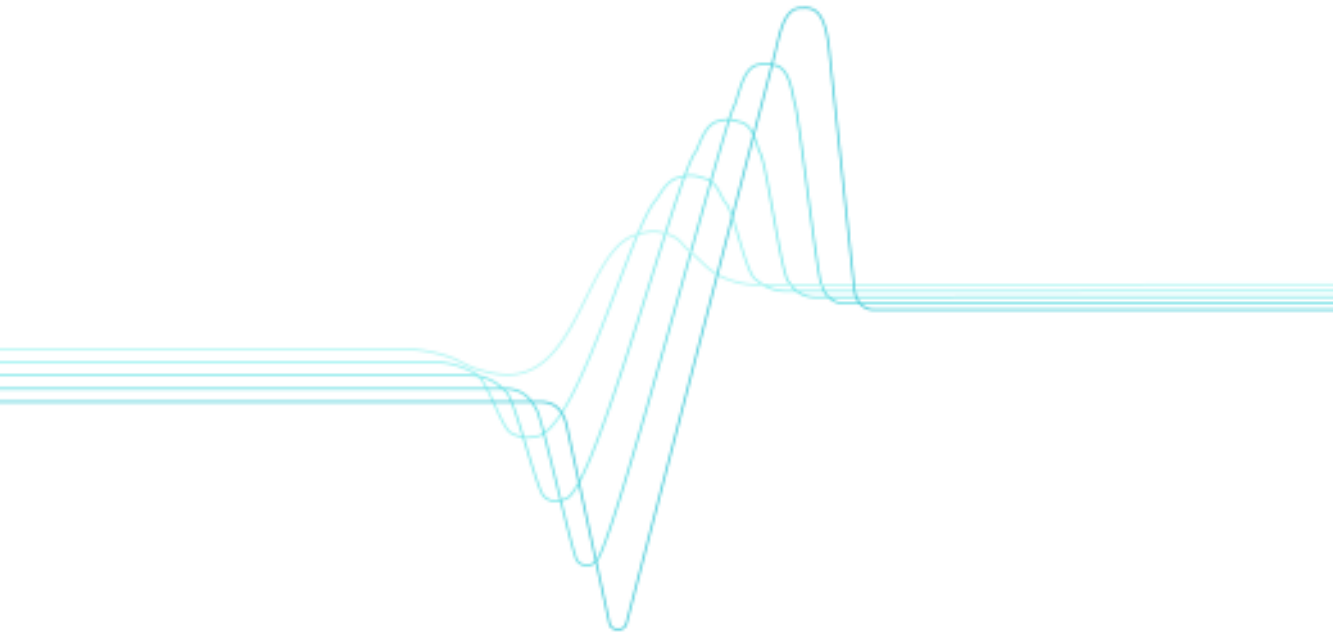

VTT PUBLICATIONS 688

Performance enhancement of small antennas and applications in RFID

Mervi Hirvonen

Dissertation for the degree of Doctor of Science in Technology to be presented with due permission for public examination and debate in Auditorium S5 at Helsinki University of Technology (Espoo, Finland) on the 7th of October, 2008 at 12 o'clock noon.

ISBN 978-951-38-7108-6 (soft back ed.)
ISSN 1235-0621 (soft back ed.)

ISBN 978-951-38-7109-3 (URL: http://www.vtt.fi/publications/index.jsp)
ISSN 1455-0849 (URL: http://www.vtt.fi/publications/index.jsp)

Copyright © VTT 2008

JULKAISIJA – UTGIVARE – PUBLISHER

VTT, Vuorimiehentie 5, PL 1000, 02044 VTT
puh. vaihde 020 722 111, faksi 020 722 7001

VTT, Bergsmansvägen 5, PB 1000, 02044 VTT
tel. växel 020 722 111, fax 020 722 7001

VTT Technical Research Centre of Finland, Vuorimiehentie 5, P.O. Box 1000, FI-02044 VTT, Finland
phone internat. +358 20 722 111, fax +358 20 722 7001

VTT, Tietotie 3, PL 1000, 02044 VTT
puh. vaihde 020 722 111, faksi 020 722 7013

VTT, Datavägen 3, PB 1000, 02044 VTT
tel. växel 020 722 111, fax 020 722 7013

VTT Technical Research Centre of Finland, Tietotie 3, P.O. Box 1000, FI-02044 VTT, Finland
phone internat. +358 20 722 111, fax +358 20 722 7013

Edita Prima Oy, Helsinki 2008

Hirvonen, Mervi. Performance enhancement of small antennas and applications in RFID [Pienten antennien suorituskyvyn parantaminen sekä sovelluksia etälukuun]. Espoo 2008. VTT Publications 688. 45 p. + app. 57 p.

Keywords small antennas, RFID, wireless sensors, quality factor, near-zero permittivity, non-Foster tuning, multi-port antennas, platform insensitivity, dual-band, backscattering measurement

Abstract

The focus of this thesis is on the performance enhancement of small antennas and design and verification of antennas for radio frequency identification (RFID) and wireless sensors. The work is presented in eight scientific papers and in a summary, which introduces relevant fundamental concepts and previous work done in the field of small antennas.

Previously, several performance enhancement methods have been proposed to improve the antenna performance especially in mobile communication applications. However, solutions for the fundamental small antenna problem, high reactive energy and low radiation resistance, which in practice lead to narrowband and low efficiency operation, are rarely provided. In this thesis, alternative methods to alleviate the high reactive energy and low radiation resistance like material loading, non-Foster tuning and multi-port loading are discussed.

Also, lately antennas for RFID and wireless sensor applications have gained growing interest. However, several characteristic design features exist for these antennas. Especially, the concept of platform insensitivity is essential and discussed in detail. Also, antenna designs and dual-band tuning technique applicable to RFID antennas are presented. In addition, wireless measurement techniques for RFID antenna verification are reported.

Hirvonen, Mervi. Performance enhancement of small antennas and applications in RFID [Pienten antennien suorituskyvyn parantaminen sekä sovelluksia etälukuun]. Espoo 2008. VTT Publications 688. 45 s. + liitt. 57 s.

Avainsanat small antennas, RFID, wireless sensors, quality factor, near-zero permittivity, non-Foster tuning, multi-port antennas, platform insensitivity, dual-band, backscattering measurement

Tiivistelmä

Väitöskirjatyö käsittelee pienten antennien suorituskyvyn parantamista sekä etälukuun (RFID) ja langattomiin antureihin soveltuvien antennien suunnittelua ja mittausta. Työ koostuu kahdeksasta tieteellisestä julkaisusta sekä yhteenvedosta, jossa on esitetty pienten antennien peruskäsitteitä sekä alan aikaisempia tutkimustuloksia.

Aikaisemmin pienten antennien suorituskykyä on pyritty parantamaan mm. matkaviestinlaitteissa. Kuitenkin ratkaisuja pienten antennien perusongelmaan, korkeaan reaktiiviseen energiatasoon sekä matalaan säteilyresistanssiin, jotka tekevät antennista käytännössä kapeakaistaisen ja hyötysuhteeltaan huonon, on harvemmin esitetty. Tässä työssä on analysoitu eri menetelmiä korkean energiatason ja matalan säteilyresistanssin lieventämiseen, kuten materiaalikuormitusta, non-Foster-viritystä sekä usean portin kuormitusta.

Viime aikoina etälukuun ja langattomiin antureihin soveltuvat antennit ovat herättäneet kasvavaa kiinnostusta. Näissä sovelluksissa antenneihin liittyy kuitenkin useita erityisiä ominaisuuksia. Erityisesti antennien alustaepäherkkyys on tärkeää, ja sitä on käsitelty työssä yksityiskohtaisesti. Lisäksi työssä on esitetty RFID-antennimalleja sekä niihin sopiva kaksitaajuusviritystekniikka. Myös RFID-antenneille soveltuvia langattomia mittaustekniikoita on esitetty.

Preface

The work for this thesis was mainly carried out at VTT Technical Research Centre of Finland during the years 2004–2008. The work has been also supported by TES Finnish Foundation for Technology Promotion. The support of both parties is gratefully acknowledged.

I would like to express my gratitude to supervising professor Sergei Tretyakov. Thank you for the co-operation and great guidance that made this work possible.

Warm thanks belong to Dr. docent Johan Sten for excellent collaboration and instructing. The conversations and suggestions have been essential. I also want to thank Arto Hujanen for the co-operation and guidance during these years at VTT. Also, Dr. Jussi Säily, Kaarle Jaakkola and Pekka Pursula deserve special thanks for collaboration and support. All my colleagues at VTT also deserve thanks. I also want to thank the pre-examiners Dr. Filiberto Bilotti and Dr. Pekka Ikonen for the comments and suggestions.

Anja, Pekka and Sirpa, your support and believe in me has been invaluable. Also, Niina, Annukka and Reetta, thanks for constant support and encouragement.

Mervi Hirvonen, Espoo, August 2008

List of publications

[P1] M. Hirvonen and J. C.-E. Sten, "Power and Q of a horizontal dipole over a metamaterial coated conducting surface", *IEEE Trans. Antennas Propagat.*, vol. 56, no. 3, pp. 684–690, March 2008.

[P2] M. Hirvonen and S. A. Tretyakov, "Near-zero permittivity substrates for horizontal antennas: Performance enhancement and limitations", *Microwave and Optical Tech. Lett.*, vol. 50, no. 10, pp. 2674–2677, Oct. 2008.

[P3] M. Hirvonen, A. Hujanen, J. Holmberg and J. C.-E. Sten, "Bandwidth limitations of dipoles matched with non-Foster impedances", *Proceedings of European Conference on Antennas Propagat., EUCAP 2007*, Nov. 2007.

[P4] J. C.-E. Sten and M. Hirvonen, "Impedance and quality factor of mutually coupled multiport antennas", *Microwave and Optical Tech. Lett.*, vol. 50, no. 8, pp. 2034–2039, August 2008.

[P5] J. C.-E. Sten and M. Hirvonen, "Decay of groundplane currents of small antenna elements", *IEEE Antennas Wireless Propagat. Lett.*, vol. 4, pp. 82–84, 2005.

[P6] M. Hirvonen, P. Pursula, K. Jaakkola and K. Laukkanen, "Planar inverted-F antenna for radio frequency identification", *Electronics Letters*, vol. 40, no. 14, pp. 848–850, July 2004.

[P7] M. Hirvonen, K. Jaakkola, P. Pursula and J. Säily, "Dual-band platform tolerant antennas for radio-frequency identification", *IEEE Trans. Antennas Propagat.*, vol. 54, no. 9, pp. 2632–2637, Sep. 2006.

[P8] P. Pursula, M. Hirvonen, K. Jaakkola and T. Varpula, "Antenna effective aperture measurement with backscattering modulation", *IEEE Trans. Antennas Propagat.*, vol. 55, no. 10, pp. 2836–2843, Oct. 2007.

Contribution of the author

[P1] The paper was initialized and developed mainly by the author. Dr. J. Sten participated in deriving the analytical expressions and preparing the paper.

[P2] The paper was developed mainly by the author. Prof. S. Tretyakov participated in deriving the analytical expressions and preparing the paper.

[P3] The paper was initialized and developed mainly by the author. A. Hujanen, J. Holmberg and Dr. J. Sten participated in defining the work.

[P4] The author prepared the paper with Dr. J. Sten. The author initialized and defined the application examples and performed the computations.

[P5] The author prepared the paper with Dr. J. Sten. The author initialized and defined the application examples and performed the computations.

[P6] The antenna structure presented in the paper was invented by the author. P. Pursula and K. Jaakkola participated in the backscattering measurements. K. Laukkanen supervised the work.

[P7] The antenna structure and tuning technique presented in the paper was invented by the author. K. Jaakkola and P. Pursula participated in the backscattering measurements. J. Säily supervised the work.

[P8] The paper is a result of collaborative work. The author participated in designing and defining the measured antennas as well as in the actual measurements and analysis of the results.

Contents

Abbreviations

AUT	Antenna Under Test
DC	Direct Current
EIRP	Effective Isotropic Radiated Power
ERP	Effective Radiated Power
GPS	Global Positioning System
HF	High Frequency
IC	Integrated Circuit
ILA	Inverted-L Antenna
MEMS	Micro-Electro-Mechanical Systems
NIC	Negative Impedance Converter
PEC	Perfect Electric Conductor
PIFA	Planar Inverted-F Antenna
PMC	Perfect Magnetic Conductor
RCS	Radar Cross Section
RF	Radio Frequency
RFID	Radio Frequency Identification
TE	Transverse Electric
TM	Transverse Magnetic
UHF	Ultra High Frequency
VSWR	Voltage Standing Wave Ratio

List of symbols

a	Radius
b	Thickness
A	Aperture
B	Bandwidth
C	Capacitance
d	Length
$\mathbf{E}$	Electric field
G	Gain
$\mathbf{H}$	Magnetic field
I	Current
k	Wave number
L	Inductance
L_{retn}	Return loss
$\mathbf{n}$	Normal
n	Mode number
P	Power
Q	Quality factor
r	Distance
R	Resistance
S	Matching level
T	Coupling factor
U	Voltage
W	Energy
Z	Impedance
ε	Permittivity
Γ	Reflection coefficient
λ	Wavelength
η	Efficiency
μ	Permeability

σ	Radar cross section
ω	Angular frequency

1 Introduction

1.1 Background

Wireless technology has become a part of our everyday life. Mobile communication, GPS navigation and wireless internet connections are the most common examples. However, wireless technology has lately found new applications also in identifying products in logistics, industrial production, theft prevention, automatic payment systems and in key cards to name but a few. Moreover, integrating sensors to wireless platforms enables the distributed monitoring of the environment. Important applications can be found for example in health care, rescue and safety. For example, one could monitor the life functions of the patient wirelessly in real time. Moreover, wireless sensor networks enable efficient monitoring of the potentially hazardous environments like traffic, volcanic or avalanching regions and industrial plants.

An important part of a wireless system is an antenna. Antenna transforms the RF signal generated in the transmitter device into a free-space wave and vice versa in the receiving end of the link. However, since the past hundred years there has been a growing interest in reducing the physical size of the antenna. Rapid development in minituarizing the electronics has also led to ever increasing demand for electrically small antennas (antennas, whose largest dimension is a fraction of the free-space wavelength). Especially in modern wireless applications, such as in radio frequency identification (RFID) and wireless sensors, the antenna has usually become the largest object and defines the physical size of the device.

However, antenna miniaturisation is a big engineering challenge because of the fundamental limitations that restrict the antenna performance. In the ideal case, all the power fed to the antenna would be radiated into free space through antenna radiation resistance and no energy (reactive fields) would be stored in the structure. However, even in a theoretical case antenna contains reactive fields, which make the antenna a frequency dependent device.

Especially problematic are electrically small antennas, because of their high reactive field level and low radiation resistance. Moreover, antennas designed to operate close to a conducting surface (ground plane) suffer from similar problems, since the radiation from impressed antenna currents flowing tangentially to the surface tend to be cancelled out by the surface currents induced on the plane. In practice, high reactive field level and low radiation resistance result in a narrowband operation and low radiation efficiency due to ohmic losses that are often considerable compared to the radiation loss.

Several solutions have been proposed to overcome the problems related to small antennas especially in the mobile communication applications. These solutions often utilize external resonators and device chassis to broaden the antenna band-

width. However, remedies for the fundamental small antenna problem, high level of stored energy and low radiation resistance, are more rarely provided.

Also, small antennas tend to be sensitive to the platform. In mobile communication applications, the platform is a fixed chassis and can be taken into account in the antenna design process. In many cases, chassis may be even exploited to enhance the radiation. However, in many novel applications like RFID, no fixed platform exists, but the antenna is attached directly to different objects or environments. Thus, a theory and antenna designs showing platform insensitive characteristics are needed.

In addition to platform insensitivity, RFID antennas posses a number of characteristic design features. In RFID, the antennas are directly matched to the reactive input impedance of the IC. Thus, the antenna is not a resonant device on its own. Also, being mass production devices, the material and manufacturing issues play an important role and need to be considered in the design process. Moreover, due to the small size and reactive impedance, RFID antennas are hard to verify with traditional measurement techniques containing the measurement cable. Instead, wireless measurement techniques need to be adopted.

1.2 Objectives and contents of the thesis

The objective of this thesis is to provide new insight and solutions to problems related to small antennas and antennas for RFID and wireless sensor applications. In this thesis, the separation between the two antenna regions, the fields assosiated with spherical multipole modes outside the smallest sphere enclosing the antenna and the internal fields, is emphasized. Alternative solutions to overcome the fundamental small antenna problem, high reactive energy and low radiation resistance, by affecting the internal fields are analysed. Also, the concept of platform insensitivity as well as new antenna designs suitable for RFID and wireless sensors are provided.

The thesis is composed of eight publications [P1]–[P8] and a summary. In general, the thesis is devided into two main parts, the first one concentrating on performance enhancement issues and the second one on RFID. In the first part, in Chapter 2, the fundamental concepts including the quality factor Q, bandwidth and efficiency of small antennas are discussed in detail. Chapter 3 deals with the performance enhancement methods of small antennas. After a brief review of basic performance enhancement methods, alternative techniques related to publications [P1]–[P4] like material loading, non-Foster tuning and multi-port loading are discussed.

In the second part, in Chapter 4, platform insensitivity of small antennas is discussed. In paper [P5] a theory for understanding platform insensitivity is pro-

posed and in papers [P6] and [P7] antenna designs showing platform insensitive characteristics are presented. Chapter 5 concentrates on antennas for RFID and wireless sensor applications. Papers [P6] and [P7] present antenna designs suitable for RFID and paper [P8] introduces a wireless measurement technique. Chapter 6 summarises the scientific contribution of publications [P1]–[P8], and the thesis is concluded in Chapter 7.

Part I

2 Fundamental concepts

2.1 Quality factor

As discussed in the introduction, stored energy and radiation resistance, which relates to radiated power, define the performance of a small antenna element. Thus, an important measure for small antennas is the quality factor Q

$$Q = \frac{\omega W}{P}, \tag{1}$$

which is known to be approximately inversely proportional to bandwidth (see Section 2.2). In equation (1) ω is the angular frequency, W the energy stored in the reactive fields and P the loss power. In a lossless case the loss power P is the power radiated to free space P_r, which is generally given by the integral [1], [2]

$$P_r = \frac{1}{2}\Re \int_S (\mathbf{E} \times \mathbf{H}^*) \cdot \mathbf{n}\, dS, \tag{2}$$

where S is an arbitrary surface enclosing the source, dS is the differential surface element and $\mathbf{n}$, the surface normal. It is often most convenient to evaluate the power in the far-field region at a certain distance r, whence (2) can be written in spherical coordinates as

$$P_r = \frac{1}{2}\sqrt{\frac{\varepsilon_0}{\mu_0}} \int_0^{2\pi} \int_0^{\pi} (|E_\theta|^2 + |E_\varphi|^2) r^2 \sin\theta \, d\theta \, d\varphi. \tag{3}$$

According to the early studies by Wheeler [3], the antenna size, quality factor Q and efficiency were found to be trade-off features. Later Chu presented a theory,

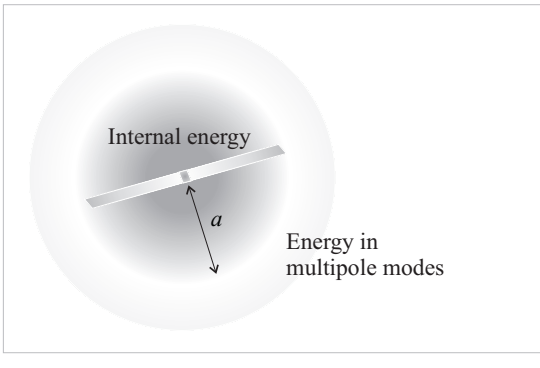

Figure 1: The smallest sphere enclosing the antenna.

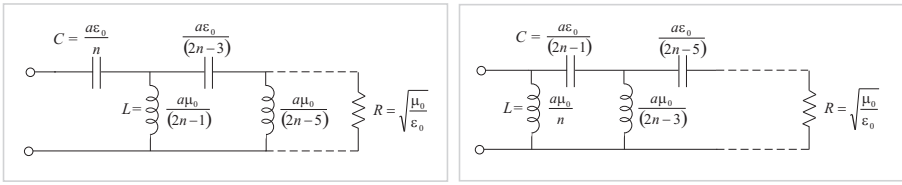

Figure 2: Equivalent circuits for spherical TM_n modes (left) and TE_n modes (right).

where the minimum quality factor of a small antenna fitting inside an enclosing sphere was derived [4]. In Chu's pioneering paper spherical harmonic wave expansions were taken to represent the fields outside the sphere and the fields inside were considered zero (see Fig. 1). Chu formulated the input impedance of the spherical fields as a continued fraction and discovered, that the radiating modes can be interpreted as a cascade of series capacitances and shunt inductances as presented in Fig. 2. As can be seen from the networks, more components are taken to model for the higher modes compared to the lower ones leading to higher level of stored energy, since [5]

$$W = \frac{1}{2}L|I_L|^2, \tag{4}$$

$$W = \frac{1}{2}C|U_C|^2, \tag{5}$$

where I_L is the local current passing through the inductance and U_C the local voltage over a capacitor. The combination of these modes would form the equivalent circuit representing the total antenna radiation, see Fig. 3. However, the power is divided to these modes by the antenna inner field, which has a major role in stored energy as discussed later in this chapter. However, in Chu's paper no representation was provided for the inner field, but it was assumed zero leading to a minimum amount of stored energy.

Finally, based on Chu's theory Collin and Rothschild presented a way to separate the propagating and reactive energy directly from the spherical wave expansion and formulated the well-known expression for the fundamental limitation of a small antenna occupying a certain volume as [6]

$$Q = \frac{1}{(ka)^3} + \frac{1}{ka}, \tag{6}$$

where a is the radius of the smallest sphere that can be drawn around the antenna and k is the wave number. In equation (6) the antenna is assumed to radiate the lowest spherical mode TM_1 or TE_1.

However, as mentioned above, Chu's theory takes into account only the electromagnetic fields stored outside the smallest sphere enclosing the antenna and

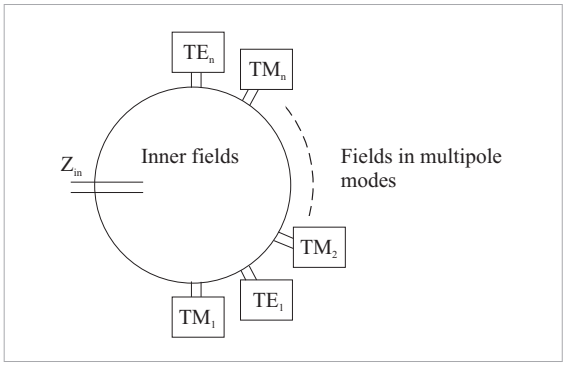

Figure 3: Antenna equivalent circuit.

assumes the fields inside the sphere to be zero. In reality, however, the antenna structure creates strong fields inside the sphere that can be considered completely stored. The total stored energy W is composed of electric W_E and magnetic W_M energies (including the effect of material dispersion) inside the smallest sphere enclosing the current carrying region (e.g. [7], [8])

$$W_{\text{int}} = \frac{1}{4}\Re \int\limits_{\text{sphere}} dV \left(\frac{\partial(\omega\varepsilon)}{\partial\omega}|\mathbf{E}|^2 + \frac{\partial(\omega\mu)}{\partial\omega}|\mathbf{H}|^2 \right), \tag{7}$$

plus the energy stored in the spherical multipole modes outside the sphere W_{ext} as given by Chu [4] and Collin and Rothchild [6]. In practice, as presented in publication [P1], the energy stored inside the smallest sphere is dominating compared to the outside energy and may be considered the performance limiting factor.

From the circuit analogy, the effect of the inner energy may be understood by adding more components to the Chu's model. For a small dipole radiating the lowest mode TM_1 an approximate circuit modeling the inner fields is introduced in publication [P3] and Section 3.2. For antennas radiating more modes, the task becomes challenging, since the power needs to be correctly divided between the modes. However, as more components form the network presenting the antenna impedance, less current fed to the antenna input port is drawn to the free-space resistances R in the radiating modes leading to lower radiated power. The same conclusion can be understood by normalizing the free-space resistances R to the feed port resistance $\Re\{Z\}$, which is the same as the radiation resistance R_r in the lossless case, whose low values lead to low radiated power.

At resonance, the electric and magnetic energies become equal. Thus, as antennas are typically considered to operate at resonance ranges, in many references, e.g. [4], [9], [10], the stored energy is often stated as two times the larger of the energies outside the resonance region as

$$W_{\text{int}} = \frac{1}{2}\Re \int\limits_{\text{sphere}} dV \left(\frac{\partial(\omega\varepsilon)}{\partial\omega}|\mathbf{E}|^2 \right), \quad \text{if } W_E > W_M \text{ and} \tag{8}$$

$$W_{\text{int}} = \frac{1}{2}\Re \int\limits_{\text{sphere}} dV \left(\frac{\partial(\omega\mu)}{\partial\omega}|\mathbf{H}|^2 \right), \quad \text{if } W_M > W_E. \tag{9}$$

However, in many modern antenna applications the antenna is directly matched to the reactive input impedance of the IC or the antenna is tuned with active components and thus, the antenna is not a resonant device on its own. Based on this, the general approach to stored energy expressed in equation (7) is considered.

Also, e.g. in [11] and [P4], the total stored energy W was shown to be related to the imaginary part of the antenna input impedance $Z(\omega)$ as

$$W \approx \frac{\partial\Im\{Z\}}{\partial\omega}\frac{|I|^2}{4}, \tag{10}$$

where I denotes the input current. On the other hand, loss power may be presented in terms of the real part of the input impedance (radiation resistance R_r in the lossless case) as

$$P = \frac{1}{2}\Re\{Z\}|I|^2. \tag{11}$$

Thus, the quality factor becomes

$$Q_z \approx \frac{\omega}{2\Re\{Z\}}\frac{\partial\Im\{Z\}}{\partial\omega}. \tag{12}$$

However, formula (12) can be applied only to small antennas with impedance level near resonance ranges. As shown in [12], a fair estimate for the Q-factor for any impedance level, even near antiresonance, may be expresssed as

$$Q_z \approx \frac{\omega}{2\Re\{Z\}}\left|\frac{dZ}{d\omega}\right|. \tag{13}$$

As presented in publication [P1], the quality factors derived either by direct integration of the energies or by taking an impedance derivative leads to well correlating results.

2.2 Bandwidth

Antenna bandwidth defines the frequency range $\Delta\omega$ where the antenna performance, usually impedance, conforms to a specified standard [13]. In other words, the impedance bandwidth is always defined with certain matching condition, for example return loss L_{retn} [5]

$$L_{\text{retn}} = 10\log|\Gamma|^2 \tag{14}$$

or voltage standing wave ratio level

$$\mathrm{VSWR} = \frac{1+|\Gamma|}{1-|\Gamma|}, \tag{15}$$

where Γ is the reflection coefficient from load $Z_L(\omega)$ to antenna $Z_A(\omega)$ as

$$\Gamma = \frac{Z_A - Z_L^*}{Z_A + Z_L}. \tag{16}$$

The antenna quality factor Q, on the other hand, only refers to the element performance itself, since no port load is considered. However, there is a direct link between the antenna quality factor and impedance bandwidth: as shown in equations (10)–(13), the higher the reactive fields and stored energy, the larger the impedance derivative of the antenna. Thus, the higher the quality factor, the more rapidly the antenna impedance varies as a function of the frequency leading to a narrowband operation.

In many references, e.g. [14], [15], the relationship between the antenna Q and the bandwidth is written as

$$B = \frac{1}{Q}\sqrt{\frac{(TS-1)(S-T)}{S}}, \tag{17}$$

where S is the matching level VSWR$< S$ and $T = \Re\{Z_L(\omega_0)\}/\Re\{Z_A(\omega_0)\}$ the coupling factor referring to the matching level at the center frequency ω_0. If the bandwidth is defined as the half-power bandwidth ($|\Gamma|^2$=0.5) and at the center frequency the matching is perfect (T=1), a well-known estimate between the bandwidth and Q, $B \approx 1/Q$, is valid. However, in equation (17) the antenna impedance is considered to be near resonance ranges, and assumed to behave like an RLC circuit. However, in reality, antennas might exhibit several resonances and contain matching circuits, in which case equation (17) does not apply.

2.3 Efficiency

Antenna radiation efficiency is defined as the ratio between the radiated power P_r and the total power accepted by the antenna P_{tot}. Radiation efficiency may be also written in terms of resistance due to the relation presented in equation (11). In practice, in addition to the radiation resistance R_r the real part of the antenna impedance $\Re\{Z\}$ contains structural losses, R_{loss}, like ohmic and dielectric losses. The radiation efficiency of the antenna is defined as [16], [17]

$$\eta = \frac{R_r}{R_{\mathrm{loss}} + R_r}. \tag{18}$$

Thus, antenna structures with a low radiation resistance often suffer from poor radiation efficiency, since the effect of even small structural losses become significant. However, as can be detected from equation (11), the antenna resistance

$\Re\{Z\}$ including both radiation and loss resistances is always normalized to the current level at that point. Thus, increasing the radiation resistance with an impedance transformer in the element (for example a folded dipole), the loss resistance increases correspondingly leading to low radiation efficiency.

3 Performance enhancement

3.1 Background

As discussed in the previous section, an important measure for the performance of a small antenna is the quality factor Q, which can be considered approximately inversely proportional to the antenna bandwidth. However, the quality factor gives information about a single radiating element, but in practice the antenna bandwidth is often affected by several resonating elements or external matching components. Thus, in principle, for example multi-stage passive impedance matching can be used to achieve bandwidths somewhat larger than the $1/Q$-estimate (see e.g. [18], [19]), but the required matching circuits tend to become very complex and are, in reality, inherently lossy.

Also, parasitic elements can be used to create multiple resonances leading to larger bandwidth performance (see e.g. [20]–[22]), but are difficult to manage due to strong coupling and added physical size. Another widely used technique is to use the antenna as a coupling element and exploit the antenna platform, like a mobile phone or GPS navigator chassis, as a radiator [23], [24]. Thus, the radiator element becomes physically larger having a positive effect on the performance. Moreover, like with passive matching networks and parasitic components, coupling element-chassis combination can be used to excite a double resonance leading to a notable bandwidth enhancement. However, in modern applications like in RFID and wireless sensors, the antenna platform is not fixed and cannot be used as a radiator. Moreover, none of these methods provide a solution to the fundamental small antenna problem: the high reactive field energy and low radiation resistance of the antenna element.

In addition to a small size, also the vicinity of the ground plane has been found to cause serious degration in the antenna performance, since the radiation from the antenna currents flowing tangentially to the surface tends to be cancelled out by the surface currents induced on the ground plane. Magnetic conductors and high impedance surfaces have been proposed to attack this problem, since in this case the induced currents would flow in the same phase enhancing the radiation [25], [26]. However, since magnetic and high impedance conductors do not exist in nature, problems arise in realization and usability of artificial magnetic conductors, because of the high profile feature and losses [26]–[28].

In the following, alternative approaches to improve the antenna performance are discussed. By material loading one can increase the radiation resistance of the element leading to enhanced radiation. Also, active impedance tuning, or non-Foster tuning, shows a very promising way to enhance antenna bandwidth properties by canceling some reactance from the antenna impedance. In addition, multi-port antennas provide new insight to the problem since their current distribution may be adjusted in a favourable way by means of distributed feeding and loading.

3.2 Material loading

Permeable materials as antenna substrates have been found to lead to lower quality factors than air and permittivity fillings [29], [30]. However, exploiting permeability is not straightforward, since natural magnetics loose their properties at higher frequencies. Lately, nanoparticle technology has been able to demonstrate higher-frequency magnetics (see e.g. [31]), but these substances are not widely available and are generally toxic. Still, permeability is also possible to achieve with artificial composite materials containing resonant inclusions, although in this case the performance is limited by dispersion. In addition to permeability, substrates containing unnatural, however also artifially tailorable, negative material parameters have been proposed in the literature to lead to enhanced antenna properties (e.g. [32], [33]).

In publication [P1], the effect of different material parameters, both natural and metamaterial parameters ($\varepsilon_r < 1$ and $\mu_r < 1$), as a substrate for a horizontal dipole over a ground plane (see Fig. 4) was studied. From the curves denoting the radiated power P_r one could detect not only the radiation enhancement due to permeable and negative-parameter materials, but also a notable enhancement for the material, which had permittivity close to zero. Accordingly, the radiation resistance of a dipole with such a near-zero permittivity increases leading in a practical case to higher element efficiency. Moreover, while keeping the feed current constant, one could found the internal stored energy of such a system being roughly in the same magnitude compared to the air filling case leading to low radiation Q and notable bandwidth enhancement. Prior to [P1], near-zero materials were studied only to enhance the directional properties of radiated fields [34], [35].

However, in practice near-zero permittivity is difficult to implement. Like permeability at high frequencies and negative material parameters, near-zero permittivity is implemented with artificial composite materials, in this case wire grids, containing resonant inclusions (see e.g. [36]). Such materials tend to be highly dispersive, which increase the internal stored energy of the element, as can be seen from equation (7). For example, in the case of a microstrip patch antenna loaded with artificial permeability material presented in [37], dispersion was found to

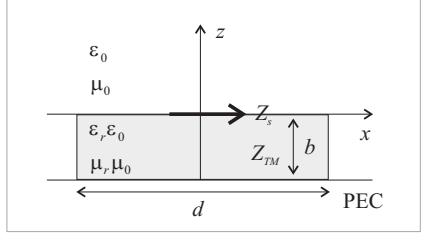

Figure 4: Horizontal electric dipole on a conductor-backed slab.

overcome the favourable enhancement leading to narrower bandwidths. Also, in [33] dispersion of negative-parameter material was found to decrease the antenna bandwidth notably.

In the case of a near-zero permittivity substrate, the favourable effect of the radiated power depends on the size of the substrate, as studied in publication [P2]. In the case of the horizontal dipole over a ground plane, the radiated power of the antenna was found to decrease drastically as the low epsilon substrate size decreases. From the surface impedance point of view, as shown in [P2], the near-zero permittivity substrate behaves partly as a magnetic conductor. As studied in [38], the near field of a wire source near a PMC spreads to a large area demanding the use of a larger screen. Also, inside the near-zero permittivity susbtrate the wavelength gets longer, and more space is needed to realize the effect.

Also, as presented in [P2], the stored energy of the element increased notably as the dispersion of a near-zero permittivity material was taken into account. As a result, the use of a near-zero permittivity substrate measuring $\lambda/4$ times $\lambda/4$ had a higher radiation Q compared to the air-filled case. On the other hand, even while including the dispersion effect, substrate $\lambda/2$ times $\lambda/2$ in size was found to already give notable enhancement in radiation Q compared to the air filling.

3.3 Non-Foster tuning

Compared to the traditional passive-component tuning, non-Foster tuning provides a whole new way to enhance the impedance performance of antennas. According to experimental results in [39]–[41], notable bandwidth enhancements have been reported. In the non-Foster technique, instead of tuning an antenna to resonance with external components, which increase the total stored energy of the system, one rather cancels the reactance seen from the input port of the antenna with negative-reactance (active) components. In the ideal case, all the reactance is canceled out and only the antenna radiation resistance is seen from the input port leading to infinite impedance bandwidth. However, in reality limitations exist.

In publication [P3] these limitations were studied. If only the energy stored outside the smallest sphere enclosing the antenna is considered, infinite bands are possible with very small dipoles by tuning the antenna with only one negative capacitance. However, in a more realistic case, the energy stored inside the smallest sphere enclosing the antenna makes the situation more complicated.

In terms of the circuit model, more components need to be included to Chu's radiation model to account for the effect of internal energy. Previously, several circuit models for small dipoles have been proposed (see e.g. [42]–[44]), but none of these makes a distinction between the inner fields and fields outside the smallest sphere. In publication [P3] a circuit model consisting of a voltage divider (two

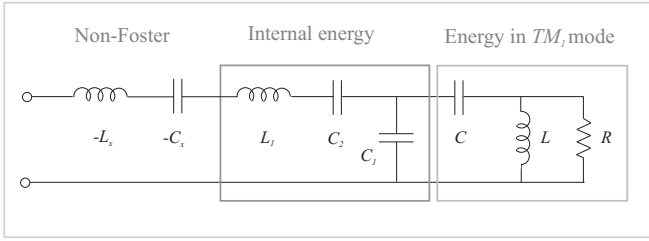

Figure 5: Approximate model for the impedance of a small dipole including the inner energy and non-Foster tuning.

capacitances) and a series inductor is proposed to model for the internal fields of a small dipole (see Fig. 5). A series inductor can be understood to relate to the physical wire carrying the current and the capacitances relate to the shunt capacitance between the dipole branches and the field capacitance tangential to the wire. Because of this voltage division, less power is drawn to the free space resistance and the element performance gets poorer compared to the case where the inner fields are considered zero.

While including the inner energy, only limited bands were achieved while tuning small dipoles with one negative capacitance. However, the bands were larger compared to the case where similar dipoles were tuned with the infinite number of passive components. On the other hand, while tuning small dipoles with two negative components, capacitor and an inductor, bands over 200 per cents were achieved.

Although these results are promising, component tolerances were found to be strict making the realization of such a system challenging. Negative-impedance components are implemented in practice with negative impedance converter (NIC) circuits, where also the performance and noise of the transistors limit the highest realizable frequency and overall performance. Moreover, power supply arrangements needed for active components make the system complex.

3.4 Multi-port elements

By feeding or loading the antenna element with multiple ports current distribution and impedance of the antenna may be modified more efficiently compared to the traditional single-port devices. The radiation Q of the antennas with multiple feed ports has been previously observed to lead to an increasing radiation Q [45]. However, in [45] only the energy stored outside the smallest sphere was considered in the case, where the ports were totally isolated. However, as presented in publication [P1], energy stored inside the smallest sphere plays the dominant role, and in practice, mutual coupling between the elements may be strong. Multiport loading schemes have been studied for example in the case of spiral and slot an-

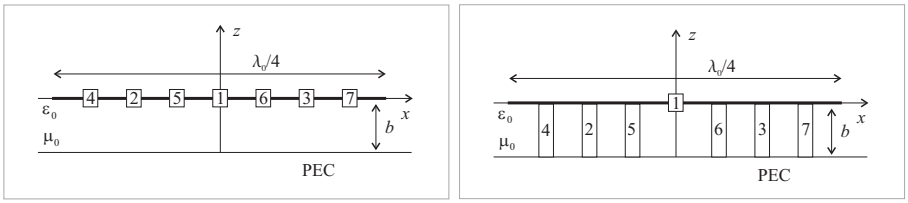

Figure 6: Multiple feeding (left) and loading (right) of a horizontal dipole over a conducting surface.

tennas in [46] and [47]. In these papers distributed loading was found to offer potential way to minimize the physical size of the antenna and control the input impedance of the antenna efficiently.

In publication [P4] the effect of multiple feeding and loading of a horizontal dipole over a ground plane was studied (see Fig. 6). In [P4] the inner energy as well as mutual coupling between the elements was included. By computational examples it was shown, that by feeding a dipole at multiple ports with suitable amplitudes, a slightly lower Q can be achieved than by feeding a similar dipole from a single port. Also, distributed loading of a similar element was analysed. According to a computational example, by tuning the element to resonance with suitable distributed shunt capacitors, notably lower Q values can be achieved compared to the case where the element is conjugately tuned with an inductor from a single port.

Thus, it can be concluded, that distributed feeding and loading provides a way to affect the inner fields created by the element. However, in realization challenges exist. In distributed feeding a complex network would be needed to match the feed lines and divide the power accurately between the ports. In distributed loading external wires would be needed to connect passive capacitors in the ports affecting the situation. On the other hand, capacitors could also be easilly realized with pieces of high-ε materials.

Part II

4 Platform insensitivity

The input impedance, radiation pattern and performance of small antennas are typically highly platform dependent. In modern applications, like RFID, the antenna may be attached directly on top of different kinds of objects and the platform effect becomes a performance spoiling feature. On the other hand, as discussed in the previous section, in some applications, like mobile phones, the effect of the platform can be exploited to enhance the antenna performance by controlled coupling. Still, also mobile phones suffer from the impedance and efficiency shifting effect in the vicinity of hand and head [48], [49]. To account for the impedance shifting effects of the platform, for example, adaptive varactor or MEMS tuning circuits have been proposed [50], [51]. However, these are complex and expensive systems and often not possible in low-cost applications like RFID.

The effects of the platform may be decreased by using a ground plane in the antenna structure to shield the element from the environment underneath. In addition to high reactive field level and low radiation resistance arising while operating in the vicinity of a conducting surface, there is also a challenge to minimize the size of the plane. For example, according to [52]–[54], a ground plane of wavelengths in size is needed to stabilize the input impedance of a vertical monopole. Also, results concerning circular microstrip antennas have been reported in [55]. The study shows that a ground plane radius beyond 1.3 times the patch radius is enough to stabilize the input impedance. A similar study concerning a PIFA structure has been reported in [56]. In the study the ground plane less than 0.2 λ in size had a major impact on the input impedance.

Platform insensitivity of the element may be understood by analysing the currents induced to the shielding ground. In publication [P5] the currents induced by vertical and horizontal point sources above an infinite perfect electric conductor were solved. In [P5] it was concluded that in addition to the height between the element and the ground plane, the induced surface currents were notably affected by the source orientation. The currents induced by vertical sources decayed proportionally to the inverse distance while the currents induced by horizontal sources decayed as the inverse distance squared. Thus, antennas with dominating horizontal current distribution concentrate the induced current to the smaller area and tend to be less sensitive to the platform as presented in the case of inverted-L antennas in Fig. 7.

However, dominating vertical current distribution is typical in many antenna structures designed to operate near a ground plane, like PIFA structures, since a vertical short tends to attract the current. In many applications, like mobile phones, this is an advantage, since induced current spreads to a wider area improv-

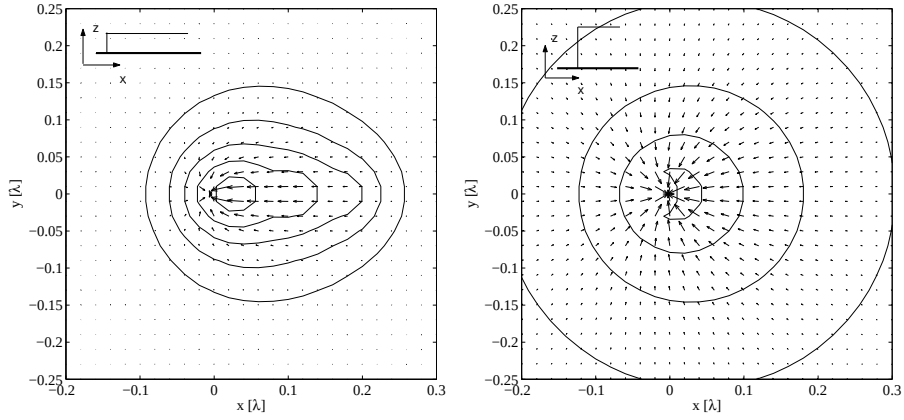

Figure 7: Surface current induced by flat (left) and high profile (right) inverted-L antenna.

ing the radiation performance of the antenna. However, if platform insensitivity is preferred, as presented in publication [P6], by widening the short of the PIFA element, i.e., reducing the inductance of the vertical part and lowering the height of the antenna, dominating horizontal current distribution and insensitivity to platform is achieved.

In addition to low profile PIFAs presented in [P6] and [P7], self-balanced structures like folded loops have been proposed as platform insensitive solutions (see e.g. [57], [58]) due to their concentrated ground current distribution. However, these antenna structures float above a ground plane, increasing the total thickness of the structure.

5 RFID and wireless sensors

5.1 Background

Lately, antennas for RFID and wireless sensor applications have gained growing interest in the research world and markets. In radio frequency identification (RFID) a reader device transmits a signal to the identification tags, in which the data is stored [59]. Thus, in a sense RFID can be understood to be similar to the bar code systems. However, the amount of data and reading ranges are much higher. Also, reading is possible without visual contact. Thus, RFID systems can be used to identify objects for example in logistics and industrial production or in key cards. Moreover, sensors can be attached to RFID platforms to allow the distributed monitoring of the environment [60], [61]. Thus, a plethora of applications exist for example in healt care, security and traffic.

Generally two kinds of RFID systems exist: near-field (HF) and far-field (UHF) RFID. In near-field systems, the wireless coupling is done through magnetic or electric field with inductors or capacitors as coupling elements and thus, the reading distances tend to be in the order of a few centimeters. On the other hand, in far-field RFID, electromagnetic coupling is utilized and the reading distances are several meters. In this thesis UHF RFID is considered.

In passive and semi-passive UHF RFID the systems operate with backscattering technique [59], [62]. Unlike in the conventional communication, the other part of the system, RFID tag, does not contain a transmitter, but the information is modulated to the backscattered signal (see. Fig 8). The identification tags contain the IC, possibly sensors and an antenna. In passive systems, the DC power needed for IC is generated from the incoming RF field with rectifier unit and no external power source exists making the lifetime of the tags limitless. However, the reading distances stay within a few meters, since only from 2W ERP (Europe) to 4W EIRP (N. America and Japan) is allocated for RFID readers. Thus, also the antenna performance and power transfer (impedance matching) to the IC become very critical features in succesfull system operation.

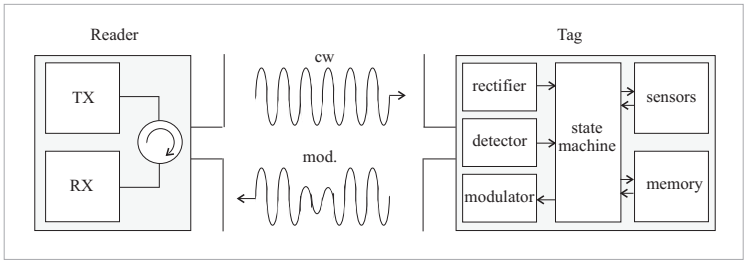

Figure 8: UHF-RFID system.

In semi-passive systems a battery supplies power to the IC. Still, the system works with backscattering technique lacking a transmitter in the tag. On the other hand, in active systems the tag contains a battery as well as a transmitter. Thus, for active systems the read ranges can extend up to hundreds of meters.

5.2 RFID antennas

As mentioned earlier, the electronics part of the tag is extremely small and in many cases, is embedded in the antenna substrate making the antenna the largest component. In other words, no fixed device chassis exist, but the antenna is directly attached to different objects or environments to be identified and monitored. Thus, small size and platform insensitivity are the main design characteristics of RFID antennas. Also, the antenna is matched directly to the reactive impedance of the IC, and thus, the antenna impedance is not real as in traditional antenna design cases. In addition, RFID tags are mass production items, and thus the material and manufacturing issues need to be considered in the antenna design process.

In order to make an RFID system insensitive to tags orientation, the majority of RFID readers are circularly polarized, however, the handedness of the polarization may vary. Thus, linear polarization of the tag is preferred to sustain operation in different orientations and with different readers.

The majority of the RFID tag antennas on the market today are two-dimensional structures, mainly printed dipoles (see Fig. 9 left [59]). Two-dimensional structures are small in size, inexpensive and suitable for mass production. In the literature many examples exist, e.g. [63], [64]. The desired input impedance of dipoles is achieved simply by making the antenna longer than the resonant length and asymmetrically feeding the antenna. Also, impedance transformers, like loops around the feed, may be utilized to gain the desired impedance. Dipoles may be shaped to many forms, even into the form of text [65]. In addition to dipoles, also slot structures have been proposed [66].

However, two-dimensional structures have a major drawback: as the antenna is attached to different objects or environments, operation starts to fail due to dramatic shifts in impedance and efficiency [67], [68]. As discussed in Chapter 4, an antenna structure containing a ground plane needs to be used to make the antenna platform insensitive and usable in different environments, especially on metal. In Fig. 9 right an example of platform insensitive PIFA antennas similar to [P6] are presented. After the publication of [P6] several platform insensitive antennas for RFID have appeared in the literature (e.g. [69]–[71]).

Currently, different frequency bands are allocated for UHF RFID use in Europe (866–868 MHz), North America (902–928 MHz) and Japan (950–956 MHz) [72].

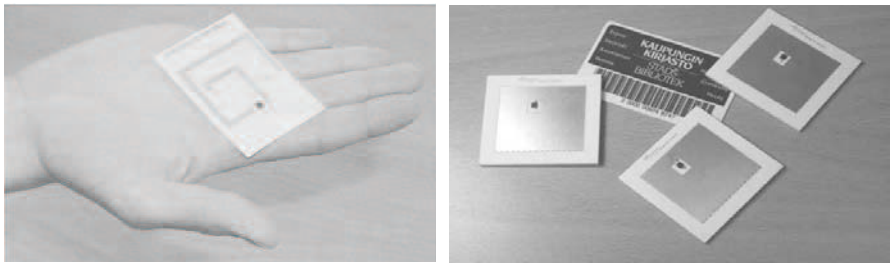

Figure 9: Printed RFID dipole (left) [59] and platform insensitive PIFAs (right) fed with RFID microchips.

Also 2.45 GHz and 5.8 GHz bands are available globally, but seldomly used because of the limited read range. Evidently, there is a demand for a universal tag containing a multi-band antenna. Fortunaly, unlike in mobile communication applications, the required operating bands are narrow, allowing the use of higher-Q antenna elements. On the other hand, low radiation resistance typically related to high-Q elements is a problem in practice due to low radiation efficiencies. However, this can be somewhat compensated by shaping the element as uniformly as possible to avoid ohmic losses and using low loss substrates.

As already mentioned in the antenna performance enhancement section, multiple resonances may be created to antennas by several elements or external circuit components. However, parasitic elements increase the antenna size and external components tend to be lossy. Also, in RFID antennas, external circuit components increase the cost of the tag, which in many cases is intolerable. Multi-band dipoles for RFID exploiting several resonator elements have been reported in the literature [73], [74].

In publication [P7], a dual-band antenna using an alternative approach is presented. In a PIFA structure, a floating port is utilized and the ground pin of

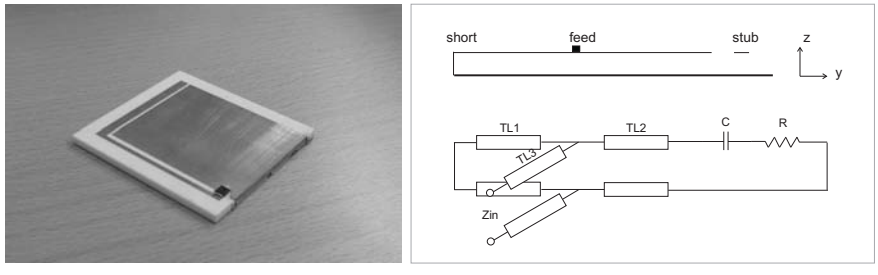

Figure 10: Dual-band, platform insensitive antenna (left) and an approximate circuit model (right).

the IC is connected to nominally a quarter-wavelength microstrip line to form a virtual ground (see. Fig. 10). In addition to the ease of manufacturing compared to vias, floating port offers a dual-band tuning possibility. In RFID, the desired input impedance of the antenna is usually strongly inductive and the resistance is low due to the direct matching to the capacitive IC. As presented in Fig. 10 right, a microstrip line acting as a virtual ground may be modeled as feed inductance ($TL3$), which can be used to move the impedance locus towards generator in the Smith chart. On the other hand, by bending the microstrip line towards the end of the patch element forms a series capacitance C, which controls the locus size. Thus, the antenna impedance can be led to pass the desired impedance level laying near the outer rim of the Smith chart twice leading to dual-band operation. Also, the current distribution of the antenna presented in [P7] is mostly horizontal, making the antenna platform insensitive.

5.3 Measurement techniques

Traditionally, antennas are verified with cable measurements. In this technique the antenna under test is connected to a network analyser, which measures the antenna impedance from reflection coefficients directly at the cable connection point (feed port), see Fig. 11. Similarly, radiation characteristics are verified by measuring transmission at different space angles between the antenna under test and a reference antenna. However, in the case of small antennas, the cable interferes with the radiated fields and affects the measurement results strongly. To minimize these effects, ferrite chokes can be used around the cable or the cable may be oriented at the angle where the field is the weakest.

However, in modern antenna applications like RFID, the antenna impedance is not real like the cable characteristic impedance leading to a huge mismatch and reflections at the connection point. Matching networks can be utilized between the antenna and the cable, but also the network platform itself may disturb the radiation. Thus, wireless measurement techniques are preferred to verify RFID antennas. Generally two kinds of measurements exist: backscattering and modulated backscattering measurements.

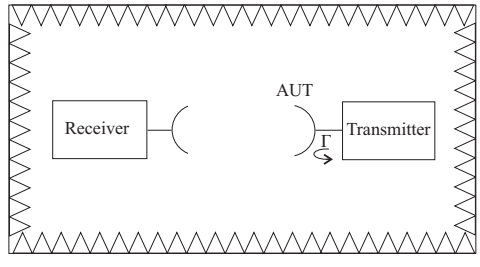

Figure 11: Measurement setup in a cable measurement.

5.3.1 Backscattering

In the backscattering the radar cross section (RCS) of the antenna is measured with different feed loads. The measurement setup of the backscattering method (also modulated backscattering) in presented in Fig. 12. In a simplified model, as the antenna is illuminated with RF power, antenna radiates back a portion of the power due to the impedance mismatch in the antenna feed. The RCS of such a system may be written as [75], [P8]

$$\sigma = \frac{4\pi A_e^2 |1-\Gamma|^2}{\lambda^2}, \tag{19}$$

where Γ is the reflection coefficient from antenna to the load resistance

$$\Gamma = \frac{Z_L - Z_A^*}{Z_L + Z_A}, \tag{20}$$

and A_e is the antenna effective aperture, which is related to the antenna gain G as

$$A_e = \frac{G\lambda^2}{4\pi}. \tag{21}$$

As presented in [76] the antenna under test and the transmitting and receiving antennas can be modeled as a linear three port network characterised by three impedance parameters. Thus, as presented in [77], [78], by measuring the antenna backscattering with three known loads information about antenna input impedance may be derived. After solving antenna input impedance, also the antenna gain can be calculated according to equations (19)–(21).

However, in practice limitations exist. In backscattering measurement, the method assumes the antenna radiation mode to be similar with all loads. In the case of simple antennas like dipoles, only one mode exists and the radiation pattern is similar in every case. However, if the antenna structure is more complex, different modes may be excited with different loads. Also, as the transmitted and backscattered signals are at the same frequency band backscattering measurement requires very low environmental interference and high resolution measurement equipment.

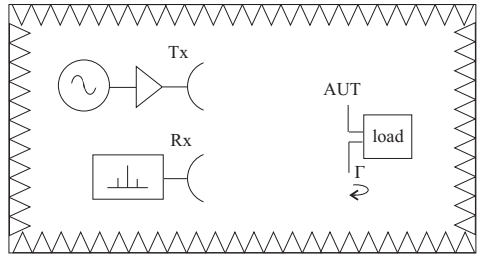

Figure 12: Measurement setup in backscattering methods.

5.3.2 Modulated backscattering

In the modulated backscattering the scattered signal from the antenna mode is transferred to the sidebands [P8]. Thus, the environmental reflections are reduced and less performance is needed from the measurement environment and equipment.

In the modulated backscattering an oscillator chip with a known input impedance is connected as a load to the antenna under test. As the oscillator drives the varactor at the input of the chip, the reactance of the chip varies modulating the phase of the current in the antenna circuit. The scattered field is thus phase modulated, which is seen as sidebands in the scattered signal. In the measurement, the transmitted power P_{tx} is increased until the IC chip gets enough power to wake up and the sidebands appear in the backscatter data. As the RF power P_{req} needed to start the modulation is known, the antenna gain G including the impedance mismatch $1-|\Gamma|^2$ can be calculated using the Friis equation

$$G(1-|\Gamma|^2) = \frac{P_{\mathrm{req}}}{G_{\mathrm{tx}} P_{\mathrm{tx}}} \left(\frac{4\pi r}{\lambda}\right)^2, \tag{22}$$

where G_{tx} is the transmitter gain and r the measurement distance. The drawback of the method is that the mismatch between the antenna and the load cannot be extracted from the results. Measuring the required transmit power as a function of the frequency gives information about the antenna bandwidth. Moreover, the radiation pattern of the antenna may be measured by recording the critical transmitted power P_{tx} as a function of space angles.

In publication [P8] the theory of the modulated backscattering as well as the accuracy of antenna gain and pattern measurements are discussed. Also, the harmfull effect of the measurement cable is demonstrated compared to the wireless measurement technique. Furthermore, modulated backscattering has been used in verifying the RFID antennas presented in publications [P6] and [P7].

6 Summary of publications

[P1] Power and Q of a horizontal dipole over a metamaterial coated conducting surface

The paper presents the power radiated by a conductor-backed horizontal dipole with different substrate material parameters. The radiation enhancement due to permeability, negative parameters and more importantly, near-zero permittivity is discussed. Also, a notable decrease in the quality factor with near-zero permittivity substrates in a dispersionless case is reported. In addition, the dominating role of the internal stored energy is showed compared to the energy stored outside the smallest sphere enclosing the element.

[P2] Near-zero permittivity substrates for horizontal antennas: Performance enhancement and limitations

The paper continues the work published in [P1]. In the paper, the role of dispersion and size of a near-zero permittivity substrate is discussed. The paper concludes, that the power enhancement achieved with near-zero permittivity is greatly affected by the size of the substrate. Also, the dispersion is found to increase the stored energy leading in higher quality factors than estimated in publication [P1]. However, it is reported that already half-wavelength times half-wavelength size substrate leads to remarkably lower quality factors even while including the material dispersion compared to the air-filling case.

[P3] Bandwidth limitations of dipoles matched with non-Foster impedances

The paper presents new results concerning the negative-reactance matching. First, a new equivalent circuit model for small dipoles is proposed. The model includes a circuit model for TM_1 field derived by Chu and a network modeling the fields stored inside the smallest sphere enclosing the antenna. In the paper it is concluded that the internal fields limit the bands achieved with non-Foster components. However, drastic bandwidth improvements are reported while tuning small dipoles with two non-Foster components. Also, the component tolerance issues are discussed.

[P4] Impedance and quality factor of mutually coupled multi-port antennas

The paper presents results gained by feeding and loading a horizontal dipole over a conducting surface at multiple input ports. It is concluded, that by multi-port feeding slightly lower quality factors are possible compared to the single-port case. Moreover, a notable decrease in the quality factor is reported while loading the antenna with shunt capacitors.

[P5] Decay of ground plane currents of small antenna elements

In the paper the ground plane currents induced by horizontal and vertical point sources are derived. It is reported that currents induced by horizontal point sources above a ground decay more rapidly compared to the vertical sources leading to less platform sensitive behaviour.

[P6] Planar inverted-F antenna for radio frequency identification

A novel PIFA structure for RFID is proposed having platform insensitive characteristics due to dominating horizontal current distribution.

[P7] Dual-band platform tolerant antennas for radio-frequency identification

The paper presents a new PIFA structure for RFID showing dual-band and platform insensitive operation. A novel dual-band tuning technique exploiting the reactive matching level and floating port is presented.

[P8] Antenna effective aperture measurement with backscattering modulation

In the paper a novel wireless measurement technique for verifying RFID antennas is presented. In the measurements a test chip, with known characteristics, is attached to the antenna feed and the antenna gain including the impedance mismatch and pattern may be measured using a modulated backscatterign signal. In the example measurements also the hazardous effect of the measurement cable is indicated compared to the wireless technique.

7 Conclusions

In this thesis, theory and solutions for problems related to small antennas are discussed. Small antennas, and especially antennas operating close to a conducting surface, tend to have high reactive field level and low radiation resistance leading to high radiation quality factor. In reality, this leads to narrowband operation and low radiation efficiency.

Performance limitations of small antennas are typically studied while taking only into account the fields associated with spherical multipole modes outside the smallest sphere enclosing the antenna and assuming the internal fields zero. However, in practice, the energy stored in the reactive internal fields is dominating compared to the fields outside the sphere, and is, in fact, the performance limiting feature. Thus, in this thesis, the separation between these two antenna regions and the importance of the internal fields are emphasized.

In the first part of the thesis, alternative approaches to overcome the small antenna problem by affecting the antenna inner fields have been analysed. First, it has been concluded that with certain material loadings, permeability, negative-parameter materials and, more importantly, near-zero permittivity, the radiation resistance and radiated power of a horizontal antenna above a ground plane may be increased notably. However, in practice near-zero permittivity is implemented with dispersive structures, which increase the stored energy and lead to higher radiation quality factor. Also, the finite size of the substrate limits the achievable increase in radiation resistance. Moreover, the realization of near-zero permittivity materials, especially as compact structures, is challenging and expensive.

Another way to improve the antenna performance is to use non-Foster (negative reactance) components to cancel some reactive energy from the antenna impedance. In this thesis a new equivalent circuit for a small dipole element, which makes a separation between the fields inside and outside the smallest sphere enclosing the antenna, is derived. By exploiting this equivalent circuit, it was concluded that the internal stored energy of the antenna limited the achievable bandwidths. Still, while tuning even very small dipoles with two negative components, drastic bandwidth enhancements could be achieved. However, with very small antennas, the active component tolerances get strict limiting the realization possibilities of the system. All in all, as non-Foster tuning contains active components and complex circuitry, it is suitable only for high-end products.

Yet another approach to the small antenna problem is multi-port feeding and loading technique. With both methods, antenna inner fields could be slightly affected in a favourable way leading to enhanced antenna performance. Being passive and simple method, multi-port feeding and loading could find potential also in low-end bulk products.

In the second part of this thesis small antennas for RFID and wireless sensors are discussed. For these antennas, several characteristic design features exist. For example, the impedance of the RFID antenna is directly matched to the reactive input impedance of the IC. Also, RFID tags are mass production devices, and material and manufacturing issues play a key role. More importantly, RFID antennas are directly attached on different objects and environments and thus, platform insensitive behaviour is needed. Thus, in this thesis a theory and implementation methods for platform insensitive antennas are proposed. Also, a few antenna designs showing platform tolerant characteristics and direct impedance matching to the IC are introduced. Also, an easy dual-band tuning technique is presented. In addition, a new wireless measurement method is presented for verifying RFID antennas.

References

[1] W. L. Stutzman and G. A. Thiele, *"Antenna theory and design"*, Wiley, 1981.

[2] C. H. Papas, *"Theory of electromagnetic wave propagation"*, Dover publications, 1988.

[3] H. A. Wheeler, "Fundamental limitations in small antennas", *Proc. IRE*, vol. 35, pp. 1479–1484, Dec. 1947.

[4] L. J. Chu, "Physical limitations on omni-directional antennas", *J. Appl. Phys.*, vol. 19, pp. 1168–1175, Dec. 1948.

[5] R. E. Collin, *"Foundations for microwave engineering"*, 2nd edition, Wiley 2001.

[6] R. E. Collin and S. Rothchild, "Evaluation of antenna Q", *IEEE Trans. Antennas Propagat.*, vol. 12, pp. 23–27, Jan. 1964.

[7] L. D. Landau and E. M. Lifshitz, *"Electrodynamics in continuous media"*, 2nd edition, Pergamon press, 1984.

[8] J. D. Jackson, *"Classical electrodynamics"*, 3rd edition, Wiley, 1999.

[9] R. L. Fante, "Quality factor of general ideal antennas", *IEEE Trans. Antennas Propagat.*, vol. 17, no. 2, pp. 151–155, March 1969.

[10] J. S. McLean, "A re-examination of the fundamental limits on the radiation Q of electrically small antennas", *IEEE Trans. Antennas Propagat.*, vol. 44, pp. 672–676, May 1996.

[11] J. C.-E. Sten and A. Hujanen, "Notes on the quality factor and bandwidth of radiating systems", *Electrical Engineering 84*, pp. 189–195, 2002.

[12] A. D. Yaghjian and S. R. Best, "Impedance, bandwidth and Q of antennas", *IEEE Trans. Ant. Propag.*, vol. 53, no. 4, pp. 1298–1324, April 2005.

[13] *"IEEE standard definitions of terms for antennas"*, IEEE std 145-1993, March 1993.

[14] I. J. Bahl and P. Bhartia, *"Microstrip antennas"*, Artech house, Dedhem, 1980.

[15] R. Garg, P. Bhartia, I. Bahl and A. Ittibiboon, *"Microstrip antenna design handbook"*, Artech house, Norwood, 2001.

[16] K. Fujimoto, A. Henderson, K. Hirasawa and J. R. James, *"Small antennas"*, Research studies press ltd., Wiley, 1987.

[17] J. D. Kraus and R. J. Marhefka, *"Antennas for all applications"*, 3rd edition, Mc Graw-Hill, 2002.

[18] A. Hujanen, J. Holmberg and J.C.-E. Sten, "Bandwidth limitations of impedance matched ideal dipoles", *IEEE Trans. Ant. Propag.*, vol. 53, no. 10, pp. 3236–3239, Oct. 2005. (See also "Correction" in vol. 54, no. 9, p. 2694.)

[19] M. Gustafsson and S. Nordebo, "Bandwidth, Q factor, and resonance models of antennas", *Progress In Electromagn. Res.*, vol. 62, pp. 1–20, 2006.

[20] H. Nakano, N. Ikeda, Y.-Y. Wu, R. Suzuki, H. Mimaki and J. Yamauchi, "Realization of dual-frequency and wide-band VSWR performances using normal-mode helical and inverted-F antennas", *IEEE Trans. Ant. Propag.*, vol. 46, no. 6, pp. 788–793, June 1998.

[21] T. M. Au and K. M. Luk, "Effect of parasitic element on the characteristics of micstrip antenna", *IEEE Trans. Ant. Propag.*, vol. 39, no. 8, pp. 1247–1251, Aug. 1991.

[22] J. Ollikainen and P. Vainikainen, "Radiation and bandwidth characteristics of two planar multistrip antennas for mobile communication systems", *Proc. Vehicular Technology Conf., VTC'98*, vol. 2, pp. 1186–1190, May 1998.

[23] P. Vainikainen, J. Ollikainen, O. Kivekäs and I. Kelander, "Resonator-based analysis of the combination of mobile handset antenna and chassis", *IEEE Trans. Ant. Propag.*, vol. 50, no. 10, pp. 1433–1444, Oct. 2002.

[24] J. Villanen, J. Ollikainen, O. Kivekäs and P. Vainikainen, "Coupling element based mobile terminal antenna structures", *IEEE Trans. Ant. Propag.*, vol. 54, no. 7, pp. 2142–2153, July 2006.

[25] J. A. Kong, *"Electromagnetic wave theory"*, Wiley, 1986.

[26] N. Engheta and R. W. Ziolkowski *"Metamaterials: physics and engineering explorations"*, Wiley, 2006.

[27] D. Sievenpiper "High-impedance electromagnetic surfaces with a forbidden frequency band", *IEEE Trans. Microw. Theory Tech.*, vol. 47, no. 11, pp. 2059–2074, Nov. 1999.

[28] A. Erentok, P. L. Luljak and R. W. Ziolkowski, "Characterization of a volumetric metamaterial realization of an artificial magnetic conductor for antenna applications", *IEEE Trans. Ant. Propag.*, vol. 53, no. 1, pp. 160–172, Jan. 2005.

[29] R. C. Hansen and M. Burke, "Antenna with magnetodielectrics", *Microw. Opt. Technol. Lett.*, vol. 26, no. 2, pp. 75–78, 2000.

[30] P. M. T. Ikonen, K. N. Rozanov, A. V. Osipov, P. Alitalo and S. A. Tretyakov, "Magnetodielectric substrates in antenna miniaturization: Potentials and limitations", *IEEE Trans. Antennas Propagat.*, vol. 54, no. 6, pp. 1654–1662, June 2006.

[31] P. Markondeya Raj, P. Muthana, T. D. Xiao, L. Wan, D. Balaraman, I. R. Abothu, S. Bhattacharya, M. Swaminathan and R. Tummala, "Magnetic nanocomposites for organic miniaturized antennas and inductors", *IEEE International Symposium on Advanced Packaging Materials, Proc.*, pp. 272–275, March 2005.

[32] A. Alu, F. Bilotti, N. Engheta and L. Vegni, "Subwavelength, compact, resonant patch antennas loaded with metamaterials", *IEEE Trans. Antennas Propagat.*, vol. 55, no. 1, pp. 13–25, Jan. 2007.

[33] M. E. Ermutlu and S. Tretyakov, "Patch antennas partially loaded with a dispersive backward-wave material", *IEEE Antennas Propagat. Int. Symp.*, vol. 2A, pp. 6–9, July 2005.

[34] A. Alu, N. Engheta, A. Erentok and R. W. Ziolkowski, "Single-negative, double-negative, and low-index metamaterials and their electromagnetic applications", *IEEE Antennas and Propagation Magazine*, vol. 49, no. 1, Feb. 2007.

[35] B.-I. Wu, W. Wang, J. Pacheco, X. Chen, T. Grzegorczyk and J. A. Kong, "A study of using metamaterils as antenna substrate to enhance gain", *Progress In Electromagnetics Reseach, PIER*, vol. 51, pp. 295–328, 2005.

[36] S. A. Tretyakov, *Analytical modeling in applied electromagnetics*, Artech House, 2003.

[37] P. M. T. Ikonen, S. I. Maslovski, C. R. Simovski and S. A. Tretyakov, "On artificial magnetodielectric loading for improving the impedance bandwidth properties of microstrip antennas", *IEEE Trans. Antennas Propagat.*, vol. 54, no. 6, pp. 1654–1662, June 2006.

[38] S. A. Tretyakov and C. R. Simovski, "Wire antennas near artificial impedance surfaces", *Microw. Opt. Technol. Lett.*, vol. 27, no. 1, pp. 46–50, Oct. 2000.

[39] J. T. Aberle and R. Loepsinger-Romak, *"Antennas with non-Foster matching networks"*, Morgan & Claypool, 2007.

[40] S. E. Sussman-Fort, "Matching network design using non-Foster impedances", *Int. Journal of RF and Microw. Computer-Aided Engineering*, Feb. 2005.

[41] A. Kaya and E. Y. Yuksel, "Investigation of a compensated rectangular microstrip antenna with negative capacitor and negative inductor for bandwidth

enhancement", *IEEE Trans. Antennas Propagat.*, vol. 55, no. 5, pp. 1275–1282, May 2007.

[42] T. G. Tang, Q. M. Tieng and M. W. Gunn, "Equivalent circuit of a dipole antenna using frequency-independent lumped elements", *IEEE Trans. Antennas Propagat.*, vol. 41, no. 1, pp. 100–103, Jan. 1993.

[43] M. Hamid and R. Hamid, "Equivalent circuit of a dipole antenna of arbitrary length", *IEEE Trans. Antennas Propagat.*, vol. 45, no. 11, pp. 1695–1696, Nov. 1997.

[44] B. Long, P. Werner and D. Werner, "A simple broadband dipole equivalent circuit model", *IEEE Antennas Propagat. Int. Symp.*, vol. 2, pp. 1046–1049, July 2000.

[45] H. D. Foltz and J. S. McLean, "Bandwidth limitations on antenna systems with multiple isolated input ports", *Microw. Opt. Technol. Lett.*, vol. 19, no. 4, pp.301–304, 1998.

[46] M. Lee, B. A. Kramer, C.-C. Chen and J. L. Volakis, "Distributed lumbed loads and lossy transmission line model for wideband spiral antenna miniaturization and characterization", *IEEE Trans. Antennas Propag.*, vol. 55, no. 10, pp. 2671–2678, Oct. 2007.

[47] N. Behdad and K. Sarabandi, "Slot antenna miniaturization using distributed inductive loading", *IEEE Antennas Propagat. Int. Symp.*, vol. 1, pp. 308–311, June 2003.

[48] J. Toftgård, S. N. Hornsleth and J. B. Andersen, "Effect on portable antennas of the presence of a person", *IEEE Trans. Antennas Propag.*, vol. 41, no. 6, pp. 739–746, June 1993.

[49] J. T. Rawley and R. B. Waterhouse, "Performance of shorted microstrip patch antennas for mobile communications handsets at 1800MHz", *IEEE Trans. Antennas Propag.*, vol. 47, no. 5, pp. 815–822, May 1999.

[50] K. Ogawa, T. Takahashi, Y. Koyanagi and K. Ito, "Automatic impedance matching of an active helical antenna near a human operator", *33rd European Microw. Conf.*, vol. 3, pp. 1271–1274, Oct. 2003.

[51] A. van Bezoojien et al., "RF-MEMS based adaptive antenna matching module", *IEEE Radio. Freq. Integrated Circuits (RFIC) Symp.*, pp. 573–576, June 2007.

[52] A. S. Meier and W. P. Summers, "Measured impedance of vertical antennas over finite ground planes", *Proc. IEEE*, vol. 37, pp. 609–616, June 1949.

[53] K. H. Awadalla and T. S. M. Maclean, "Input impedance of a monopole antenna at the center of a finite ground plane", *IEEE Trans. Antennas Propag.*, vol. AP26, no. 2, pp. 244–248, Mar. 1978.

[54] J. H. Richmond, "Monopole antenna on circular disk", *IEEE Trans. Antennas Propag.*, vol. AP32, no. 12, pp. 1282–1287, Dec. 1984.

[55] K. Antoszkiewicz and L. Shafai, "Impedance characteristics of circular microstrip patches", *IEEE Trans. Antennas Propag.*, vol. AP38, no. 6, pp. 942–946, June 1990.

[56] M. C. Huynh and W. Stutzman, "Ground plane effects on planar inverted-F antenna (PIFA) performance", *IEE Proc. Microw. Antennas Propag.*, vol. 150, no. 4, pp. 209–213, August 2003.

[57] S. Hayashida, H. Morishita and K. Fujimoto, "Self-balanced wideband folded loop antenna", *IEE Proc. Microw. Antennas Propag.*, vol. 153, no. 1, pp. 7–12, February 2006.

[58] C. C. Chiau, X. Chen and C. G. Parini, "A miniature dielectric-loaded folded half-loop antenna and ground plane effects", *IEEE Antennas Wireless Propagat. Lett.*, vol. 4, pp. 459–462, 2005.

[59] K. Finkenzeller, *"RFID handbook"*, 2nd edition, Wiley, 2003.

[60] P. Pursula, J. Marjonen, H. Ronkainen and K. Jaakkola, "Wirelessly powered sensor transponder for UHF RFID", *Solid-State Sensors, Actuators and Microsystems Int. Conf., TRANSDUCERS 07*, pp. 73–76, June 2007.

[61] N. Cho, S. Song, S. Kim and H. Yoo, "A 5.1μW UHF RFID tag chip integrated with sensors for wireless environmental monitoring", *Proceedings of ESSCIRC*, pp. 279–282, 2005.

[62] H. Stockman, "Communication by means of reflected power", *Proc. IRE*, vol. 36, no. 10, pp. 1196–1204, Oct. 1948.

[63] X. Qing and N. Yang, "A folded dipole antenna for RFID", *IEEE Antennas Propagat. Int. Symp.*, vol. 1, June 2004.

[64] P. V. Nikitin, S. Lam and K. V. S. Rao, "Low cost silver ink RFID tag antennas", *IEEE Antennas Propagat. Int. Symp.*, vol. 2B, July 2005.

[65] M. Keskilammi and M. Kivikoski, "Using text as meander line for RFID transponder antennas", *IEEE Antennas Wireless Propag. Lett.*, vol. 3, pp. 372–374, 2004.

[66] S. K. Padhi, G. F. Swiegers and M. E. Bialkowski, "A miniaturized slor ring antenna for RFID applications", *Int. Conf. on Microwave, Radar and Microwave Communications*, May 2004.

[67] J. D. Griffin, G. D. Durgin, A. Haldi and B. Kibbelen, "RF tag antenna performance on various materials using radio link budgets", *IEEE Antennas Wireless Propag. Lett.*, vol. 5, pp. 247–250, Dec. 2005.

[68] J. T. Prothro, G. D. Durgin and J. D. Griffin, "The effects of a metal ground plane on RFID tag antennas", *IEEE Antennas Propagat. Int. Symp.*, pp. 3241–3244, July 2006.

[69] Y. Byunggil, K. Sung-Joo, J. Byungwoon, F. J. Harackiewicz , P. Myon-Joo and L. Byungie, "Balanced RFID tag antenna mountable on metallic plates", *IEEE Antennas Propagat. Int. Symp.*, pp. 3237–3240, July 2006.

[70] Y. C. Or, K. W. Leung, R. Mittra and K. V. S. Rao, "Platform tolerant RFID tag antenna", *IEEE Antennas Propagat. Int. Symp.*, pp. 5491–5494, June 2007.

[71] H.-E. Nilsson, J. Siden, T. Olsson, P. Jonsson and A. Koptioung, "Evaluation of a printed patch antenna for robust microwave RFID tags", *IET Microwave, Antennas Propagat.*, vol. 1, no. 3, pp. 775–781, June 2007.

[72] http://www.epcglobalinc.org

[73] S. Jeon, Y. Yu and J. Choi, "Dual-band slot-coupled dipole antenna for 900MHz and 2.45GHz RFID tag application", *Electronics Letters*, vol. 42, no. 22, pp. 1259–1260, Oct. 2006.

[74] Z. Fang, R. Jin, J. Geng and J. Sun, "Dual band RFID transponder antenna designed for a specific chip without additional impedance matching networks", *Microwave and Optical Tech. Lett.*, vol. 50, no. 1, pp. 58–60, Jan. 2008.

[75] P. V. Nikitin and K. V. S. Rao, "Theory and measurement of backscattering from RFID tags", *IEEE Trans. Antennas Propag. Magazine*, vol. 48, pp. 212–218, Dec. 2006.

[76] R. F. Harrington, "Theory of loaded scatterers", *Proc. IEE.*, vol. 111, pp. 617–623, April 1964.

[77] J. T. Mayhan, A. R. Dion and A. J. Simmons, "A technique for measuring antenna drive port impedance using backscatter data", *IEEE Trans. Antennas Propag.*, vol. 42, no. 4, pp. 526–533, April 1994.

[78] P. Pursula, D. Sandström and K. Jaakkola, "Backscattering-based measurement of reactive antenna input impedance", *IEEE Trans. Antennas Propag.*, vol. 56, no. 2, pp. 469–474, Feb. 2008.

Errata

In [P1], at page 685, equation (10)

$$F_\theta(\theta) \approx \begin{cases} -2jk_0b/(\varepsilon_r \sin^2\theta) & \text{if } |\varepsilon_r| \gg k_0b \\ 2\cos\theta & \text{if } |\varepsilon_r| \ll k_0b \end{cases}$$

should be

$$F_\theta(\theta) \approx \begin{cases} -2jk_0b\sin^2\theta/\varepsilon_r & \text{if } |\varepsilon_r| \gg k_0b \\ 2\cos\theta & \text{if } |\varepsilon_r| \ll k_0b \end{cases}$$

In [P1], at page 689, equation (26)

$$P = \int_0^{2\pi}\int_0^{\pi/2} p\,\sin\theta d\theta d\varphi = \frac{\pi}{k^2}\sqrt{\frac{\varepsilon_0}{\mu_0}}\sum_{n=1}^{\infty}(a_n^2 + b_n^2)$$

should be

$$P = \int_0^{2\pi}\int_0^{\pi/2} p\,r^2\sin\theta d\theta d\varphi = \frac{\pi}{k^2}\sqrt{\frac{\varepsilon_0}{\mu_0}}\sum_{n=1}^{\infty}(a_n^2 + b_n^2)$$

PUBLICATION 1

Power and *Q* of a horizontal dipole over a metamaterial coated conducting surface

In: IEEE Transactions on Antennas and Propagation 2008.
Vol. 56, No. 3, pp. 684–690.
© 2008 IEEE.
Reprinted with permission from the publisher.

This material is posted here with permission of the IEEE. Such permission of the IEEE does not in any way imply IEEE endorsement of any of the VTT Technical Research Centre of Finland's products or services. Internal or personal use of this material is permitted. However, permission to reprint/republish this material for advertising or promotional purposes or for creating new collective works for resale or redistribution must be obtained from the IEEE by writing to pubs-permissions@ieee.org.

Power and Q of a Horizontal Dipole Over a Metamaterial Coated Conducting Surface

Mervi Hirvonen and Johan C. -E. Sten

***Abstract*—The radiation properties of an electrically small antenna attached to an infinite conducting ground plane covered by a thin sheet of a metamaterial medium are considered. Using analytical field expressions, the radiation of an electric point dipole with arbitrary constitutive parameters of the material coating is studied. Attention is paid especially to permittivity values close to zero. Finite element simulations are employed to confirm the radiation enhancement and low quality factor Q characteristic of a zero-index coating as compared with regular "air-filling." The Q is evaluated partly through integration of the energy of the FEM-simulated fields within the antenna region and partly from the nonradiating component of the multipole fields outside the antenna region. Additionally, the influence of surface wave power is analyzed through simulations.**

***Index Terms*—Conducting surface, dipole antenna, Q factor, radiated power, zero-index materials.**

I. Introduction

ANTENNA miniaturization is a big engineering challenge because of the fundamental limitations that restrict the performance of electrically small antennas. Especially problematic are antennas designed to operate close to a conducting surface (ground plane) [1], since the radiation from impressed antenna currents flowing tangentially to the surface tend to be cancelled out by the surface currents induced on the plane [2]. Usually, this results in a high reactive field level, low radiation resistance as well as a narrow resonant bandwidth. In addition, the efficiency may be poor due to ohmic losses that are sometimes considerable compared to the radiation loss. An important approximate measure for the bandwidth capacity of a small antenna (an antenna whose largest dimension is a minor fraction of the free-space wavelength) is the reciprocal of the radiation quality factor Q. The quality factor is generally defined for ideal lossless antennas (see, e.g., [3] and references therein)

$$Q = \frac{\omega W}{P_r} \tag{1}$$

where ω is the angular frequency of the oscillation, W the total energy (both electric and magnetic) stored by the electromagnetic fields produced by the antenna and P_r, the total amount of radiated power (for lossy antennas, P_r is to be replaced by P_r plus the power lost within the antenna structure). In principle, multistage impedance matching can be used to achieve bandwidths somewhat larger than the $1/Q$-estimate (see, e.g., [4], [5]), but the required matching circuits tend to grow very complex and are, in practice, inherently lossy. In the present paper, matching issues are not considered, however, and therefore, the Q refers to the quality factor of the radiating element itself.

The theoretical limitations for the radiation Q for the most general multipole field [6] are based on the nonradiating energy (which, in turn, is proportional to the imaginary, reactive, power [7]) stored by the spherical multipole fields outside the source region, which is determined by the smallest sphere that encloses the current carrying region. These limitations are usually considered as unattainable because they neglect the energy inside the "source sphere," which, however, is often predominant in practice. Thus, in order to achieve the theoretical limit for the Q, the power radiated by the antenna should be maximized while, simultaneously, the electromagnetic energy stored by the antenna inside the "source sphere" should ideally vanish totally, or at least be minimized. To achieve this, according to an old maxim, one should "spread out" the source current to fill the spherical volume most efficiently, thereby avoiding the emergence of energetic field concentrations and singularities.

The rapid theoretical as well as experimental advances made recently in the field of artificially tailored media, so-called metamaterials (see, e.g., [8], [9] for recent reviews), characterized by unusual electromagnetic constitutive parameters, suggests yet another way of optimizing the power and Q of antennas [10]. In particular, the use of materials having a dielectric permittivity ε and a magnetic permeability μ near or equal to zero, also known as *zero-index* [8] or *nihility* medium [11], as a substrate for the antenna structure, could provide a natural means to minimize the radiation Q and maximize the power radiated into the far zone. In [12] it has actually been suggested that a certain kind of rod array exhibits a zero index of refraction on its plasma frequency, which property can be used to focus and enhance dipole radiation. In the present paper, we explore the consequences of the application of such a metamaterial substrate backed by an infinite conducting ground plane to the radiation performance and Q of a small dipole antenna attached to the substrate.

We begin this paper by introducing expressions for the far field radiated by an elementary electric point dipole attached to a dielectric/magnetic slab with arbitrary combinations of μ_r and ε_r, involving particularly the cases $\mu_r = 1, 0$ or -1 and $\varepsilon_r = 1$, 0 or -1. We evaluate the radiated power both numerically and analytically and verify the results with Ansoft's HFSS finite element simulator for a short dipole. Radiation Q is analyzed by means of a spherical wave expansion of the approximate expressions for the fields radiated by the dipole and by integrating

Manuscript received January 29, 2007; revised October 30, 2007.

The authors are with the VTT Technical Research Centre of Finland, 02044 VTT Espoo, Finland (e-mail: mervi.hirvonen@vtt.fi).

Digital Object Identifier 10.1109/TAP.2008.916937

0018-926X/$25.00 © 2008 IEEE

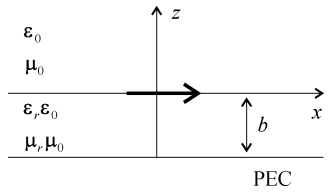

Fig. 1. Dipole on conductor backed slab.

the stored energy in the antenna structure. For comparison, Q is also derived from the antenna input impedance. Furthermore, we consider the amount of power propagating as surface waves, which is not accounted for by the expressions used for the radiated field. The pertinent question of realizability of such a special medium – albeit admittedly a very important one – is left out of the scope of the present study.

II. Fields Due to a Horizontal Dipole on Conductor Backed Slab

Consider a horizontal x-directed point dipole, or an electric current moment of magnitude IL, situated on the z-axis on a planar substrate layer backed by a perfectly conducting surface coinciding with the xy-plane (Fig. 1). The thickness of the layer is denoted b and its electric and magnetic material parameters relative to the ambient medium (say, vacuum) ε_r and μ_r, respectively. For the sake of simplicity it is assumed throughout that these parameters are real valued. All the field quantities are assumed to obey the harmonic $e^{j\omega t}$-time dependence, where $j = \sqrt{-1}$.

The electric field radiated into the far-zone (that is, $r \to \infty$, $\theta \in [0, \pi/2]$, $\varphi \in [-\pi, \pi]$) is given by Jackson and Alexopoulos [13] as

$$\mathbf{E}(r,\theta,\varphi) = j\omega\mu_0 IL\Big[\mathbf{u}_\varphi \sin\varphi\, F_\varphi(\theta) - \mathbf{u}_\theta \cos\varphi\, F_\theta(\theta)\Big]\frac{e^{-jk_0 r}}{4\pi r} \tag{2}$$

where

$$F_\varphi(\theta) = \frac{2\tan(\beta b)}{\tan(\beta b) - \frac{jN(\theta)}{(\mu_r \cos\theta)}} \tag{3}$$

$$F_\theta(\theta) = \frac{2\tan(\beta b)\cos\theta}{\tan(\beta b) - \frac{j\varepsilon_r \cos\theta}{N(\theta)}} \tag{4}$$

and $\beta = k_0 N(\theta)$, $k_0 = \omega\sqrt{\mu_0\varepsilon_0}$, $N(\theta) = \sqrt{n^2 - \sin^2\theta}$ and $n = \sqrt{\mu_r\varepsilon_r}$. In addition to space wave, a part of the power will be launched as a TM_0-surface wave if $\varepsilon_r \neq \mu_r^{-1}$. Surface wave power is discussed in Section III.

If the layer is electromagnetically thin, $\beta b \ll 1$, the expressions can be approximated as

$$F_\varphi(\theta) \approx \frac{2k_0 b}{k_0 b - \frac{j}{(\mu_r \cos\theta)}} \tag{5}$$

$$F_\theta(\theta) \approx \frac{2k_0 (N(\theta))^2 b\cos\theta}{k_0 (N(\theta))^2 b - j\varepsilon_r \cos\theta} \tag{6}$$

which are the basis for the subsequent developments. Below, we examine a few particular cases where these expressions can be expected to yield analytically tractable results.

1. When $kb\mu_r \ll 1$, a Taylor-expansion of $F_\varphi(\theta)$ gives

$$F_\varphi(\theta) \approx 2jk_0 b\mu_r \cos\theta(1 - jk_0 b\mu_r \cos\theta + \cdots) \tag{7}$$

plus terms involving higher powers of $k_0 b\mu_r$ (presumed negligible).

2. When $\varepsilon_r = 1$ and $\mu_r = 1$ simultaneously, there is no substrate. Then

$$F_\varphi(\theta) \approx 2jk_0 b\cos\theta(1 - jk_0 b\cos\theta + \cdots) \tag{8}$$

through substitution in (7) while $F_\theta(\theta)$ is

$$F_\theta(\theta) \approx 2jk_0 b\cos^2\theta(1 - jk_0 b\cos\theta + \cdots). \tag{9}$$

This case of "air filling" has been examined in [1].

3. In the case $\varepsilon_r \ll 1$ there are two possibilities

$$F_\theta(\theta) \approx \begin{cases} -\frac{2jk_0 b}{\varepsilon_r \sin^2\theta} & \text{if } |\varepsilon_r| \gg k_0 b \\ 2\cos\theta & \text{if } |\varepsilon_r| \ll k_0 b \end{cases}. \tag{10}$$

4. In the case of an "anti-vacuum", $\varepsilon_r = -1$ and $\mu_r = -1$

$$F_\varphi(\theta) \approx -2jk_0 b\cos\theta(1 + jk_0 b\cos\theta + \cdots) \tag{11}$$

$$F_\theta(\theta) \approx -2jk_0 b\cos^2\theta(1 + jk_0 b\cos\theta + \cdots). \tag{12}$$

The fields are in this case the complex conjugates of those of the $\varepsilon_r = 1$ and $\mu_r = 1$-case mentioned above.

III. Radiated Power

The radiated power is generally given by the integral

$$P_r = \frac{1}{2}\Re\int_S (\mathbf{E}\times\mathbf{H}^*)\cdot\mathbf{n}\, dS \tag{13}$$

where S is an arbitrary surface enclosing the source, dS is the differential surface element and $\mathbf{n}$, the surface normal. It is often most convenient to evaluate the power in the far field at a certain distance r, whence (13) can be written in spherical coordinates as

$$P_r = \frac{1}{2}\sqrt{\frac{\varepsilon_0}{\mu_0}}\int_0^{2\pi}\int_0^{\pi}(|E_\theta|^2 + |E_\varphi|^2) r^2 \sin\theta\, d\theta\, d\varphi \tag{14}$$

which is easily computed numerically. However, in the special cases mentioned previously the radiated power can be obtained also analytically by direct integration. In particular, using (2) and the approximations (8) and (9) we get from (14)

$$P_r = (IL)^2\sqrt{\frac{\varepsilon_0}{\mu_0}}\frac{(\omega\mu_0)^2 (k_0 b)^2}{15\pi} \tag{15}$$

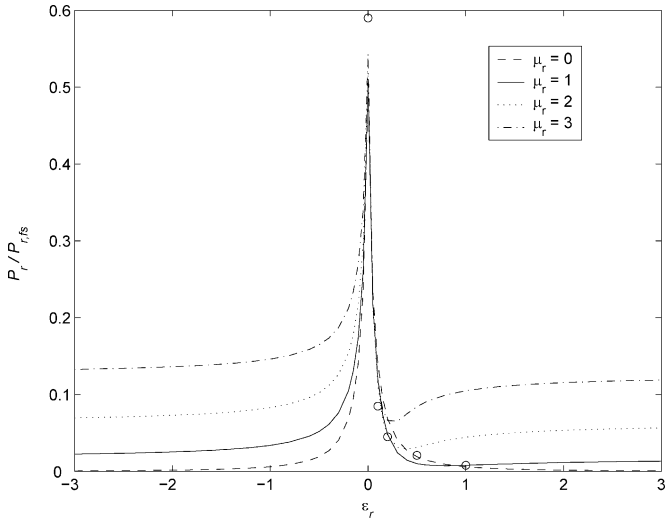

Fig. 2. Radiated power with positive μ_r values. Circles represent the analytical values gained from (15), (16) and (17) in the case $\mu_r = 1$.

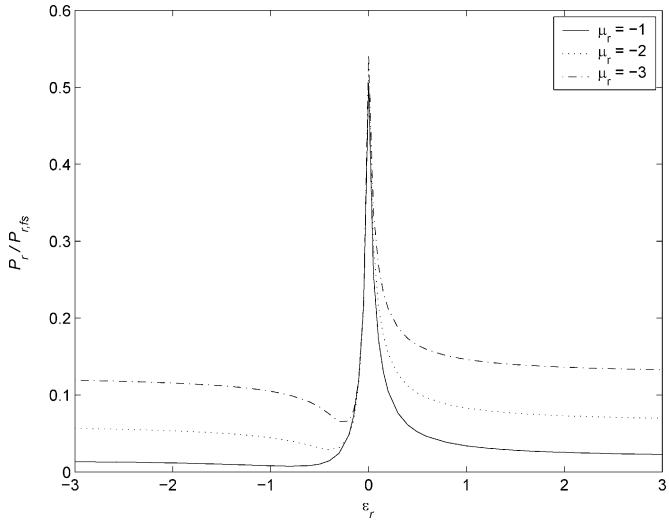

Fig. 3. Radiated power for negative μ_r values.

when $\varepsilon_r = 1$, $\mu_r = 1$ (note: the same power is obtained in the case $\varepsilon_r = -1, \mu_r = -1$) and from (2), (7), and (10)

$$P_r = (IL)^2 \sqrt{\frac{\varepsilon_0}{\mu_0}} \frac{(\omega\mu_0)^2 (\frac{8}{5\varepsilon_r} + \mu_r)(k_0 b)^2}{24\pi} \tag{16}$$

when $1 \gg |\varepsilon_r| \gg k_0 b$ and

$$P_r = (IL)^2 \sqrt{\frac{\varepsilon_0}{\mu_0}} \frac{(\omega\mu_0)^2 (1 + \mu_r k_0 b)^2}{24\pi} \tag{17}$$

when $1 \gg |\varepsilon_r| \ll k_0 b$. In these cases (where a ground plane is involved) the integrals are of course evaluated over the upper hemisphere only ($\theta \in [0, \pi/2]$). In comparison, a dipole in free space radiates the power

$$P_{r,\mathrm{fs}} = (IL)^2 \sqrt{\frac{\varepsilon_0}{\mu_0}} \frac{(\omega\mu_0)^2}{12\pi} \tag{18}$$

over the entire sphere ($\theta \in [0, \pi]$).

Figs. 2 and 3 depict the radiated power for different combinations of ε_r and μ_r. The distance of the dipole to the conducting plane in all these examples is $k_0 b = 0.1$ and the feed current is considered constant. The values of (14) are normalized to the power radiated by the same dipole source in free space (18).

For $\varepsilon_r, \mu_r > 1$ a growing permittivity or permeability leads to an enhanced radiated power, i.e., the radiation resistance increases, although for μ_r the enhancement is notably stronger, as has been noticed in [14]. Similarly in the case of negative parameters, $\varepsilon_r, \mu_r < -1$, the smaller ε_r and μ_r, the more power is radiated. However, when ε_r approaches zero, the power increases and reaches its peak at $\varepsilon_r = 0$, in accordance with (17). The radiated power with permittivity zero is (in this particular case of $k_0 b = 0.1$) roughly 75 times larger than in the case $\varepsilon_r = 1$, corresponding to $(1 + \mu_r k_0 b)^2/2$ times (i.e., more than a half of) the power radiated by the same dipole source in free space. This is a remarkable improvement.

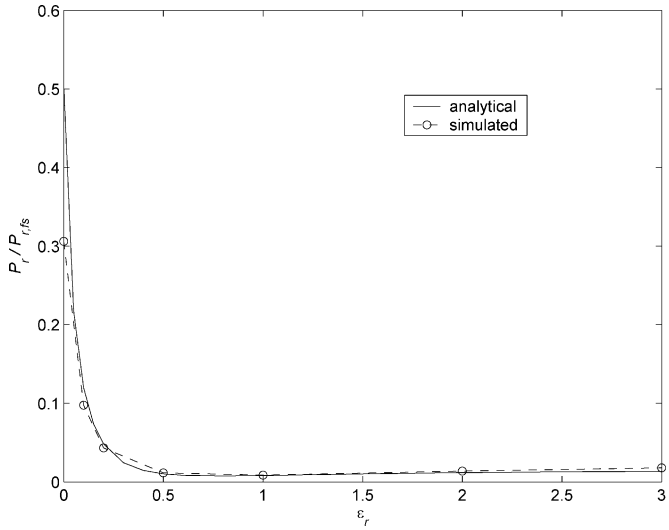

Fig. 4. Simulated radiated power versus the power given by the theoretical field expressions.

In Fig. 4 the radiated power of the quarter wave dipole simulated with HFSS (Ansoft Corp.) is compared with the theoretical result of Fig. 2 in the case of $\mu_r = 1$. In the simulations the dipole was a center fed infinitesimally thin PEC strip of width 0.0033 λ. Again, the height of the dipole over the conducting plane $k_0 b$ is 0.1 and the values are normalized to the radiated power of the corresponding dipole source in free space. As can be seen, the simulated results resemble very closely the numerical ones, a part of the difference being due to surface-wave power. Only positive ε_r- values are considered here, because HFSS (Version 10.1.2) can only handle material parameters having a positive real part with a reasonable accuracy [15].

In the previous formulas the surface wave power is not taken into account. The amount of surface wave power P_{sw} carried by

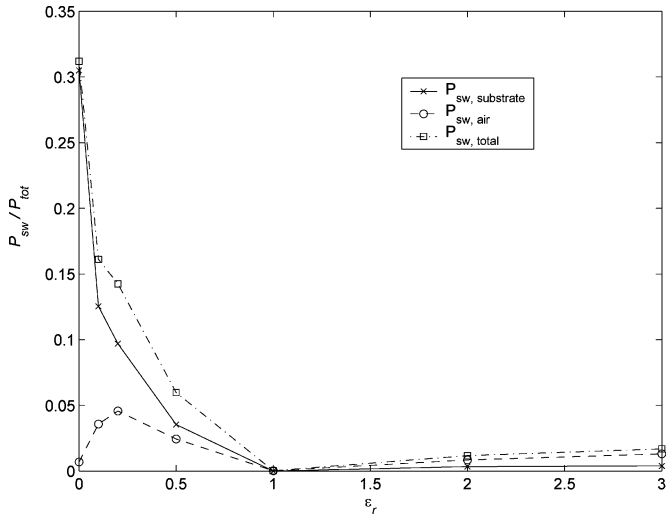

Fig. 5. Surface wave power of the quarter wave dipole extracted from HFSS simulations.

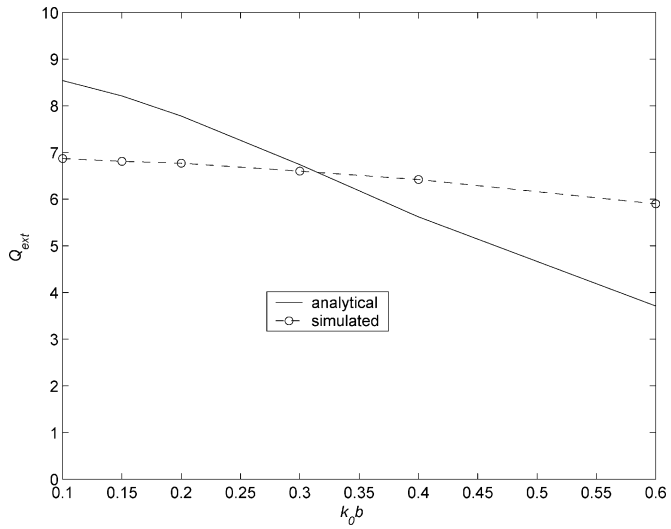

Fig. 6. External Q factor as a function of the layer thickness.

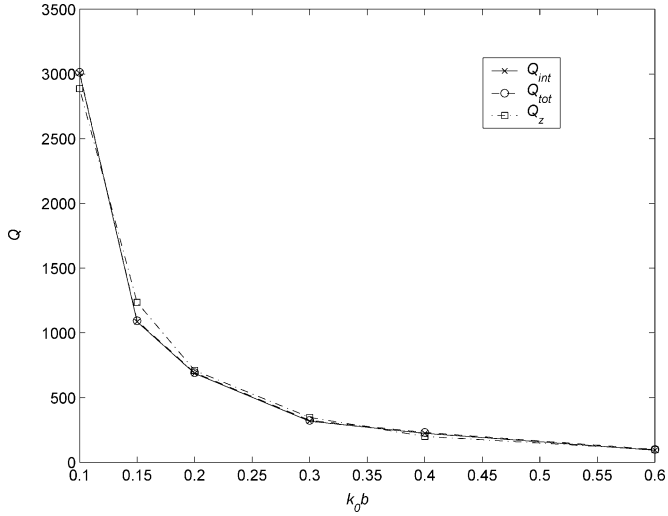

Fig. 7. Internal and total Q factors as a function of the layer thickness.

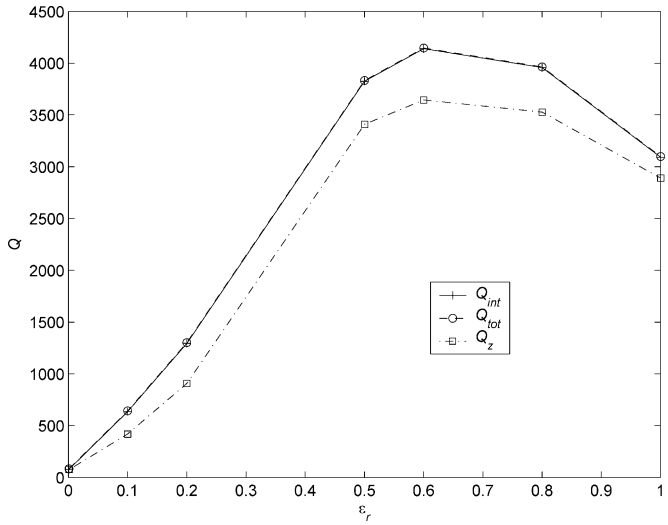

Fig. 8. Internal and total Q factors when ε_r varies and $k_0 b = 0.1$ and $\mu_r = 1$.

the E_z and H_φ components of the fields of the dominant TM_0 surface wave can be evaluated from [13]

$$P_{\mathrm{sw}} = -\frac{1}{2}\Re \int_0^\infty \int_0^{2\pi} E_z H_\varphi^* \rho \, d\varphi \, dz \tag{19}$$

using the values of E_z, H_φ given by the simulator program at the interface along the boundary surface of the simulation volume. The resulting surface wave power of a quarter wave long dipole as a function of ε_r is illustrated in Fig. 5. The distance to the conducting plane $k_0 b$ is 0.1 and the power values are normalized to the amount of total power (i.e., the power radiated into free space plus the surface wave power). For all the cases $\mu_r = 1$.

In Fig. 5 the surface wave power is drawn separately for the substrate and in the "air region" above the interface. It turns out that for $\varepsilon_r < 1$, the largest part of the surface wave power flows inside the substrate while for $\varepsilon_r > 1$ above it. The total surface wave power can be seen to grow as a function of index of refraction at the interface, thus reaching its maximum at $\varepsilon_r = 0$ and minimum at $\varepsilon_r = 1$.

IV. Quality Factor

The quality factor Q, being a ratio between energy and power (1), is not as such directly measurable. The theoretical limitations for the radiation Q are based on the nonradiating energy stored by the spherical multipole fields outside the smallest sphere enclosing the current carrying region. The formulas for determining this external energy W_{ext} and hence the external quality factor Q_{ext} are based on [6] and summarized in the Appendix .

However, in real antenna structures also the energy stored inside the smallest enclosing sphere, W_{int}, needs to be considered. Although expressions for internal energy are generally impossible to describe analytically, finite element simulation programs (such as Ansoft's HFSS) allow the electromagnetic en-

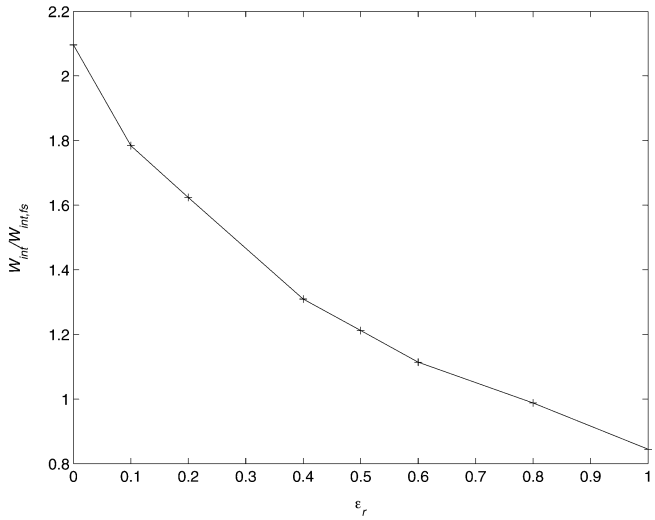

Fig. 9. Internal stored energy $W_{\rm int}$ when ε_r varies and $k_0 b = 0.1$ and $\mu_r = 1$.

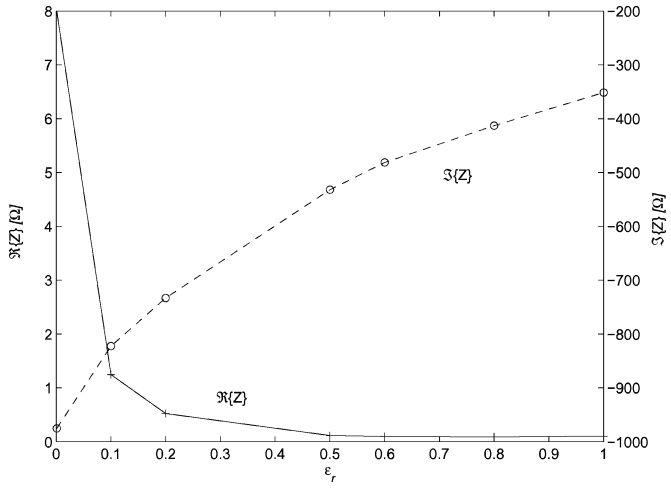

Fig. 10. Input impedance Z when ε_r varies and $k_0 b = 0.1$ and $\mu_r = 1$.

ergy in a given region of space (for a specific excitation) to be integrated numerically. Thus, one may estimate the quantity

$$W_{\rm int} = \frac{1}{4}\Re \int_{\rm sphere} dV\,(\varepsilon|\mathbf{E}|^2 + \mu|\mathbf{H}|^2) \tag{20}$$

where the integration volume "sphere" signifies the smallest spherical volume that surrounds the current carrying region. In the following dispersionless, positive material parameters are considered. For a discussion on the exact definitions of the electric, magnetic and magnetoelectric energies in a general, dispersive metamaterial medium, we refer to [3], [10], [16].

Moreover, as shown in [3] a fair estimate of the Q-factor can be achieved by means of the input impedance $Z(\omega)$ through the formula

$$Q_Z \approx \frac{\omega}{2\Re\{Z\}}\left|\frac{dZ}{d\omega}\right|. \tag{21}$$

In Fig. 6 the external quality factor $Q_{\rm ext}$ of the simulated quarter wave dipole on top of an air-filled conductor backed slab as a function of thickness $k_0 b$ of the slab is illustrated. Again, the feed current is considered constant. Although the analytical formula given in the Appendix predicts a deeper slope compared to the simulated one, the order of magnitude of the results is the same. For comparison, the external quality factor of the same dipole in free space is approximately 3.5. In Fig. 7 the internal quality factor $Q_{\rm int}$ and total quality factor $Q_{\rm tot}$ (the external plus the internal Q) are presented in the same case. For reference, the quality factor Q_Z evaluated from the simulated input impedance Z is also shown. Clearly, the Q's given by the different methods are seen to increase exponentially as the thickness of the slab decreases. The internal quality factor $Q_{\rm int}$, being proportional to the energy $W_{\rm int}$ stored inside the smallest sphere, is in the order of total Q and is thus dominant.

Fig. 8 displays the simulated internal and total quality factors of the quarter wave dipole for different values of permittivity. The distance to the conducting plane $k_0 b$ is 0.1 and the permeability value one. The external quality factor in this case is small compared to the internal one, near 7 for all values of permittivity. The internal Q decreases from 3000 to 120 as the permittivity goes from one to zero, which is also in tune with the simultaneously increasing radiated power. As a reference, the internal Q of a similar dipole in free space would be around 30. On the other hand, the internal stored energy presented in Fig. 9 slightly increases as ε_r approaches zero. The values in Fig. 9 are normalized to the stored energy of a similar dipole in free space. The stored energy is of the same order of magnitude as in the free space case indicating the dominant role of the radiated power in the Q value. To understand this, we remind that in these examples the feed current is held constant. If the radiated power or input power in matched case would be held constant instead, one would encounter notably larger levels of internal energy compared to the free space case and a steeply decreasing trend as permittivity approaches zero.

In Fig. 10 the input impedance of the simulated dipole is presented. The real part of the impedance increases as the permittivity approaches zero indicating an increasing radiation resistance. The result parallels the increasing radiated power illustrated in the Figs. 2–4. On the other hand, the imaginary part of the input impedance decreases somewhat as the permittivity becomes smaller. This phenomenon can be understood by the growth of the wavelength in a low epsilon substrate, which makes the dipole appear electromagnetically smaller than in the air.

V. Conclusion

In this paper we have considered both theoretically and computationally the effect on the quality factor Q and radiated power of letting the permittivity and permeability of an antenna substrate be less than the free space values ε_0 and μ_0, respectively. Attention was paid especially to the case of zero or near-zero permittivity, that can potentially be achieved using special microstructured substrate materials exhibiting a "plasma resonance" frequency. It was shown that a remarkable increase of the radiated power (due to a simultaneously growing radiation resistance) compared to the stored internal energy would occur for such a near-zero permittivity substrate medium,

leading to exceptionally low quality factor in dispersionless case. These properties are highly desirable, because antennas attached to a ground plane suffer from both low radiation resistance and narrow bandwidth.

For comparison, different methods to evaluate the quality factor were provided. One of the methods is based on a division of the stored electromagnetic energy into two respective volumes – the antenna region (where the energy is computed using simulated fields) and the free-space surrounding the antenna (where the stored energy is associated with the reactive near fields of the antenna) while the other method employs the frequency derivative of the input impedance. To our satisfaction, both methods were found to yield similar results.

APPENDIX

In this Appendix, expressions for the radiated power and Q in terms of multipole moments are summarized [6]. We write a spherical harmonics expansion of outward propagating electric and magnetic fields as

$$\mathbf{E}(\mathbf{r}) = \sum_{n=1}^{\infty}\sum_{m=-n}^{n}\Big[a_{mn}\mathbf{M}_{mn} + b_{mn}\mathbf{N}_{mn}\Big] \tag{22}$$

$$\mathbf{H}(\mathbf{r}) = \frac{jk}{\omega\mu_0}\sum_{n=1}^{\infty}\sum_{m=-n}^{n}\Big[a_{mn}\mathbf{N}_{mn} + b_{mn}\mathbf{M}_{mn}\Big] \tag{23}$$

where the spherical vector wavefunctions $\mathbf{M}_{mn}$ and $\mathbf{N}_{mn}$ are defined

$$\mathbf{M}_{mn}(r,\theta,\varphi) = \nabla\times\Big\{\mathbf{r}h_n^{(2)}(kr)\,P_n^{|m|}(\cos\theta)\,e^{-jm\varphi}\Big\} \tag{24}$$

and $\mathbf{N}_{mn}(r,\theta,\varphi) = (1/k)\nabla\times\mathbf{M}_{mn}$, $\mathbf{r}$ being the position vector, $h_n^{(2)}$ the spherical Hankel function and $P_n^{|m|}$ the associated Legendre function.

By defining the power density in the far field as

$$p(r,\theta,\varphi) = \frac{1}{2}\sqrt{\frac{\varepsilon_0}{\mu_0}}\mathbf{E}\cdot\mathbf{E}^\star = \frac{1}{2}\sqrt{\frac{\varepsilon_0}{\mu_0}}(|E_\theta|^2 + |E_\varphi|^2) \tag{25}$$

the power radiated into the upper half-space can be obtained by integration over the hemisphere as

$$P = \int_0^{2\pi}\int_0^{\pi/2} p\,\sin\theta d\theta d\varphi = \frac{\pi}{k^2}\sqrt{\frac{\varepsilon_0}{\mu_0}}\sum_{n=1}^{\infty}(a_n^2 + b_n^2) \tag{26}$$

where

$$a_n^2 = \sum_{m=-n}^{n}\Lambda_{mn}|a_{mn}|^2 \qquad b_n^2 = \sum_{m=-n}^{n}\Lambda_{mn}|b_{mn}|^2 \tag{27}$$

$$\Lambda_{mn} = \frac{n(n+1)(n+|m|)!}{(2n+1)(n-|m|)!}. \tag{28}$$

To compute the Q from (1) we need an expression for the total energy stored by the multipole moments outside the sphere, defined as the smallest sphere of radius r_0 that can be drawn outside the source. Such an expression has been derived in [6], but since only one half-space is of concern, only one half of this expression is taken viz.

$$W = \frac{\pi\varepsilon_0}{4k^3}\sum_{n=1}^{\infty}(a_n^2 + b_n^2)w_n \tag{29}$$

where

$$w_n = 2x - x^3(|h_n^{(2)}|^2 - j_{n-1}j_{n+1} - y_{n-1}y_{n+1}) - x^2(j_n j_n' + y_n y_n') - x|h_n^{(2)}|^2. \tag{30}$$

For brevity, the argument $x = kr_0$ of the spherical Hankel functions $h_n^{(2)}$, the spherical Bessel j_n and Neumann functions y_n is omitted. The lowest five w_n's are given by

$$w_1 = (1+2x^2)x^{-3} \tag{31}$$

$$w_2 = (18+9x^2+6x^4)x^{-5} \tag{32}$$

$$w_3 = 3(225+60x^2+12x^4+4x^6)x^{-7} \tag{33}$$

$$w_4 = 5(8820+1575x^2+180x^4+20x^6+4x^8)x^{-9} \tag{34}$$

$$w_5 = 15(297675+39690x^2+3150x^4+210x^6 + 15x^8+2x^{10})x^{-11}. \tag{35}$$

The case $\varepsilon_r = \mu_r = 1$ can be handled explicitly. In effect, the field (2) including the approximations (8) and (9) can be matched with a spherical wave expansion (22) by means of the following pair of dominant multipole moments

$$a_{\pm1,1} = \pm jILb\frac{k^3}{8\pi}\sqrt{\frac{\mu_0}{\varepsilon_0}} \qquad \text{and} \qquad b_{\pm1,2} = ILb\frac{k^3}{24\pi}\sqrt{\frac{\mu_0}{\varepsilon_0}}. \tag{36}$$

Hence, from (1) and (29) the Q-factor is

$$Q = \frac{27+16x^2+14x^4}{16x^5} \tag{37}$$

while the radiated power is given by (17).

REFERENCES

[1] J. C.-E. Sten, A. Hujanen, and P. K. Koivisto, "Quality factor of an electrically small antenna radiating close to a conducting plane," *IEEE Trans. Antennas Propag.*, vol. 49, no. 5, pp. 829–837, May 2001.

[2] J. C.-E. Sten and M. Hirvonen, "Decay of groundplane currents of small antenna elements," *IEEE Ant. Wireless Propag. Lett.*, vol. 4, pp. 82–84, 2005.

[3] A. D. Yaghjian and S. R. Best, "Impedance, bandwidth and Q of antennas," *IEEE Trans. Antennas Propag.*, vol. 53, no. 4, pp. 1298–1324, Apr. 2005.

[4] A. Hujanen, J. Holmberg, and J. C.-E. Sten, "Bandwidth limitations of impedance matched ideal dipoles," *IEEE Trans. Antennas Propag.*, vol. 53, no. 10, pp. 3236–3239, Oct. 2005.

[5] M. Gustafsson and S. Nordebo, "Bandwidth, Q factor, and resonance models of antennas," *Progress Electromagn. Res.*, vol. 62, pp. 1–20, 2006.

[6] R. L. Fante, "Quality factor of general ideal antennas," *IEEE Trans. Antennas Propag.*, vol. AP-17, no. 2, pp. 151–155, Jan. 1969.
[7] E. A. Marengo, A. J. Devaney, and F. K. Gruber, "Inverse source problem with reactive power constraint," *IEEE Trans. Antennas Propag.*, vol. 52, no. 6, pp. 1586–1595, Jun. 2004.
[8] N. Engheta and R. W. Ziolkowski, "A positive future for double-negative metamaterials," *IEEE Trans. Microw. Theory Tech.*, vol. 53, no. 4, pp. 1535–1556, Apr. 2005.
[9] H. Chen, B.-I. Wu, and J. A. Kong, "Review of electromagnetic theory in left-handed materials," *J. Electromagn. Waves Applicat.*, vol. 20, no. 15, pp. 2137–2151, 2006.
[10] R. W. Ziolkowski and A. D. Kipple, "Application of double negative materials to increase the power radiated by electrically small antennas," *IEEE Trans. Antennas Propag.*, vol. 51, no. 10, pp. 2626–2640, Oct. 2003.
[11] A. Lakhtakia and T. G. Mackay, "Fresnel coefficients for a permittivity-permeability phase space encompassing vacuum, anti-vacuum, and nihility," *Microw. Opt. Tech. Lett.*, vol. 48, no. 2, pp. 265–270, Feb. 2006.
[12] B.-I. Wu, W. Wang, J. Pacheco, X. Chen, T. Grzegorczyk, and J. A. Kong, "A study of using metamaterials as antenna substrate to enhance gain," *Progress Electromagn. Res.*, vol. 51, pp. 295–328, 2005.
[13] D. R. Jackson and N. G. Alexopoulos, "Simple approximate formulas for input resistance, bandwidth and efficiency of resonant rectangular patch," *IEEE Trans. Antennas Propag.*, vol. 39, no. 3, pp. 407–410, Mar. 1991.
[14] R. C. Hansen and M. Burke, "Antennas with magneto-dielectrics," *Microw. Opt. Tech. Lett.*, vol. 26, no. 2, pp. 75–78, Jul. 2000.
[15] A. Erentok and R. W. Ziolkowski, "HFSS modelling of a dipole antenna enclosed in an epsilon-negative (ENG) metamaterial shell," in *Proc. Antennas and Propagation Soc. Int. Conf.*, 2005, vol. 3B, pp. 22–25.
[16] S. A. Tretyakov and S. I. Maslovski, "Veselago materials: What is possible and impossible about the dispersion of the constitutive parameters," *IEEE Antennas Propag. Mag.*, vol. 49, no. 1, Feb. 2007.

Mervi Hirvonen received the Master of Science (Tech.) and Licentiate of Science (Tech.) degrees in electrical engineering from Helsinki University of Technology (TKK), Espoo, Finland, in 2004 and 2006, respectively.

Since 2002 she has been with the VTT Technical Research Centre of Finland. Her current research interests include electromagnetics and antenna theory, wireless sensors, RFID systems and mobile communications.

Johan C.-E. Sten received the degrees of diplomingenjör and teknologie doktor (Dr. Sci.) degrees in electrical engineering from Helsinki University of Technology (TKK), Espoo, Finland, in 1992 and 1995, respectively.

From 1991 to 1994, he was with the Laboratory of Electromagnetics at TKK and since 1995 with VTT Technical Research Centre of Finland, Espoo. His interests include electromagnetic theory, especially antennas and scattering. He is an editor of the *Progress in Electromagnetics Research* (PIER) book series.

PUBLICATION 2

Near-zero permittivity substrates for horizontal antennas

Performance enhancement and limitations

In: Microwave and Optical Technology Letters 2008.
Vol. 50, No. 10, pp. 2674–2677.
Reprinted with permission from the publisher.

an EYDF amplifier, the amplified spontaneous emission intensity can be more than 40 dBm suppressed over the tunable range, and the power conversion efficiency can achieve 10.5%. The tunable laser is a potential candidate for communication and optical measurement.

ACKNOWLEDGMENTS

This research was supported by Hebei Natural Science Foundation (F2006000183), Hebei Natural Science Foundation (2001241), The Science Foundation of Hebei Normal University (L2005B05).

REFERENCES

1. H.Y. Ryu, W.K. Lee, H.S. Moon, and H.S. Suh, Tunable erbium-doped fiber ring laser for applications of infrared absorption spectroscopy, Opt Commun 275 (2007), 379–384.
2. H.M. Pask, J.C. Robert, C.H. David, et al., Ytterbium doped silica fiber lasers versatile sources for the 1-12 mm region IEEE J Selected Topics Quant Electron 1 (1995), 2–13.
3. Y.L. Yu, H. Tan, and Q. Wang, Technique for wavelength selectable fiber ring-laser, Chin J Lasers 29 (2002), 1–4.
4. S.M. Zhang, F.Y. Lu, J. Wang, and C.X. Xie, High-power narrow-linewidth tunable Er^{3+}/Yb^{3+} co-doped cladding-pumped fiber ring laser, Process SPIE 5644 (2005), 242–247.
5. D. Zhou, P.R. Prucnal, and I. Glesk, A widely tunable narrow linewidth semiconductor fibre ring laser, IEEE Photon Technol Lett 10 (1998), 781–783.
6. S.K. Liaw, K.L. Hung, Y.T. Lin, et al., C-band continuously tunable lasers using tunable fiber Bragg grating, Optic Laser Technol 39 (2007), 1214–1217.
7. X.J. Huang, X. Li, and S. Zhan, et al., Widely tunable Yb^{3+}-doped laser with all fiber structure, Optik 12 (2007), 575–578.
8. Y.H. Li, C.Y. Lou, B.Y. Wu, et al., Novel method to simultaneously compress pulses and suppress supermode noise in actively mode-locked fiber ring laser, IEEE Photon Technol Lett 10 (1998), 1250–1252.
9. M. Ding and P.K. Cheo, Effect of Yb:Er codoping on suppressing in Er doped fiber, Photon Technol Lett 9 (1997), 324–326.

© 2008 Wiley Periodicals, Inc.

NEAR-ZERO PERMITTIVITY SUBSTRATES FOR HORIZONTAL ANTENNAS: PERFORMANCE ENHANCEMENT AND LIMITATIONS

Mervi Hirvonen[1] and Sergei A. Tretyakov[2]

[1] VTT Technical Research Centre of Finland, P.O. Box 1000, 02044 VTT Espoo, Finland

[2] Department of Radio Science and Engineering, Helsinki University of Technology, P.O. Box 3000, 02015 TKK, Finland; Corresponding author: mervi.hirvonen@vtt.fi

Received 19 February 2008

ABSTRACT: *In this letter the advantages offered by ε-near-zero materials as substrates for horizontal dipole antennas near a ground plane are theoretically studied. From the previous work it is known that substrates with extremely low values of permittivity dramatically enhance radiation from horizontal currents over a ground plane. On the other hand, as reported in this letter, frequency dispersion and the finite size of the substrate limit the achievable enhancement in antenna performance.* © 2008 Wiley Periodicals, Inc. Microwave Opt Technol Lett 50: 2674–2677, 2008; Published online in Wiley InterScience (www.interscience.wiley.com). DOI 10.1002/mop.23739

Key words: *dipole antenna; conducting surface; near-zero permittivity; dispersion; quality factor*

1. INTRODUCTION

Antenna miniaturization is one of the most difficult challenges for antenna designers due to the low radiation resistance and high reactive field level (stored energy), which are inherent features of electrically small antennas. Moreover, horizontal antennas designed to operate in the vicinity of a ground plane suffer from these problems even more, since the currents induced to the ground plane tend to cancel out the radiating ones. High reactive energy accumulated in the vicinity of a small antenna and low radiation resistance allow in practice only extremely narrow operational bandwidth and low efficiency of the antenna.

From the above discussion it is clear that one needs to find antenna solutions that would enhance radiating power and lower the amount of stored electromagnetic energy. One known approach is to use permeable material loadings [1–3]. That approach is limited by dispersion and losses in available magnetic materials. More recently, when possibilities to realize artificial materials with exotic properties (metamaterials) have been discovered, possibilities of using media with $\varepsilon_r < 1$ and $\mu_r < 1$ were considered. In particular, in [4], the effect of substrates with various material parameters were studied in the case of a horizontal dipole over a ground plane (see Fig. 1). From the radiated power P_r analysis one could detect not only the radiation enhancement in the presence of permeable and negative-index materials, but also a notable enhancement with materials having permittivity close to zero. Prior to [4], near-zero materials have been studied to enhance the directional properties of antennas [5–7].

Calculations in [4] revealed that in the dispersion-free low-epsilon case the internal stored energy was roughly at the same level of magnitude as compared with the air-filling case. This lead to low quality factor values and rather broadband operation. However, in [4] the effect of dispersion of the low-epsilon material was left out of the scope of the study, although it is known to play a major role in antenna applications of metamaterials [2, 3]. In this article, we provide more insight to potential performance of antennas using artificial low-epsilon materials and study the effect of dispersion and the size of the substrate on the antenna performance.

2. THEORY

To understand the enhancement in radiated power of a horizontal dipole in the case of a low-permittivity substrate, one can analyze the surface impedance of the slab Z_s seen by a horizontal electric dipole. In the case of a low-surface impedance, the reflection coefficient from the impedance boundary is close to -1, which means cancellation of radiation. On the other hand, a high-surface impedance is preferable, since radiation from the dipole can be

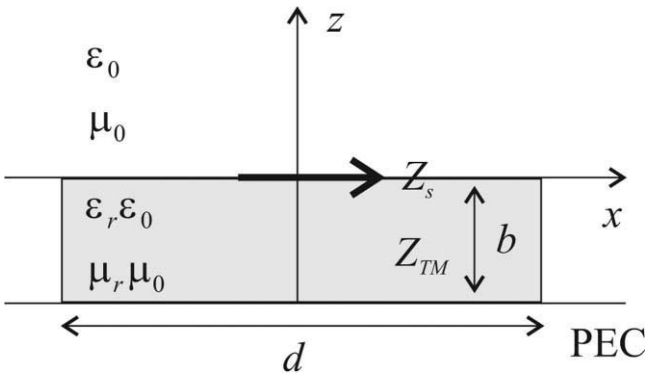

Figure 1 Electric dipole on a conductor-backed slab

enhanced. A horizontal dipole over a material slab on a ground plane (see Fig. 1) generates a wide spectrum of spatial harmonics, and we need to consider surface impedance for plane-wave components with arbitrary tangential wavenumbers k_t. The surface impedance can be written as (e.g., [8])

$$Z_s = jZ^{TM}\tan(\beta b), \tag{1}$$

where b is the thickness of the slab and β is the vertical component of the propagation constant given by

$$\beta^2 = \omega^2\varepsilon\mu - k_t^2. \tag{2}$$

Z^{TM} is the wave impedance of TM waves in the slab:

$$Z^{TM} = \sqrt{\frac{\mu}{\varepsilon}}\sqrt{1 - \frac{k_t^2}{\omega^2\varepsilon\mu}}. \tag{3}$$

For the spatial harmonic propagating in the vertical direction ($k_t = 0$), and for electrically thin slabs the permittivity ε cancels out: The slab impedance becomes $Z_s \approx j\mu\omega b$. Thus, if the thickness b is small compared to the wavelength, the slab impedance is small and acts as an electric conductor, unless a high-permeability substrate is used. However, if the tangential wave number k_t is nonzero (all other spatial harmonics, propagating in oblique directions or evanescent fields), the tangent function is finite and for the case when ε tends to zero, the surface impedance becomes infinite and acts as a magnetic conductor enhancing the antenna radiation. Although the enhancement is smaller than for the ideal case of a perfect magnetic conductor ground plane, it can be very significant. The results presented in publication [4] strongly support this hypothesis.

3. EFFECT OF FREQUENCY DISPERSION

In publication [4], calculations in the dispersion-free low-epsilon case showed that the stored energy W was roughly of the same magnitude as compared to the air-filling case. Thus, the enhancement in radiated power P_r, which is easily computed numerically from the far-field data as

$$P_r = \frac{1}{2}\sqrt{\frac{\varepsilon_0}{\mu_0}}\int_0^{2\pi}\int_0^{\pi}(|E_\theta|^2 + |E_\varphi|^2)r^2\sin\theta\, d\theta\, d\varphi, \tag{4}$$

led to a low radiation quality factor Q, since

$$Q = \frac{\omega W}{P_r}, \tag{5}$$

and to a wide antenna bandwidth.

However, in [4] dispersion of the material parameters and its effects on the stored energy and the radiation Q were left out of the scope. In practice, dispersion plays an important role. Like permeability in high microwave frequencies, near-zero permittivity is realized with passive artificial composite materials. As one possible realization, one can use meshes of thin metal wires, possibly loaded by inductors to reduce structural dimensions. It is well known, that frequency dispersion of the material parameters cannot be neglected in calculation of the stored energy, if the permittivity and/or permeability values are smaller than unity (e.g., [9, 10]). For these materials, the stored energy is calculated as

$$W = \frac{1}{4}\mathrm{Re}\int_{\text{sphere}} dV\left(\frac{\partial(\omega\varepsilon)}{\partial\omega}|\mathbf{E}|^2 + \frac{\partial(\omega\mu)}{\partial\omega}|\mathbf{H}|^2\right). \tag{6}$$

This formula assumes that the substrate losses can be neglected. While the permittivity values can approach zero, the coefficient $\frac{\partial(\omega\varepsilon)}{\partial\omega}$ is always larger than unity.

Thus, dispersion leads to increased stored field energy in the substrate. In estimating the antenna quality factor we integrate the energy density over the smallest sphere that can completely enclose the antenna. The energy stored outside this volume can be estimated using the spherical-mode expansion of the antenna fields. In paper [4] it is shown that the energy stored outside the antenna sphere is small compared to the internal energy, and in this study it is neglected.

In antenna design low-loss substrates are clearly preferable, which suggests the use of non-resonant microstructures for the realization of near-zero permittivity materials. In this case the dispersion can be usually well approximated by the Drude law as

$$\varepsilon = \varepsilon_0\left(1 - \frac{\omega_p^2}{\omega^2}\right), \tag{7}$$

where ω_p is the plasma frequency. If the permeability is nondispersive (we assume nonmagnetic substrates in this study), we get for the field energy

$$W = \frac{1}{4}\mathrm{Re}\int_{\text{sphere}} dV\left[\varepsilon_0\left(1 + \frac{\omega_p^2}{\omega^2}\right)|\mathbf{E}|^2 + \mu_0|\mathbf{H}|^2\right]. \tag{8}$$

4. RESULTS

In the case of a microstrip antenna loaded with artificial magnetic materials studied in [2], it was found that the bandwidth enhancement due to magnetic properties of the substrate was negated by the effect of increased stored energy due to material dispersion. In the present case of low-epsilon substrate the favorable effect on increased radiation depends on the size of the substrate. In paper [4] the size of the low-ε substrate was considered infinite. However, empirically one can expect considerable decrease in the radiated power as the substrate size becomes smaller. If the antenna system is assumed to be similar to the case presented in the earlier work [4] (a horizontal dipole over a material-coated ground plane), the radiated power curves presented in Figure 2 can be drawn showing the decrease in the radiated power as the length d of the substrate is decreased from infinity to the quarter of the wavelength in free space. The normalized distance $k_0 b$ to the ground plane equals 0.1, and the primary radiator is a quarter-wavelength dipole. In the simulations, the dipole was metal strip with width 0.0033λ and fed in the center with ideal current source. In Figure 2 the ground plane is considered infinite and the radiated power is normalized to the power radiated by the same dipole in free space without the ground.

The internal stored energy of the same antenna is presented in Figure 3. In the calculations, the internal energy was numerically evaluated from the field data simulated with HFSS software and the dispersion factor was included. In all the simulation cases the feed current was considered constant and the stored energy was normalized to the stored energy of a similar dipole in free space.

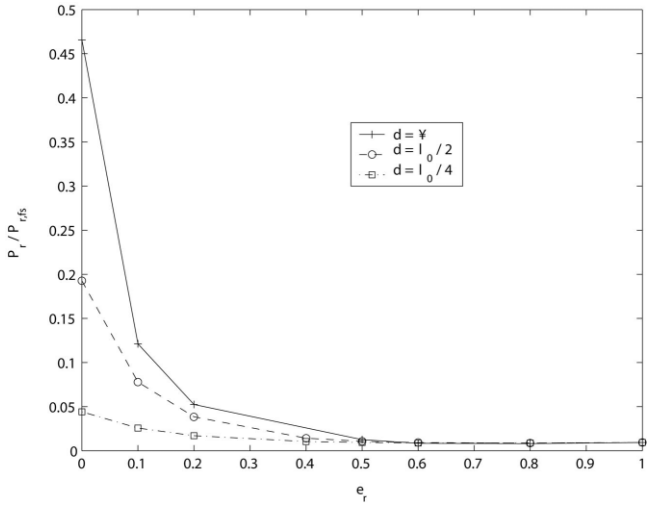

Figure 2 Radiated power for different sizes of low-ε substrate

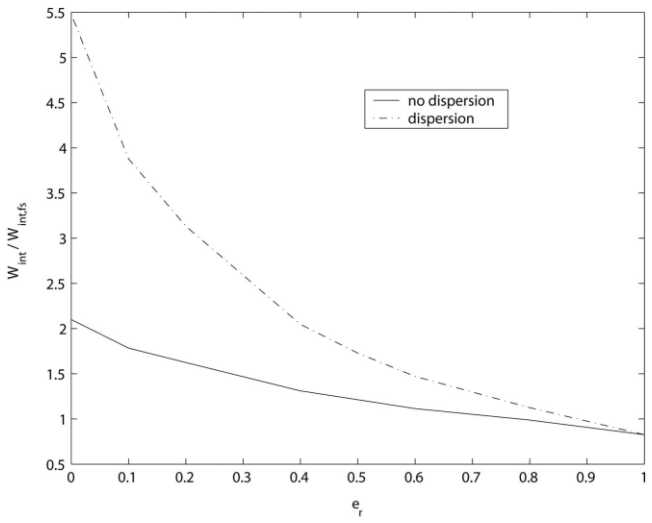

Figure 3 Stored reactive energy

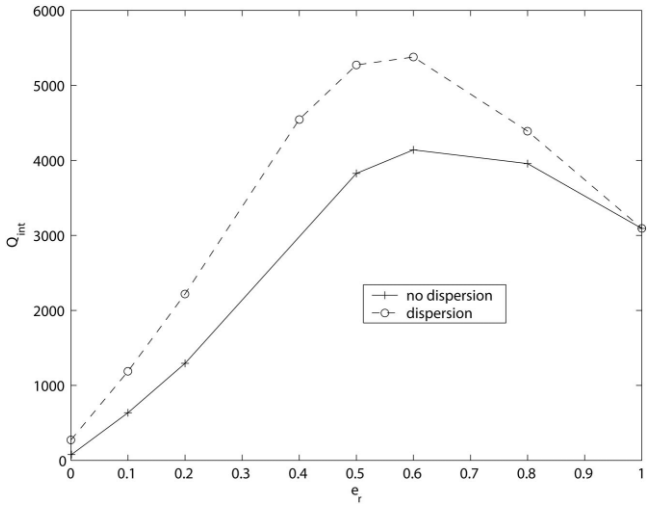

Figure 4 Radiation quality factor in the case of an infinite substrate

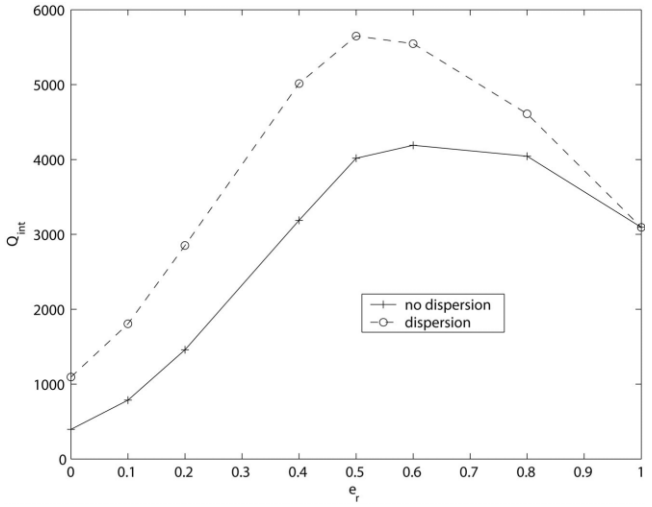

Figure 5 Radiation quality factor in the case of a $\lambda/2 \times \lambda/2$ substrate

As can be seen from Figure 3, the internal stored energy increases notably due to dispersion of the substrate permittivity.

From the radiated power and the stored energy data, the radiation quality factors for different sizes of dispersive low-epsilon substrates can be plotted (Figs. 4–6). The radiation quality factors first increase as ε decreases, but start to decrease sharply as ε gets closer to zero. For the case where dispersion is included in the analysis, the values are expectedly higher as compared to the dispersion-free situation. However, the size of the substrate (which determines the radiated power) plays a major role. For an infinite substrate (see Fig. 4) and for a substrate measuring $\lambda/2 \times \lambda/2$ (see Fig. 5), even for the dispersive case, lower quality factors are possible than in the air-filling case. However, if the substrate is quarter wave in length (see Fig. 6), just filling the volume under the radiating dipole, the quality factor is higher as compared to the air-filling case.

5. CONCLUSIONS

In the earlier work it was shown, that in addition to permeable substrates under a horizontal current element, low-epsilon materials lead to higher radiation resistance and widening the antenna bandwidth [4]. However, the size of the substrate was considered

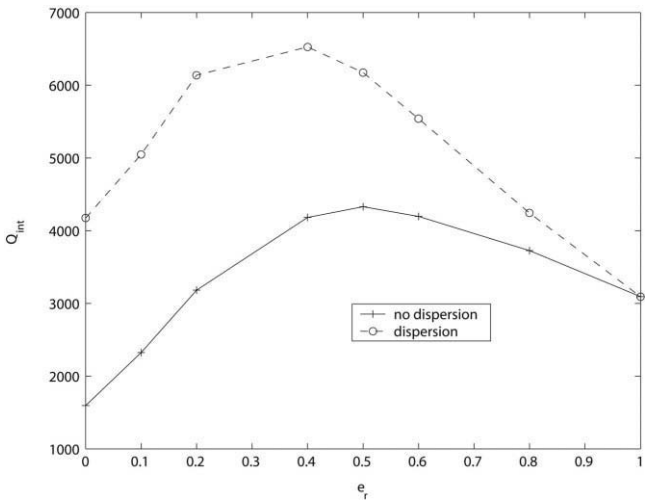

Figure 6 Radiation quality factor in the case of a $\lambda/4 \times \lambda/4$ substrate

infinite and the frequency dispersion of the material was neglected. In this article, we have taken the dispersion effects into account and have shown that the size of the substrate plays a major role in radiation enhancement. The radiated power of a dipole has been found to decrease drastically as the low-epsilon substrate size decreases. Also, the stored energy of the element increases notably with material dispersion. As a result, low-epsilon substrates measuring $\lambda/4 \times \lambda/4$ has a higher radiation Q compared to the air-filled case. On the other hand, substrates of the size of $\lambda/2 \times \lambda/2$ have been found to give notable enhancement in the radiation performance of the antenna.

REFERENCES

1. R.C. Hansen and M. Burke, Antennas with magnetodielectrics, Microwave Opt Technol Lett 26 (2000), 75–78.
2. P.M.T. Ikonen, S.I. Maslovski, C.R. Simovski, and S.A. Tretyakov, On artificial magnetodielectric loading for improving the impedance bandwidth properties of microstrip antennas, IEEE Trans Antennas Propagat 54 (2006), 1654–1662.
3. P.M.T. Ikonen, K.N. Rozanov, A.V. Osipov, P. Alitalo, and S.A. Tretyakov, Magnetodielectric substrates in antenna miniaturization: Potential and limitations, IEEE Trans Antennas Propagat 54 (2006), 3391–3399.
4. M. Hirvonen and J.C.-E. Sten, Power and Q of a horizontal dipole over a metamaterial coated conducting surface, IEEE Trans Antennas Propagat 56 (2008).
5. A. Al[bgrave]u[egrave], F. Bilotti, N. Engheta, and L. Vegni, A conformal omni-directional sub-wavelength metamaterial leaky-wave antenna, IEEE Trans Antennas Propagat 55 (2007), 1698–1708.
6. A. Al[bgrave]u[egrave], N. Engheta, A. Erentok, and R.W. Ziolkowski, Single-negative, double-negative, and low-index metamaterials and their electromagnetic applications, IEEE Antennas Propagat Mag 49 (2007).
7. B.-I. Wu, W. Wang, J. Pacheco, X. Chen, T. Grzegorczyk, and J.A. Kong, A study of using metamaterils as antenna substrate to enhance gain, Prog Electromagn Res PIER 51 (2005), 295–328.
8. S.A. Tretyakov, Analytical modeling in applied electromagnetics, Artech House, Norwood, MA, 2003.
9. L. D. Landau and E.M. Lifshits, Electrodynamics of continuous media, 2nd ed., Pergamon Press, Oxford, England, 1984.
10. S.A. Tretyakov and S.I. Maslovski, Veselago materials: What is possible and impossible about the dispersion of the constitutive parameters, IEEE Antennas Propagat Mag 49 (2007), 37–43.

© 2008 Wiley Periodicals, Inc.

SMALL HANDSET ANTENNA FOR FM RECEPTION

D. Aguilar,[1] J. Anguera,[1,2] C. Puente,[2] and M. Ribó[1]
[1] Communications and Signal Theory Department, Universitat Ramon Llull, Barcelona, Spain
[2] Technology and Intellectual Property Rights Department, Fractus, Barcelona, Spain; Corresponding author: jaume.anguera@fractus.com

Received 19 February 2008

ABSTRACT: *A passive internal handset antenna for FM reception is presented using electromagnetic simulations as well as laboratory experiments. Received signal for the antennas have been demodulated and the quality of the audio signal evaluated. Results have been compared with a long antenna (λ/4) confirming that the proposed solution is a good candidate to migrate to a full wireless FM system that may be integrated into a handset phone.* © 2008 Wiley Periodicals, Inc. Microwave Opt Technol Lett 50: 2677–2683, 2008;

Published online in Wiley InterScience (www.interscience.wiley.com). DOI 10.1002/mop.23774

Key words: *handset antennas; FM antennas; small antennas*

1. INTRODUCTION

Up to the moment and during several years the design of antennas for handset and wireless devices in CDMA, GSM, UMTS, Bluetooth, among other bands, has evolved and numerous publications on this topic appeared [1–14]. None the less to our knowledge, there is no scientific literature to design passive embedded antennas for handset/wireless device at FM band (100 MHz). At the beginning of this research, a benchmarking has been done to confirm that nowadays there are no commercial mobile phones that include a wireless FM system having an internal FM antenna. Therefore it is a challenge to design such an antenna.

In this article, we present a miniature FM internal antenna for mobile terminals that obtains reasonable levels of bandwidth and radiating efficiency. To prove its behavior, three prototypes have been simulated using a commercial code and then implemented. Each prototype is representative of a particular handset platform.

In Section 2 the precedents of the antenna design is presented. Some of the problems about miniaturizing an antenna are indicated and it is shown how efficiency and bandwidth are critically affected when trying to fit a FM antenna into a phone case. A common solution to overcome the bandwidth (BW) difficulties is also commented and its drawbacks are explained. In Section 3 the antenna design is presented. The benefits of using this technique are clearly remarked because it improves both efficiency and BW without increasing the antenna dimensions ($l_{max} \approx \lambda/30$). In Section 4 the measurements of received power and gain of three prototypes are shown. The results are also compared with the ones obtained using a larger antenna ($\lambda/4$ monopole over a ground plane). Section 5 summarizes and concludes the work.

2. BACKGROUND

When the operating frequency of a mobile wireless device is at a lower part of the spectrum such as FM, $\lambda/4$ antennas as PIFA or monopole become not practical. Nevertheless when the operating frequencies of the devices are above 800–900 MHz these designs are valid since λ is shorter than 350 mm, so antennas with lengths of 87 mm ($\lambda/4$) can be packed into a small space [1]. However commercial FM spectrum is placed between 88 and 108 MHz (λ of 3061 mm at 98 MHz). At these frequencies, a design of a $\lambda/4$ monopole antenna would require a wire of 765 mm! In this case, a typical $\lambda/4$ monopole would not be a practical solution because

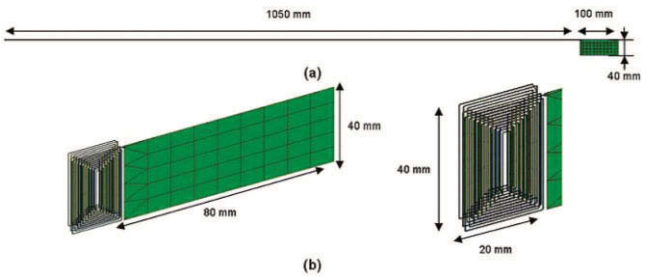

Figure 1 (a) Straight/reference monopole (wire length = 1050 mm, wire width = 0.5 mm), (b left) packed monopole (wire length = 2262 mm, wire width = 0.25 mm) and (b right) zoom of the antenna: $40 \times 20 \times 5$ (h) mm^3. [Color figure can be viewed in the online issue, which is available at www.interscience.wiley.com]

PUBLICATION 3

Bandwidth limitations of dipoles matched with non-Foster impedances

In: Proceedings of European Conference on Antennas Propagat., EUCAP 2007, Nov. 2007. 5 p.
Reprinted with permission from the publisher.

BANDWIDTH LIMITATIONS OF DIPOLES MATCHED WITH NON-FOSTER IMPEDANCES

Mervi Hirvonen, Arto Hujanen, Jan Holmberg and Johan C.-E. Sten

VTT Technical Research Centre of Finland
P.O. Box 1000, 02044 VTT, Finland
mervi.hirvonen@vtt.fi

Keywords: Bandwidth, dipole, non-Foster impedances.

Abstract

In this paper, the bandwidth limitations of dipoles matched with negative impedance components are discussed. In theory, infinite impedance bands are possible with non-Foster impedances, but in practice the fields stored inside the smallest sphere enclosing the antenna limit the band. Both theoretical and practical achievable bandwidths as well as non-Foster component tolerance issues are reported in this paper.

1 Introduction

Theoretical bandwidths of small antenna elements are traditionally limited by the size of the smallest sphere enclosing the current carrying region [1, 2]. In these formulations given for the radiation quality factor *Q* (which is taken to be inversely proportional to the fractional bandwidth), however, the limit takes only into account the non-radiating energy stored outside the smallest sphere. In principal, multi-stage matching can be used to achieve bandwidth enhancement. In the earlier work [3] the impedance matching properties of ideal dipoles achieved with infinite amount of passive matching components has been analysed. Promising results were shown, but still the actual size of the antenna limited the achievable bandwidth.

On the other hand, in theory, infinite bandwidths are achievable by cancelling out the antenna capacitance and inductance with corresponding negative reactances. Nevertheless, in practice limitations exist. In reality, also the energy stored inside the smallest sphere enclosing the antenna affects the radiation *Q* and decreases the bandwidth dramatically. In this paper, the bandwidth limitations of dipoles matched with one and two non-Foster impedance components are analysed both in the sense of theoretical limits based on energy outside the smallest sphere and in a practical case including the inner energy. The realization of the negative impedances has been left out scope of this paper, although implementations exist [4, 5].

2 Theory

In the model described by Chu [1], the antenna impedance linked to the fields outside the smallest enclosing sphere is represented by a ladder *RLC*-network. For the ideal electric dipole, TM_1, the equivalent circuit is presented in Fig. 1. The component values are $C = a\varepsilon_0$, $L = a\mu_0$, $R = \sqrt{\mu_0 / \varepsilon_0}$, where a is a radius of the smallest sphere enclosing the antenna. The wave impedance seen by the fields propagating outwards from the surface of the enclosing sphere is thus

$$Z_{Chu} = \sqrt{\frac{\mu_0}{\varepsilon_0}}\left(\frac{1}{jka} + \frac{jka}{jka+1}\right). \quad (1)$$

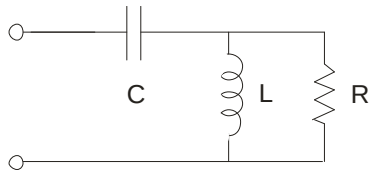

Fig. 1. Chu circuit model.

However, in practice strong fields are stored inside the enclosing sphere and thus, more circuit components are needed to model for the antenna impedance. According to Hansen [6] the measured input impedance of a short wire dipole can be described approximately as

$$Z_{Hansen} = 20(ka)^2 - j120\frac{\ln(a/t)-1}{\tan ka}, \quad (2)$$

where *2a* is the length and *t* thickness of the dipole. In Fig. 2 and 3 the real and imaginary parts of impedances calculated with above models are illustrated. The impedance described by Hansen predicts lower resistance value than Chu model. The imaginary part in Hansen model is greatly affected by the thickness of the wire. At thickness ratio $a/t = 50$, however, the imaginary part becomes similar to the one predicted by Chu model. By adding a network of two capacitances and an inductor to Chu circuit (see Fig. 4.), the impedance behaviour predicted by Hansen model may be achieved. Two capacitances act as voltage divider, which illustrates the ratio

of the power transformed from the total power circulating in the antenna region to TM_1 mode. The inductor, together with shunt capacitance, represents a transmission line due to physical nature of the wire dipole. The input impedance of this extended Chu model is described as

$$Z_{Chu,extended} = \sqrt{\frac{\mu_0}{\varepsilon_0}}\left(jka\frac{L_1}{L} + \frac{1}{jka\dfrac{C_2}{C}} + \frac{\dfrac{1}{jka} + \dfrac{jka}{jka+1}}{1+\dfrac{C_1}{C}\left(1-\dfrac{(ka)^2}{jka+1}\right)} \right) \tag{3}$$

With ratios C_1/C = 3.95, C_2/C = 1.48 and L_1/L = 0.32 the impedance match very well with Hansen model for thickness ratio $a/t = 50$ as illustrated in Fig. 2 and 3. Simulations of similar dipoles conducted with IE3D electromagnetic simulator based on MoM agree remarkably well with the results gained from the extended Chu and Hansen models for $ka << 1$.

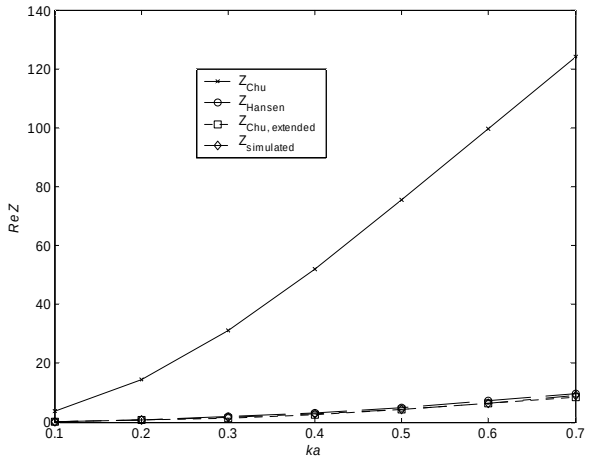

Fig. 2. Real part of impedance predicted with different models.

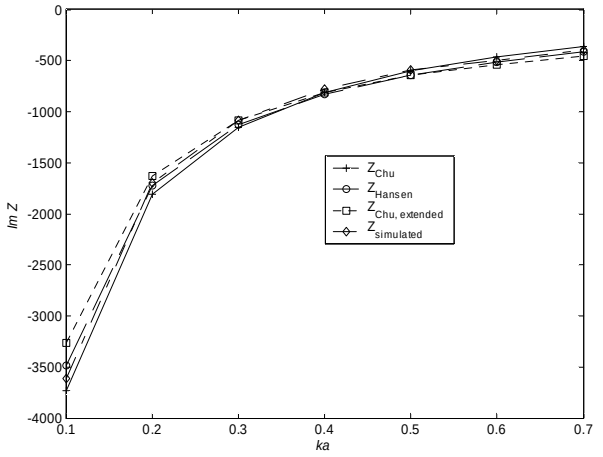

Fig. 3. Imaginary part of impedance predicted with different models.

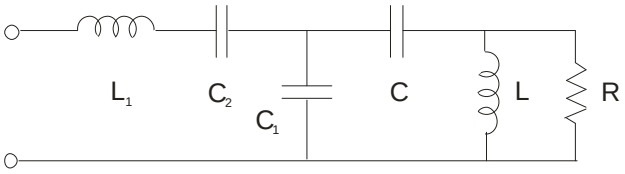

Fig. 4. Extended Chu circuit model describing approximately a short wire dipole.

3 Matching with a single non-Foster component

3.1 Ideal case

In the Chu model, the impedance of a small electric dipole is inherently capacitive. Cancelling out this capacitance by a single series negative capacitance leads to remarkable bandwidth enhancements. In the bandwidth calculation the antenna circuit including the negative C_x component is considered to be fed from an ideal impedance transformer, i.e.

$$\rho = \frac{Z_{in} - \mathrm{Re}\{Z_{in}\}}{Z_{in} + \mathrm{Re}\{Z_{in}\}}, \tag{4}$$

where Z_{in} in this case is Z_{chu} (see equation 1) in series with tuning capacitance C_x. From equation (4) the optimal value for C_x/C may be solved as

$$\frac{C_x}{C} = \frac{1}{\dfrac{(ka)^2}{(ka)^2+1} + \dfrac{2(ka)^3}{(ka)^2+1}\dfrac{|\rho|}{\sqrt{1-|\rho|^2}} - 1}. \tag{5}$$

On the other hand solving equation (4) as a function k leads to bandwidth information. Equation (4) may be presented as a third order polynomial for k as

$$k^3 - k^2\frac{a^2 C}{y C_x} - \frac{\dfrac{C}{C_x}+1}{y} = 0, \tag{6}$$

where

$$y = \frac{2|\rho|a^3}{\sqrt{1-|\rho|^2}}. \tag{7}$$

Third order polynomial (6) has three real solutions at C_x/C(k = 1). The roots represent three points where the matching curve passes the matching limit $|\rho|$. One of the solutions is a trivial solution, $k = 1$, representing the lower limit of the band. Second solution represents the upper band limit and the third solution the third passing point, which, however, is irrelevant in the bandwidth calculation.

The maximum relative bandwidth achieved with an ideal negative C_x matching component is presented in Fig. 5 as a function of antenna size ka. Above certain size of the antenna ka, the second root gives imaginary values indicating infinite impedance bandwidth. The numerical circuit simulator calculations conducted with Microwave Office agree very well with the analytical results. The corresponding relative bandwidth values achieved with infinite amount of passive components [3] is presented in Fig. 6. In theory, larger bandwidths are possible with smaller size antennas with one negative C_x component that with infinite amount of passive components.

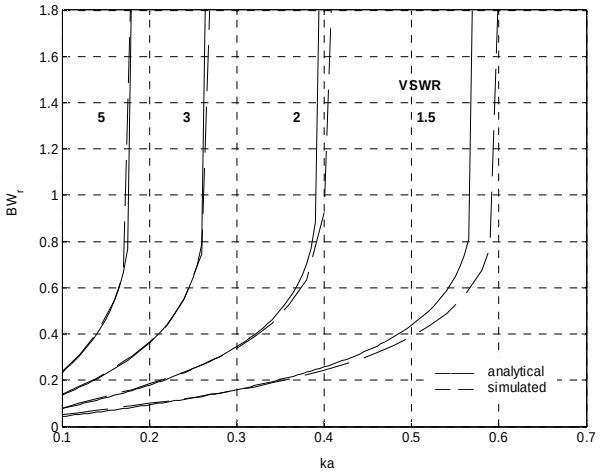

Fig. 5. Maximum bandwidth achieved with negative C_x component.

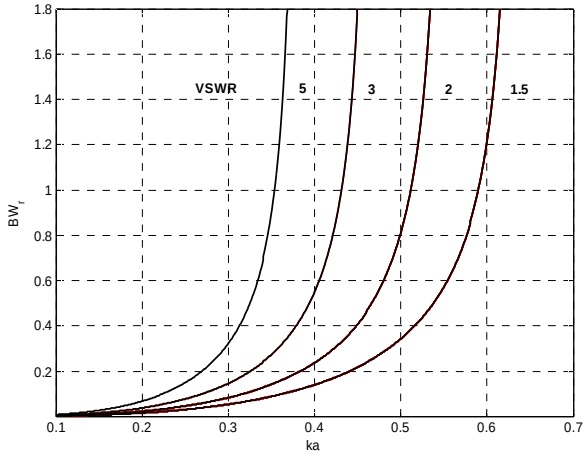

Fig. 6. Maximum bandwidth achieved with infinite amount of passive components.

3.2 Practical case

In a case of a real antenna, the achievable bandwidths with negative C_x element tuning are considerably smaller due to the fields stored inside the smallest sphere. The analytical solution for C_x/C from equation (4), where in this case Z_{in} is $Z_{Chu,extended}$ (see equation 3) in series with negative capacitance C_x, leads to complicated formula and k is a function of sixth order. The function is, however, analytically solvable with symbolic computation solvers like Mathematica. k has two real solutions at $C_x/C(k = 1)$. First real solution is a trivial solution, $k = 1$, representing the lower limit of the band and the second real solution the upper band limit. The functions are, however, extremely sensitive to C_1/C, C_2/C, L_1/L and ρ parameter values.

In Fig. 7 the maximum achievable bandwidths with an ideal negative C_x component in a case including the inner field model are illustrated as a function of size of the antenna ka. Also the maximum bandwidths of corresponding simulated electric dipoles tuned with negative C_x component are presented. The analytical and simulated bandwidths correspond very well. As can be seen from Fig. 7 in reality only limited bands are possible with negative capacitance matching. For comparison, the maximum bandwidths of dipoles tuned with infinite amount of passive components are presented in Fig. 8. Infinite amount of passive components was modelled here as a cascade of 14 LC resonators generated by Genesys circuit simulator as in [3]. Tuning with negative capacitance shows considerably larger bands than tuning with passive components.

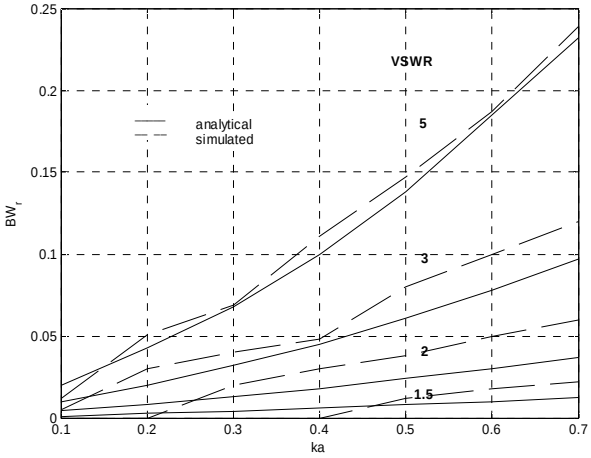

Fig. 7. Maximum bandwidth achieved with negative C_x component

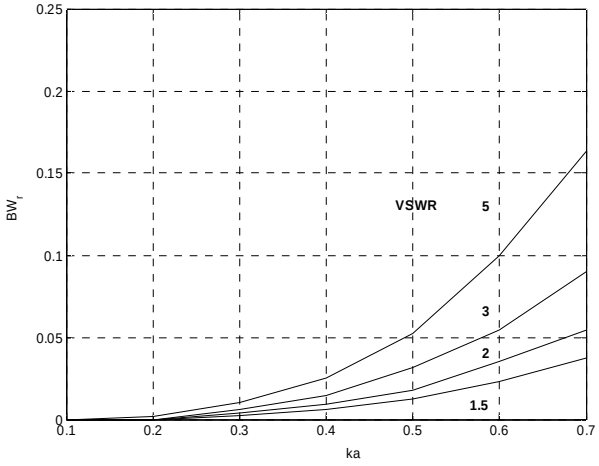

Fig. 8. Maximum bandwidth achieved with infinite amount of passive components.

The variation tolerance of the negative C_x component is illustrated in Fig. 9. The tolerance is defined in a margin, where frequency shifts maximum of 1.0 per cents from the base frequency f_0. The tolerance is really low and increases as a function of antenna size ka.

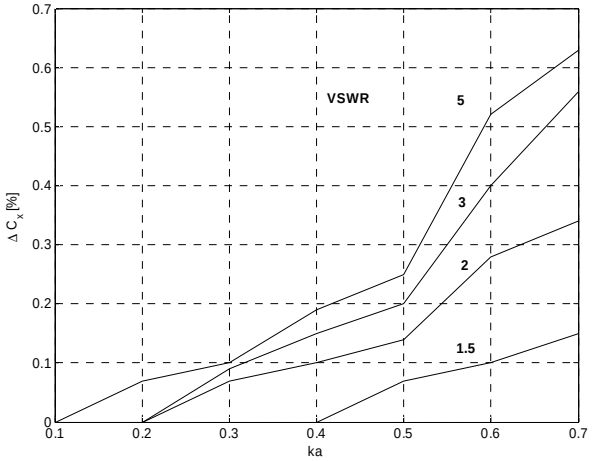

Fig. 9. Variation tolerance of negative C_x component.

4 Matching with two non-Foster components

4.1 Ideal case

In the Chu model, cancelling out the dominating capacitance led to remarkable bandwidth enhancements. However, by adding a parallel negative inductor to the model, the input impedance of the circuit may be written as

$$Z_{in} = \frac{j\omega L_x\left(\frac{1}{j\omega C}+\frac{1}{j\omega C_x}+\frac{j\omega LR}{j\omega L+R}\right)}{j\omega L_x+\left(\frac{1}{j\omega C}+\frac{1}{j\omega C_x}+\frac{j\omega LR}{j\omega L+R}\right)}. \quad (8)$$

If $-L_x$ is equal to L and simultaneously $-C_x$ is equal to C, equation (8) becomes

$$Z_{in} = R, \quad (9)$$

indicating frequency independent, infinite band.

4.2 Practical case

In practice, as already mentioned, the inner field limits the bandwidth behaviour. In this case, the function for impedance ($Z_{Chu,extended}$ in series with negative C_x and L_x components) has two variables and analytical formulation gets difficult. However, according to the numerical optimization done with simulated dipoles, relative bandwidths more than 2 are possible with two negative series tuning components. Unfortunately, the tuning is very sensitive to matching component values. In Fig. 10 and 11 the component tolerances at 1 per cent margin are presented.

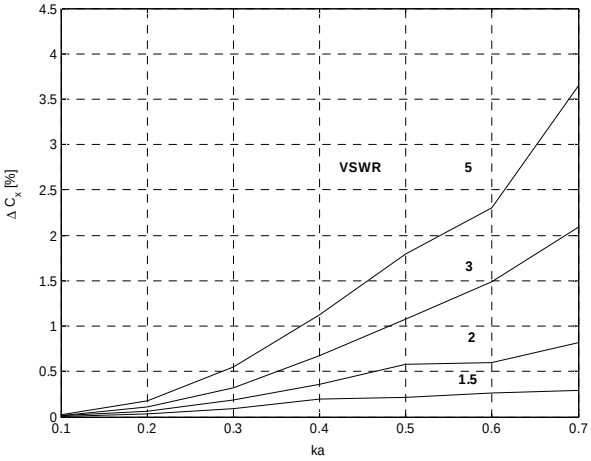

Fig. 10. Variation tolerance of negative C_x component.

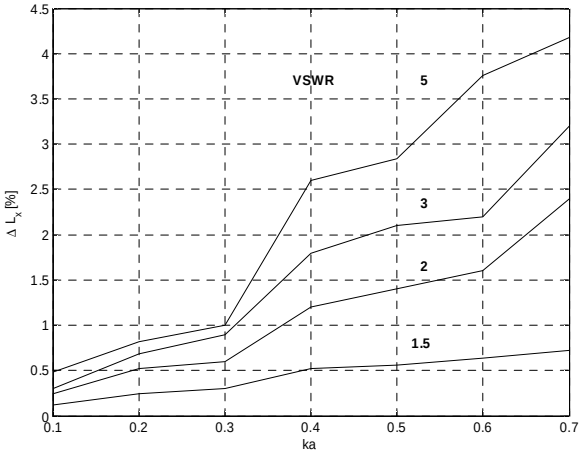

Fig. 11. Variation tolerance of negative L_x component.

5 Conclusions

In this paper, the active element tuning for small antennas is analysed. In theory, infinite bandwidths are achievable with very small antennas using only one negative tuning element. However, in practice strong near fields limit the antenna Q and only limited bands are achievable with one active element. On the other hand, by using two negative tuning elements bandwidths larger than 200 % are achievable even with very small antennas. Still, the variation tolerances are very small and limit the component implementation possibilities in practice.

References

[1] L.J. Chu, "Physical Limitations of Omni-Directional Antennas," *Journal of Applied Physics*, Vol. 19, December 1948.

[2] J. S. McLean, "A Re-Examination of the Fundamental Limits on the Radiation Q of Electrically Small

Antennas," *IEEE Transactions on Antennas and Propagation*, Vol. 44, No.5, May 1996.

[3] A. Hujanen, J. Holmberg and J. C.-E, Sten, "Bandwidth Limitations of Impedance Matched Ideal Dipoles," *IEEE Transactions on Antennas and Propagation*, Vol. 53, No. 10, October 2005.

[4] S. E. Sussman-Fort, "Matching Network Design Using Non-Foster Impedances," *International Journal of RF and Microwave Computer-Aided Engineering*, February 8, 2005.

[5] S. E. Sussman-Fort, "Non-Foster Impedance Matching for Transmit Applications," *IEEE International Workshop on Antenna Technology, Small Antennas and Novel Metamaterials*, March 2006.

[6] R.C. Hansen, "Fundamental Limitations in Antennas," *Proceedings of the IEEE*, Vol. 69, No. 2, February 1981.

PUBLICATION 4

Impedance and quality factor of mutually coupled multiport antennas

In: Microwave and Optical Technology Letters 2008.
Vol. 50, No. 8, pp. 2034–2039.
© 2008 IEEE.
Reprinted with permission from the publisher.

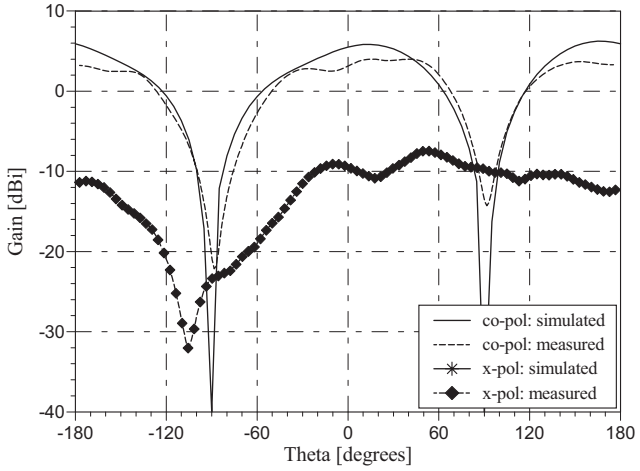

Figure 8 Simulated and measured E-plane radiation patterns at 5.2 GHz for the dual-band CPW-fed slot antenna [$\varphi = 180°$, with reference to Fig. 1(a)]

and 8. The maximum simulated gain of the antenna was found to be ~6 dBi in both the lower and upper frequency bands, and the measured gain was slightly lower. The irregularities in the E-plane measured results around $\theta = 90°$ for both the co- and cross-polarization patterns are because of the feed cable, which was connected in the measurement plane.

4. CONCLUSIONS

In this article, a simple impedance matching design approach to obtain dual-band performance from a single CPW-fed slot was described. Although the upper and lower bandwidths were only 8 and 6%, respectively, the antenna is ideal for dual-band WLAN applications in the 2.4 and 5.2 GHz bands. The same design approach can also be followed to design dual-band antennas with different f_2/f_1 ratios. The two elements (slot and terminated stub) forming the antenna can be designed separately and then combined—final tuning of the stub parameters can then be done to satisfy the design requirements. The radiation patterns at both the upper and lower band were well-formed, had similar gain in both frequency bands, and good cross-polarization characteristics.

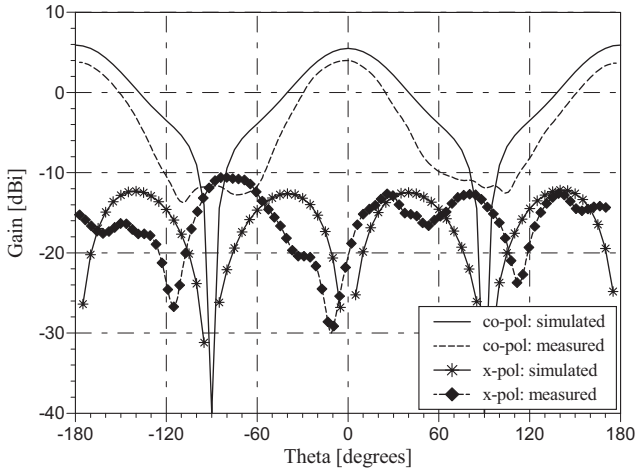

Figure 9 Simulated and measured H-plane radiation patterns at 5.2 GHz for the dual-band CPW-fed slot antenna [$\varphi = 90°$, with reference to Fig. 1(a)]

REFERENCES

1. M.-H. Ho and G.-L. Chen, Reconfigured slot-ring antenna for 2.4/5.2 GHz dual-band operations, IET Microwave Antennas Propag 1 (2007), 712–717.
2. A.A. Omar, M.C. Scardelletti, Z.M. Hejazi, and N. Dib, Design and measurement of self-matched dual-frequency coplanar waveguide-fed-slot antennas, IEEE Trans Antennas Propag AP-55 (2007), 223–226.
3. D. Llorens, P. Otero, and C. Camacho-Penalosa, Dual-band, single CPW port, planar-slot antenna, IEEE Trans Antennas Propag AP-51 (2003), 137–139.
4. Y.-C. Lin and K.-J. Hung, Design of dual-band slot antenna with double T-match stubs, Electron Lett 42 (2006), 438–439.
5. Y.-C. Chen, S.-Y. Chen, and P. Hsu, Dual-band slot dipole antenna fed by a coplanar waveguide, IEEE AP-S Dig, Albuquerque, NM (2006), 3589–3592.
6. M.C. Mukandatimana, T.A. Denidni, and L. Talbi, Design of a new dual-band CPW-fed slot antenna for ISM applications, IEEE AP-S Dig, Monterey, CA (2004), 6–9.
7. Zeland Software, IE3D User's Manual, Release 12.1 (2007).

© 2008 Wiley Periodicals, Inc.

IMPEDANCE AND QUALITY FACTOR OF MUTUALLY COUPLED MULTIPORT ANTENNAS

Johan C.-E. Sten and Mervi Hirvonen
VTT Technical Research Centre of Finland, P.O. Box 1000, 02044 VTT Finland; Corresponding author: johan.sten@vtt.fi

Received 10 December 2007

ABSTRACT: *In this study, expressions for the radiation quality factor Q and the input impedance seen at any terminal of a multiport antenna are derived. It is shown computationally that because of the possibility to adjust the antenna current distribution through suitable feeding/loading a multiport antenna can perform lower Qs than a similar single-port antenna.* © 2008 Wiley Periodicals, Inc. Microwave Opt Technol Lett 50: 2034–2039, 2008; Published online in Wiley InterScience (www.interscience.wiley.com). DOI 10.1002/mop.23564

Key words: *multiport antenna; quality factor; mutual coupling; impedance matrix; input impedance*

1. INTRODUCTION

With the exception of large arrays, antennas are traditionally conceived as single-port devices. This is because mutual coupling, which is often very strong in small and compact antennas, is regarded as an unwanted nonideality to be eliminated or compensated to achieve a desired radiation characteristic [1]. In this article, a different viewpoint is taken, namely to look for the advantages of the mutual coupling for improving the antenna performance, in particular the radiation quality factor Q, which is an important design parameter for small antennas.

Previously, the Q of antennas with multiple ports have been studied in the case of totally isolated ports, which was observed to lead to an increasing Q [2]. However, in [2], only the energy involved in the reactive part of the spherical multipole fields was taken into account, whereas the interior stored energy due to the fields inside the smallest sphere that can be drawn around the antenna was assumed to be zero. Our case is more realistic as it takes into consideration the total stored energy and the mutual coupling. In this article, we show by means of computational examples that by providing an antenna—in our case a short wire

antenna near a ground plane—with several mutually coupled input/output ports and choosing their feed point amplitudes suitably, a lower Q (and, implicitly, a potentially broader bandwidth) can actually be achieved than by feeding only one port at a time. Furthermore, we compare the tuning using a single reactive element at the feed point with tuning by means of a set of distributed reactive load impedances embedded inside the antenna. For this purpose, a formula for the input impedance viewed from one of the ports of a general N-port antenna is derived and given in the Appendix.

As a preliminary, we first establish the circuit equations governing the antenna system modeled as a lossy linear network [3]. Enumerating the input/output ports of the N-port antenna $i = 1, 2, \ldots, N$, the current intensities I_i and the voltages V_i at the ports (the dimensions of which are assumed to be sufficiently small in terms of the wavelength) are interrelated by Kirchhoff's network equations, which can be condensed as an $N \times N$ impedance matrix (see, e.g., [3, 4]) viz,

$$\begin{pmatrix} V_1 \\ V_2 \\ \vdots \\ V_N \end{pmatrix} = \begin{pmatrix} z_{11} & z_{12} & \cdots & z_{1N} \\ z_{21} & \ddots & & z_{2N} \\ \vdots & & \ddots & \\ z_{N1} & \cdots & & z_{NN} \end{pmatrix} \begin{pmatrix} I_1 \\ I_2 \\ \vdots \\ I_N \end{pmatrix} \tag{1}$$

abbreviated $\bar{V} = \overline{\overline{Z}}\bar{I}$ (or equivalently $\bar{I} = \overline{\overline{Y}}\bar{V}$ in terms of the admittance matrix $\overline{\overline{Y}} = \overline{\overline{Z}}^{-1}$).

The concomitant scattering matrix $\overline{\overline{S}}$ describing the interaction of the antenna with external sources and load impedances is defined by means of the incoming and the reflected wave vectors, $\bar{w}^+$ and $\bar{w}^-$, respectively, as

$$\bar{w}^+ = \bar{V} + \overline{\overline{Z}}_L\bar{I} \quad \text{and } \bar{w}^- = \bar{V} - \overline{\overline{Z}}_L\bar{I} \tag{2}$$

where $\overline{\overline{Z}}_L$ signifies an $N \times N$ diagonal matrix having as its diagonal entries the load-impedances $z_{L1}, z_{L2}, \ldots, z_{LN}$ connected to the respective terminal. Combining (1) and (2) yields

$$\bar{w}^- = (\overline{\overline{Z}} - \overline{\overline{Z}}_L)(\overline{\overline{Z}}_L + \overline{\overline{Z}})^{-1}\bar{w}^+ \tag{3}$$

$$\text{where } \overline{\overline{S}} = (\overline{\overline{Z}} - \overline{\overline{Z}}_L)(\overline{\overline{Z}}_L + \overline{\overline{Z}})^{-1}.$$

2. ANTENNA QUALITY FACTOR

It is a well-known fact that the bandwidth of a resonant device (such as an antenna) is closely related to the quality factor Q [5–8]. The Q is generally defined as 2π times the ratio of the energy stored by the device per cycle and the energy lost during the same time interval, i.e.,

$$Q = \omega \frac{W^{\mathrm{E,stored}} + W^{\mathrm{M,stored}}}{P^{\mathrm{loss}}} \tag{4}$$

where $W^{\mathrm{E,stored}}$ and $W^{\mathrm{M,stored}}$ are, respectively, the time average electric and magnetic energy stored, and P^{loss} is the average dissipated power, which is equal to the power radiated P^{rad} when the antenna is lossless, as will be the case in the following.

However, when applying this definition to antennas, a problem arises as follows: as the electromagnetic energy of an antenna is dispersed all around the surrounding space, it is not immediately clear how the stored energy should be defined and measured. In particular, since a part of the energy is associated with the propagating fields, it is evident that this part of the energy should be extracted from the total energy. Because energy as a global quantity can be only indirectly estimated, we must find a way to relate it to the response of the device to the excitation by a time-harmonic signal (through the complex voltages and currents at the input/output ports).

To tackle the problem, we start from the identity (which Papas [9] termed as the "energy theorem")

$$\nabla \cdot \left(\frac{\partial \mathbf{E}}{\partial \omega} \times \mathbf{H}^* - \frac{\partial \mathbf{H}}{\partial \omega} \times \mathbf{E}^* \right) = -j \left[\frac{\partial(\omega\varepsilon)}{\partial \omega} \mathbf{E} \cdot \mathbf{E}^* + \frac{\partial(\omega\mu)}{\partial \omega} \mathbf{H} \cdot \mathbf{H}^* \right] - \frac{\partial \mathbf{E}}{\partial \omega} \cdot \mathbf{J}^* - \mathbf{E}^* \cdot \frac{\partial \mathbf{J}}{\partial \omega} \tag{5}$$

derivable from the time harmonic Maxwell equations by ω-differentiation [7, 9]. In deriving (5), a time dependence of $e^{j\omega t}$ has been assumed, since this will lead to a circuit description where positive reactances are interpreted as inductive and negative reactances as capacitive (the standard engineering convention). In the sequel, the last two terms involving conduction currents ($\mathbf{J}$) will be ignored as our primary interest at this point is the ideal case without (significant) losses. For a treatment of the more general case involving losses and material dispersion, we refer to [7, 10].

Let us next apply the theorem to a volume ν bounded from the inside by the antenna occupying the volume ν_0 and from the outside by a sphere $\nu_{r\to\infty}$, whose radius goes to infinity. Application of Gauss' divergence theorem gives

$$\int_{\partial\nu} \left(\frac{\partial \mathbf{E}}{\partial \omega} \times \mathbf{H}^* - \frac{\partial \mathbf{H}}{\partial \omega} \times \mathbf{E}^* \right) \cdot dS = -4j \left[\int_{\nu} \frac{1}{4} \frac{\partial(\omega\varepsilon)}{\partial \omega} \left| \mathbf{E} \right|^2 d\nu + \int_{\nu} \frac{1}{4} \frac{\partial(\omega\mu)}{\partial \omega} \left| \mathbf{H} \right|^2 d\nu \right], \tag{6}$$

where dS is a differential surface element and $\partial\nu$ is the bounding surface of the considered volume ν. The two volume integrals can be interpreted as generalizations (for dispersive materials) of the familiar energy integrals

$$W^{\mathrm{E}} = \int_{\nu} \frac{\varepsilon}{4} |\mathbf{E}(\mathbf{r})|^2 d\nu, \tag{7}$$

$$W^{\mathrm{M}} = \int_{\nu} \frac{\mu}{4} |\mathbf{H}(\mathbf{r})|^2 d\nu, \tag{8}$$

into which they reduce in the case that the medium is not dispersive ($\partial\varepsilon/\partial\omega = 0$ and $\partial\mu/\partial\omega = 0$). On the surface of the antenna $\partial\nu_0$, which we assume to be a perfectly conducting boundary, the integral vanishes everywhere except for the terminals, where it yields

$$\int_{\partial\nu_0} \left(\frac{\partial \mathbf{E}}{\partial \omega} \times \mathbf{H}^* - \frac{\partial H}{\partial \omega} \times \mathbf{E}^* \right) \cdot dS = -\sum_{i=1}^{N} \left(\frac{\partial V_i}{\partial \omega} I_i^* + \frac{\partial I_i}{\partial \omega} V_i^* \right) = - \frac{\partial \bar{V}^T}{\partial \omega} \bar{I}^* - \frac{\partial \bar{I}^T}{\partial \omega} \bar{V}^* \tag{9}$$

whereas on the radiation surface $\partial\nu_{r\to\infty}$, the integrand can be developed by using the long distance asymptotic expressions for the field vectors, viz,

$$\mathbf{E}(\mathbf{r}) \underset{r\to\infty}{\to} \mathbf{E}_\infty(\mathbf{u}_r)\frac{\exp(-jkr)}{r} \tag{10}$$

for the electric field, where $k = \omega\sqrt{\mu_0\varepsilon_0}$ and

$$\mathbf{E}_\infty(\mathbf{u}_r) = \lim_{r\to\infty}\frac{rE(r)}{\exp(-jkr)} \tag{11}$$

An exactly similar asymptotic relation applies to the magnetic field $\mathbf{H}(\mathbf{r})$. Thus, at $\partial\nu_{r\to\infty}$

$$\int_{\partial V_{r\to\infty}} \left(\frac{\partial\mathbf{E}}{\partial\omega}\times\mathbf{H}^* - \frac{\partial\mathbf{H}}{\partial\omega}\times\mathbf{E}^*\right)\cdot dS = \int_{\partial V_{r\to\infty}} \left(\frac{\partial\mathbf{E}_\infty}{\partial\omega}\times\mathbf{H}_\infty^* - \frac{\partial\mathbf{H}_\infty}{\partial\omega}\times E_\infty^* - 2jr\sqrt{\mu_0\varepsilon_0}\Re\{\mathbf{E}_\infty\times\mathbf{H}_\infty^*\}\right)\cdot\frac{dS}{r^2} \tag{12}$$

Identifying the radiated power with the expression

$$P^{\mathrm{rad}} = \int_{\partial V_{r\to\infty}} \frac{1}{2}\Re\{\mathbf{E}\times\mathbf{H}^*\}\cdot dS \tag{13}$$

and using $\mathrm{u}_r\times\mathbf{E}\infty(\mathbf{u}_r) = \sqrt{\mu_0/\varepsilon_\infty}\mathbf{H}_\infty(\mathrm{u}_r)$ and $\mathbf{u}_r\cdot\mathbf{E}\infty(\mathbf{u}_r) = 0$ the "energy theorem" (5) yields

$$\frac{\partial\bar{V}^T}{\partial\omega}\bar{I}^* + \frac{\partial\bar{I}^T}{\partial\omega}\bar{V}^* = 2\sqrt{\frac{\varepsilon_0}{\mu_0}}\int_{4\pi}\frac{\partial\mathbf{E}_\infty}{\partial\omega}\cdot\mathbf{E}_\infty^* d\Omega + 4j(W^{\mathrm{E}} + W^{\mathrm{M}} - r\sqrt{\mu_0\varepsilon_0}P^{\mathrm{rad}}) \tag{14}$$

denoting $d\Omega = \sin\theta d\theta d\varphi$. . The last term in the expression can be seen to involve three quantities having the quality of energy; W^{E}, W^{M}, and $r\sqrt{\mu_0\varepsilon_0}P^{\mathrm{rad}}$, each of which grow separately without a bound as $r\to\infty$. However, it can be shown that the quantities are interrelated and that the whole expression remains finite.

Let a be the radius of the smallest sphere that circumscribes the antenna. The total electromagnetic energy of the propagating field confined between the two concentric spheres of radii a and r must obviously be

$$W^{\mathrm{E,rad}} + W^{\mathrm{M,rad}} = \frac{(r-a)}{c_0}P^{\mathrm{rad}} \tag{15}$$

where $c_0 = \sqrt{\mu_0\varepsilon_0}$ is the speed of light. Within the sphere of radius a (the "antenna region") the energy is to be taken as completely stored, because the field in this region has strictly not been launched off the antenna, and thus it can in principle be decomposed in spherical waves propagating inward and outward. There is also some stored energy outside the sphere, which stems from the reactive part of the spherical multipole fields. Thus, in general, the total electromagnetic energy consists of a stored part and a radiated part, viz.,

$$W^{\mathrm{E}} + W^{\mathrm{M}} = W^{\mathrm{E,stored}} + W^{\mathrm{M,stored}} + \frac{(r-a)}{c_0}P^{\mathrm{rad}} \tag{16}$$

Invoking this relationship in (14) yields an expression for the requested quantity $W^{\mathrm{E,stored}} + W^{\mathrm{M,stored}}$, which inserted in (4) gives the result

$$Q = \frac{\omega}{4P^{\mathrm{rad}}}\Im\left\{\frac{\partial\bar{V}^T}{\partial\omega}\bar{I}^* + \frac{\partial\bar{I}^T}{\partial\omega}\bar{V}^*\right\} - \frac{\omega}{2P^{\mathrm{rad}}}\sqrt{\frac{\varepsilon_0}{\mu_0}}\Im\left\{\int_{4\pi}\frac{\partial\mathbf{E}_\infty}{\partial\omega}\cdot\mathbf{E}_\infty^* d\Omega\right\} + ka \tag{17}$$

In practice, either the voltages or the currents at the terminals are kept constant and independent of ω (meaning that either $\partial V_i/\partial\omega$ or $\partial I_i/\partial\omega$ vanish for every i and for all considered frequencies). Whichever condition one chooses, the same condition must also apply when the relevant field integral is computed from the fields. For instance, if $\partial I_i/\partial\omega = 0$ for all frequencies,

$$Q = \frac{\omega}{4P^{\mathrm{rad}}}\Im\left\{\sum_{i=1}^{N}\frac{\partial V_i}{\partial\omega}I_i^*\right\} - \frac{\omega}{2P^{\mathrm{rad}}}\sqrt{\frac{\varepsilon_0}{\mu_0}}\Im\left\{\int_{4\pi}\frac{\partial E_\infty}{\partial\omega}\cdot\mathbf{E}_\infty^* d\Omega\right\}_{\partial I_i/\partial\omega=0} + ka \tag{18}$$

$$P^{\mathrm{rad}} = \frac{1}{2}\Im\{\sum_{i=1}^{N}V_i I_i^*\} \tag{19}$$

In the case of a single feed point, (18) and (19) reduce to the classical formula in terms of the radiation resistance R^{rad} and reactance X [5, 6]

$$Q \approx \frac{\omega}{2R^{rad}}\frac{\partial X}{\partial\omega} \tag{20}$$

when the frequency dispersion of the far-field radiation [the integral quantity in (18)] is not evaluated due to its negligible (or zero) influence on the Q of small antennas [5]. The term ka has been dropped as well, as it is in most circumstances practically insignificant.

3. APPLICATIONS

As an application, we next present a number of simple computational examples to illustrate the use of multiple ports in connection with antennas that are small in terms of wavelength.

3.1. Optimizing Q Using Distributed Sources

First, let us consider the case of multiple feeds at different locations. For a given geometrical distribution of feed points, our aim is to find the combination of excitation current amplitudes that gives the best (lowest) antenna Q. As is well-known, the location of the feed point affects the current distribution on the antenna and the resulting radiation field pattern. In fact, even for negligible changes in the radiation pattern, the reactive near field and power may change significantly [11]. Thus, one can also expect to find clear differences between the cases in terms of antenna Q.

The antenna considered is a lossless horizontal wire tangential to a perfectly conducting ground plane. The ports are oriented horizontally and distributed evenly along the wire (see Fig. 1). The antenna Q-factor may now be calculated numerically using (18)

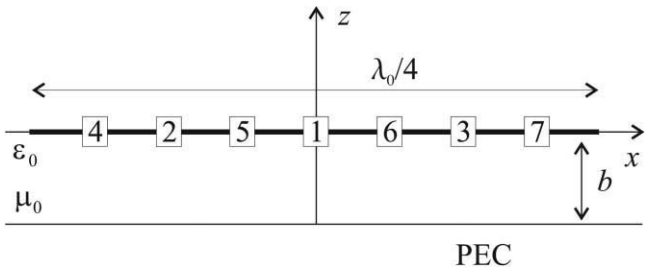

Figure 1 Horizontal dipole with multiple feed ports

and the simulated Z-matrix data by computing the port voltages V_i from the impressed excitation currents I_i. In the calculations, the second term (the far-field dispersion integral) in (18) has been neglected, since (as already mentioned) the field variations as a function ω are negligible in the case of radiation of low frequencies. In the field simulations (using HFSS by Ansoft Corp.), at the lowest considered frequency f_0 the wire has the length of $\lambda_0/4$ and the width of $0.0035\lambda_0$. The distance to the ground plane is $k_0 b = 0.1$.

In Figure 2, the Q-factors of the 1-port and 3-port cases are illustrated. In the 1-port case, the feed current $I_0 = 1$. In the 3-port case, the feed currents leading to minimum and maximum Q are sought numerically with a Matlab routine by letting the currents I_2 and I_3, which are assumed equal, to vary between 0 to 1, while keeping $I_0 = 1$. As can be seen from Figure 2, with a certain 3-port excitation of the wire, a remarkably lower Q when compared with the 1-port case can be achieved especially at lower frequencies (where the antenna is notably below resonance length). Near resonance $f/f_0 \approx 1.9$, however, the difference becomes less marked. The excitation currents leading to minimum and maximum Q values are shown in Figure 3. Evidently, the best result is obtained when the currents I_2 and I_3, appropriately weighted, reinforce the current I_1 at the middle, whereas the worst case is when $I_2 = I_3$ are both forced to zero (meaning that the antenna is made effectively shorter than its actual length). However, the Qs would be even larger if I_2 and I_3 were allowed to receive values more freely, that is, outside the range [0, 1] now considered. In Figure 3, one also notices that the values of I_2, I_3 giving optimal Q

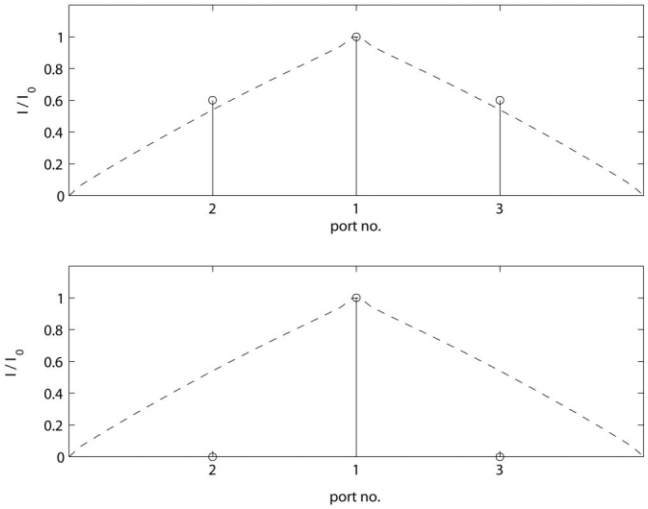

Figure 3 Excitation currents leading to minimum (top) and maximum (bottom) Q values, corresponding to Figure 2. For comparison, the current distribution along the wire in the 1-port case is depicted with a dashed line

differ only slightly from the strength of the current at the respective location of a centre-fed 1-port antenna.

Similarly, a 7-port case was calculated. The Q and the excitation currents corresponding to minimum and maximum Q-values are shown in Figures 4 and 5. As can be seen by comparing Figure 4 with Figure 2, by appropriate excitation of a 7-port antenna Q-factors slightly lower can be achieved than what is possible with a similar 3-port antenna.

3.2. Optimizing Q Using Distributed Reactive Loads

Next, let us search for the optimum (minimum) antenna Q by loading a 1-port, 3-port, and 7-port antenna, respectively, with appropriate reactive elements. In every case, the antenna structure is the same except for the varying number of ports.

Again, the antenna considered is a horizontal wire-dipole above a perfectly conducting ground plane. It is assumed to be fed horizontally at the mid-point, whereas the other ports are imposed vertically between the wire and the corresponding point on the ground plane below (see Fig. 6). For convenience, the structure is

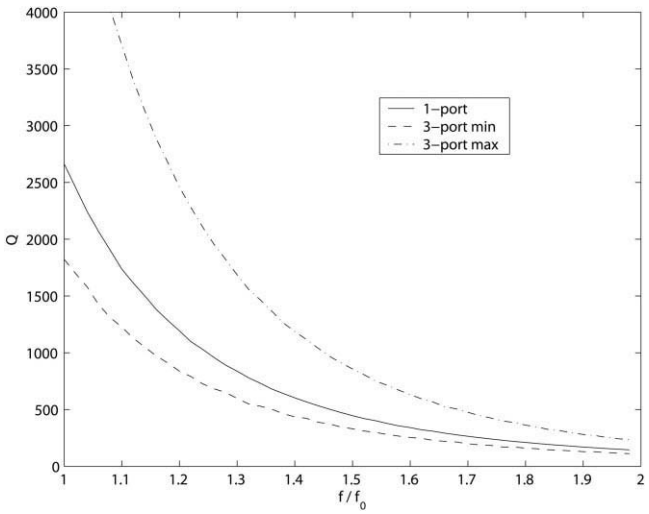

Figure 2 Minimum and maximum Q values obtained with excitation of three ports, assuming $I_2 = I_3 \in [0, 1]$

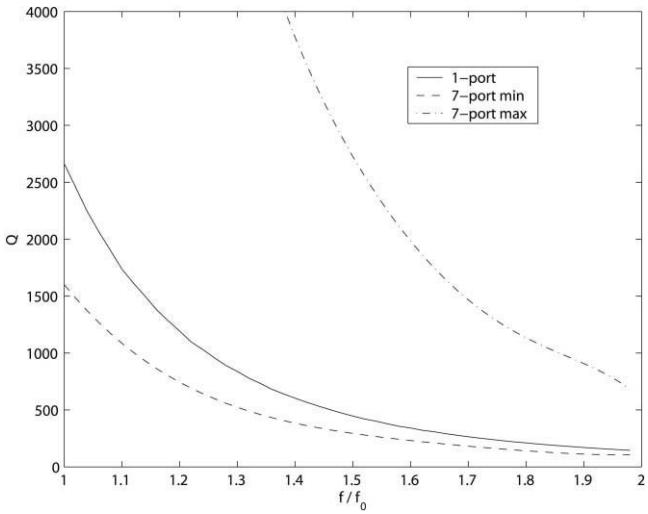

Figure 4 Minimum and maximum Q values obtained with 7-port excitation, assuming $I_2 = I_3$, $I_4 = I_7$, and $I_5 = I_6$ to vary in the range [0, 1]

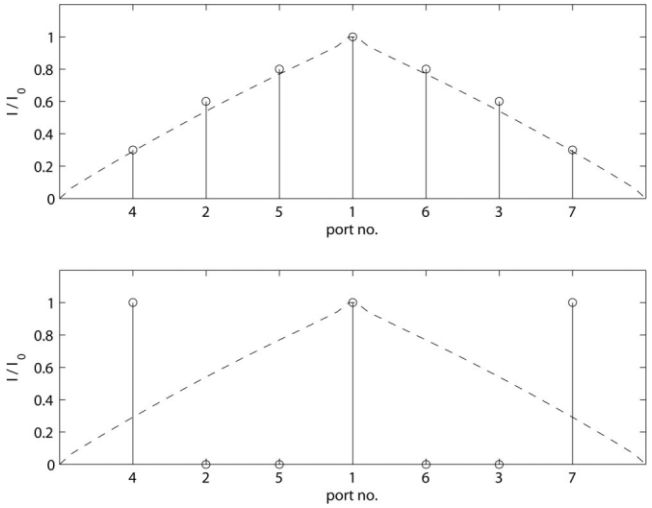

Figure 5 Excitation currents leading to minimum (top) and maximum (bottom) Q values corresponding to Figure 4. The dashed line marks the current distribution in the 1-port case

considered mirror symmetric, i.e., the same component values appear symmetrically on both sides of the wire. Now, by using the relationships of the Z-matrix of Section 2, the input impedance and Q of the antenna may be computed from the simulation data using (20). The loading is adjusted such that the antenna becomes resonant at f_0.

In Figure 7 the Q factors of the impedance loaded multiport antenna are shown. In the 1-port case the antenna is loaded with an inductor (whose reactance at $\omega_0 = 2\pi f_0$ is $\omega_0 L = 327\Omega$) at the feed point. In the 3-port case, the antenna is loaded with capacitors at ports 2 and 3, and in the 7-port case at ports 2–7. In the 7-port case, the capacitance values leading to minimum and maximum Q factors were sought with a Matlab routine when the reactances $1/\omega_0 C$ varied between 80 and 1600Ω. The reactances corresponding to the Q curves presented in Figure 7 are given in Table 1. As is seen in Figure 7, loading the antenna with an inductor at the feed port increases notably the Q factor of the antenna system compared to the unloaded 1-port element (see Figure 2). On the contrary, the capacitor loading in the 3-port case leads to remarkably smaller Qs, and with a certain 7-port capacitance loading yet smaller Q factors are possible.

4. CONCLUSIONS

In this article, we have derived an expression for the Q of a multiport antenna based on the total field energy stored by the antenna system. Some fundamental relationships derived from the basic electric network equations have also been presented that enable the design and control of the impedance properties of

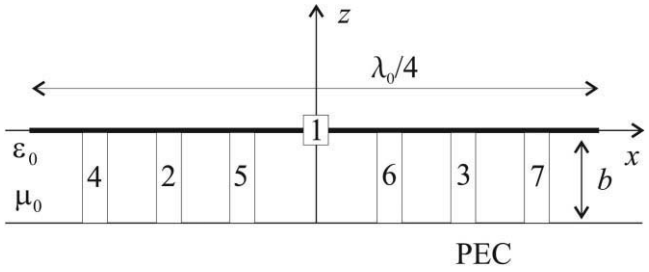

Figure 6 Horizontal dipole with multiple loading ports

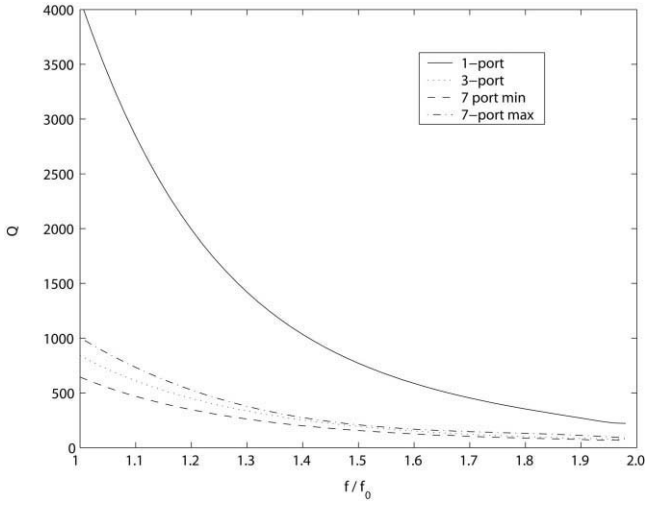

Figure 7 Q-values obtained with 1-port, 3-port, and 7-port loading

multiport antennas using the impedance (or admittance) matrix obtained, for instance, from electromagnetic simulations or real antenna measurements (by way of the relevant scattering matrix). The derived formulae were subsequently applied numerically in the search for optimal (in terms of smallest Q) loading and excitation of a multiport antenna. The example structure considered by means of HFSS simulations was an electrically short wire. The results confirm that a set of suitably chosen load impedances distributed within the antenna structure may indeed improve the Q as compared to the case where the antenna is conjugate matched at the feed point. It was also found that an appropriately chosen set of excitation currents may lead to a better Q than that obtained by feeding the antenna from a single point.

APPENDIX

In a typical multiport antenna application scenario, where one of the ports is adopted as the input/output and the others are loaded with suitable impedances z_{Li}, we are required to find the impedance seen at the input. In this case, the antenna (modeled by the impedance matrix $\bar{\bar{Z}}$) is connected through its terminals to the diagonal load impedance matrix $\bar{\bar{Z}}_L$. Thus, combining (1) with $\bar{V} = -\bar{\bar{Z}}_L \bar{I}$ renders $(\bar{\bar{Z}} + \bar{\bar{Z}}_L)\,\bar{I} = 0$. To have an existing solution, apart from the trivial $\bar{I} = \bar{0}$, the determinant of this eigenvalue equation must vanish, i.e., [12] $\det(\bar{\bar{Z}} + \bar{\bar{Z}}_L) = \bar{0}$, which leads to an equation that can be solved analytically in the case of a small number of ports and, more generally, numerically. Explicitly, we have

$$\begin{vmatrix} z_{11} + z_{L1} & z_{12} & \cdots & z_{1N} \\ z_{21} & \ddots & & z_{2N} \\ \vdots & & \ddots & \\ z_{N1} & \cdots & & z_{NN} + z_{LN} \end{vmatrix} = 0 \qquad (21)$$

and, supposing that the port number 1 be the unknown element, we obtain

Table 1 Tuning Reactances

port no.	4	2	5	6	3	7
$1/\omega_0 C$ [Ω](3-port)	-	118	-	-	118	-
$1/\omega_0 C$ [Ω](7-port min)	200	1064	1590	1590	1064	200
$1/\omega_0 C$ [Ω](7-port mx)	1590	357	82	82	357	1590

$$z_{L1} = -z_{11} + \frac{1}{M_{11}} \sum_{j=2}^{N} (-1)^j z_{1j} M_{1j} \tag{22}$$

where M_{ij} is the minor (or secondary determinant, obtained by deleting row i and column j) of the matrix $\overline{\overline{Z}} + \overline{\overline{Z}}_L$. Requiring equality of the input impedance and the load impedance, and generalizing the result to the input impedance viewed at the kth port yields

$$Z_{\text{in},k} = z_{kk} + \frac{1}{M_{kk}} \sum_{j=1, j\neq k}^{N} z_{kj} C_{kj} \tag{23}$$

where $C_{kj} = (-1)^{j+k} M_{kj}$ is the cofactor of the corresponding minor M_{kj}. In particular, for the two port system ($N = 2$), we have the well-known result [3, 12]

$$Z_{\text{in}} = z_{11} - \frac{z_{12} z_{21}}{z_{22} + z_{2L}} \tag{24}$$

where $z_{12} = z_{21}$ if the network is reciprocal, as is usually the case.

REFERENCES

1. H. Steyskal and J.S. Herd, Mutual coupling compensation in small array antennas, IEEE Trans Antennas Propag 38 (1990), 1971–1975.
2. H.D. Foltz and J.S. McLean, Bandwidth limitations on antenna systems with multiple isolated input ports, Microwave Opt Technol Lett 19 (1998), 301–304.
3. R.F. Harrington, Field computation by moment methods, Chapter 6, MacMillan, New York, 1968.
4. F. Schwering, N.N. Puri, and C.M. Butler, Modified diakoptic theory of antennas, IEEE Trans Antennas Propag 34 (1986), 1273–1281.
5. R.L. Fante, Quality factor of general ideal antennas, IEEE Trans Antennas Propag 17 (1969), 151–155.
6. W. Geyi, P. Jarmuszewski, and Y. Qi, The Foster reactance theorem for antennas and radiation Q, IEEE Trans Antennas Propag 48 (2000), 401–408.
7. A.D. Yaghjian and S.R. Best, Impedance, bandwidth and Q of antennas, IEEE Trans Antennas Propag 53 (2005), 1298–1324.
8. L. Li and C.-H. Liang, Analysis of resonance and quality factor of antenna and scattering systems using complex frequency method combined with model-based parameter estimation, Prog Electromagn Res 46 (2004), 165–188.
9. C.H. Papas, Theory of electromagnetic wave propagation, Dover, New York, 1988.
10. A.D. Yaghjian, Improved formulas for the Q of antennas with highly lossy dispersive materials, Antennas Wireless Propag Lett 5 (2006), 365–369.
11. E.A. Marengo, A.J. Devaney, and F.K. Gruber, Inverse source problem with reactive power constraint, IEEE Trans Antennas Propag 52 (2004), 1586–1595.
12. N. Marcuwitz, Network formulation of electromagnetic field problems, Proceedings of the Symposium of Modern Network Synthesis, New York, Polytechnic Institute of Brooklyn, 1952, 215–235.

© 2008 Wiley Periodicals, Inc.

INVESTIGATION OF LOW-PROFILE FRESNEL ZONE PLATE ANTENNAS

S. M. Stout-Grandy,[1] A. Petosa,[2] I. V. Minin,[3] O. V. Minin,[3] and J. S. Wight[1]

[1] Department of Electronics, Carleton University, 1125 Colonel By Drive, Ottawa, Ontario, K1S 5B6 Canada; Corresponding author: sstout@doe.carleton.ca

[2] Advanced Antenna Technology Group, Communications Research Centre Canada, 3701 Carling Ave., Ottawa, K2H 8S2 Canada

[3] Department of Information Protection, Novosibirsk State Technical University (NSTU), 20 Karl Marx Prospect, Novosibirsk, 630092 Russia

Received 14 December 2007

ABSTRACT: *This article presents low-profile configurations of the Fresnel zone plate antenna at Ka-band. The investigation involved progressively reducing the focal distance of the antenna through simulations and observing the effect on the directivity, radiation patterns, and aperture efficiency. The number of metal zones was also varied in the simulations. It was found that focal distances below 0.75λ yielded little more directivity than the feed itself. With a single zone, the 1.25λ focal distance achieved the highest overall aperture efficiency of 24%, which was a significant improvement over the larger focal distance cases. Measurements were performed to verify the simulated results.* © 2008 Wiley Periodicals, Inc. Microwave Opt Technol Lett 50: 2039–2043, 2008; Published online in Wiley InterScience (www.interscience.wiley.com). DOI 10.1002/mop.23593

Key words: *Fresnel zone plate antenna; low-profile*

1. INTRODUCTION

The Fresnel zone plate antenna (FZPA) is a type of microwave lens, which originated from the work of Augustin Fresnel in the early 19th century at optical frequencies [1]. In its standard configuration, as shown in Figure 1, it is planar in the xy plane and has a feed antenna situated at the focal point of the lens at a distance F along the z-axis. The aperture of the FZPA consists of circular zones that alternate between transparent and metal, which focus the fields using the principle of diffraction [2].

FZPAs are very attractive for applications in the Ka-band where they offer significant advantages over shaped lenses, parabolic reflectors, and planar arrays. The FZPA is much simpler to fabricate, has a reduced aperture thickness, is lighter weight, and is an overall lower cost antenna solution. Despite these tremendous advantages, they have not been widely used in the past. This is primarily because of their low aperture efficiency, which is due to the blocking of a large percentage of EM waves by the metal

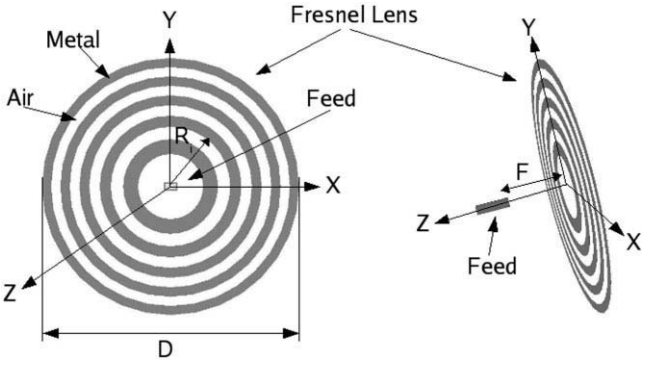

Figure 1 Fresnel zone plate antenna: (a) front view and (b) isometric view

PUBLICATION 5

Decay of groundplane currents of small antenna elements

In: IEEE Antennas and Wireless Propagation Letters 2005.
Vol. 4, pp. 82–84.
© 2005 IEEE.
Reprinted with permission from the publisher.

This material is posted here with permission of the IEEE. Such permission of the IEEE does not in any way imply IEEE endorsement of any of the VTT Technical Research Centre of Finland's products or services. Internal or personal use of this material is permitted. However, permission to reprint/republish this material for advertising or promotional purposes or for creating new collective works for resale or redistribution must be obtained from the IEEE by writing to pubs-permissions@ieee.org.

Decay of Groundplane Currents of Small Antenna Elements

J. C.-E. Sten and M. Hirvonen

***Abstract*—Expressions are derived for the surface current induced by vertical and horizontal dipoles on a nearby infinite groundplane. The expressions are obtained by means of the exact magnetic field. It is found that for a vertical dipole the surface current density decays roughly as the inverse of the distance from the source, while for a horizontal dipole it decays as the inverse distance squared. The result furnishes an explication for the empirical observation that antennas carrying mainly horizontal currents tend to be less sensitive to the dimensions of a finite groundplane than antennas carrying vertical currents. A formula is given by means of which the groundplane current of a compound source can be evaluated and controlled.**

***Index Terms*—Antennas, ground plane, surface current.**

I. Introduction

FOR SOME TIME, it has been recognized that the size and shape of the groundplane of an electrically small antenna have a significant effect not only the radiation properties [1], [2] but also the input impedance of the structure [3], [4]. Nevertheless, empirical studies aside no rigorous explanation has been given to the observation that different antennas are variously affected by the size and shape of the groundplane. In particular, antennas with an emphasis on the horizontal (or tangential) current component tend to be more independent—at least when the impedance is concerned—of the groundplane dimensions than antennas with an emphasis on the vertical (normal to the surface) current. It is thus conjectured that the distribution of surface currents is more widely spread, generally speaking, and the rate of decay of the current intensity slower for vertical sources than for horizontal ones.

In this paper we endeavour to show theoretically, by considering the near-fields of small antenna elements, that the surface currents induced by vertical and horizontal dipoles decay at a different rate according to the distance from the source region—for vertical dipoles at a rate of $1/r$, while for horizontal dipoles at $1/r^2$. The presented analysis also yields a simple means to evaluate groundplane currents for antennas with a prescribed current distribution. A numerical illustration of the method for an inverted L-structure (ILA) is presented.

II. Dipole Fields

The key to expressing the current distributions induced on an infinite groundplane is the magnetic field $\mathbf{H}$. In spherical coordinates (r,θ,φ) a z-directed infinitesimal current element (an electric point dipole) located at the origin and having the moment $\mathbf{u}_z[Il]$, creates the field (implicitly assuming harmonic $e^{j\omega t}$-time dependence) [5]

$$\mathbf{H}(\mathbf{r}) = jk[Il]\frac{e^{-jkr}}{4\pi r}\left(1-\frac{j}{kr}\right)\sin\theta\mathbf{u}_\varphi. \tag{1}$$

When a perfectly conducting plane is brought near the dipole, the plane creates a reflection which can be accounted for by means of an image source at the mirror image point. In the case of a vertical dipole (parallel to the surface normal) the image current is in phase with the original, while in the contrary case of horizontal (or tangential) current, the image is in the opposite phase [5].

A. Vertical Dipole

Let us introduce a system of two-dimensional primed coordinates (x',y') on the plane perfectly conducting surface $z=-z_0$, with the origin at $(x,y,z)=(0,0,-z_0)$. Writing the transformation

$$r=\sqrt{z_0^2+\rho'^2},\quad \theta=\frac{\pi}{2}+\arccos\frac{z_0}{r} \tag{2}$$

with $\rho'=\sqrt{x'^2+y'^2}$, we get

$$\mathbf{H}(x',y')|_{z=-z_0} = jk[Il]\frac{e^{-jkr}}{4\pi r}\left(1-\frac{j}{kr}\right)\frac{\rho'}{r}\mathbf{u}_\varphi. \tag{3}$$

The total induced current is $\mathbf{J}_s=2\mathbf{n}\times\mathbf{H}$, where $\mathbf{n}$ is the surface normal $\mathbf{u}_z$, the factor 2 being due to the reinforcing image source. Then

$$\mathbf{J}_s = -j[Il]\rho'(kr-j)\frac{e^{-jkr}}{2\pi r^3}\mathbf{u}_{\rho'} \tag{4}$$

where $\mathbf{u}_{\rho'}=(x'\mathbf{u}_x+y'\mathbf{u}_y)/\rho'$. At $\rho'=0$, immediately below the original current, the surface current can be seen to vanish, while at a far distance, when $\rho'/r\approx 1$, the surface current decays roughly as $1/r$.

B. Horizontal Dipole

A plane conducting surface is now introduced at $y=y_0$ along with an associated system of primed coordinates (x',z') originating at $(x,y,z)=(0,y_0,0)$. The transformation then reads

$$\begin{aligned} r&=\sqrt{x'^2+y_0^2+z'^2}\\ \theta&=\arccos\frac{z'}{r}\\ \varphi&=\arccos\frac{x'}{\sqrt{x'^2+y_0^2}}\end{aligned} \tag{5}$$

Manuscript received October 1, 2004; revised January 10, 2005.

The authors are with the Technical Research Centre of Finland, VTT Information Technology, Telecommunications, 02044 VTT, Espoo, Finland.

Digital Object Identifier 10.1109/LAWP.2005.844649

1536-1225/$20.00 © 2005 IEEE

where

$$\mathbf{H}(x',z')|_{y=y_0} = jk[Il]\frac{e^{-jkr}}{4\pi r}\left(1-\frac{j}{kr}\right)\frac{\sqrt{x'^2+y_0^2}}{r}\mathbf{u}_\varphi \quad (6)$$

where

$$\mathbf{u}_\varphi = \frac{(-y_0\mathbf{u}_x + x'\mathbf{u}_y)}{\sqrt{x'^2+y_0^2}}.$$

Using $\mathbf{J}_s = 2\mathbf{n}\times\mathbf{H}$, where $\mathbf{n} = -\mathbf{u}_y$, the current density induced on the surface becomes

$$\mathbf{J}_s = -j[Il]y_0(kr-j)\frac{e^{-jkr}}{2\pi r^3}\mathbf{u}_z \quad (7)$$

which is seen to decay roughly as $1/r^2$ at large distances r. In addition, when $y_0 \ll x'$ and z', the current density is directly proportional to y_0, the height of the dipole above the surface (in the limit $y_0 \to 0$ radiation ceases and $\mathbf{J}_s \to 0$).

C. General Case

Consider now a general point current element

$$\mathbf{J}(\mathbf{r}) = ([Il]_x\mathbf{u}_x + [Il]_y\mathbf{u}_y + [Il]_z\mathbf{u}_z)\,\delta(\mathbf{r}-\mathbf{r}_0) \quad (8)$$

residing at $\mathbf{r}_0 = x_0\mathbf{u}_x + y_0\mathbf{u}_y + z_0\mathbf{u}_z$ in front of a perfectly conducting surface, $z = 0$. The current distribution arising in the xy-plane may be written by transforming the expressions (4) and (7) as

$$J_{s,x} = -j(kr-j)\frac{e^{-jkr}}{2\pi r^3}([Il]_z(x-x_0) + [Il]_x z_0) \quad (9)$$

$$J_{s,y} = -j(kr-j)\frac{e^{-jkr}}{2\pi r^3}([Il]_z(y-y_0) + [Il]_y z_0) \quad (10)$$

with $r = \sqrt{(x-x_0)^2+(y-y_0)^2+(z-z_0)^2}$.

III. Application

By exploiting the general case formulas (9) and (10), the surface currents of actual antennas may now be studied. As an example, the surface currents induced by the inverted L wire antenna are presented. Two variants of the geometry are selected. Variant one, depicted in Fig. 1, is a very low-profile structure with a height of only $\lambda/28$ and a total wire length of $\lambda/4$. For variant two, appearing in Fig. 2, the vertical and horizontal components are of the same length, $\lambda/8$. For both variants, the current is assumed to be a quarter sinusoid, reaching maximum at the feed point and tending to zero at the open end of the wire. This assumption, despite being an approximation, gives an adequate picture of the surface current distribution.

In the evaluation of the currents, the ILA-structure was modeled as several vertical and horizontal point currents with amplitudes proportional to the integral of sine current. The surface currents of the two variants are presented in Figs. 1 and 2, respectively. The scale of the contour lines is the same for both cases, representing half-values. As can be seen by comparing the two figures, the surface current induced by the higher profile variant with a dominating vertical current extends in a larger area than the surface current induced by the lower profile structure with dominating horizontal current.

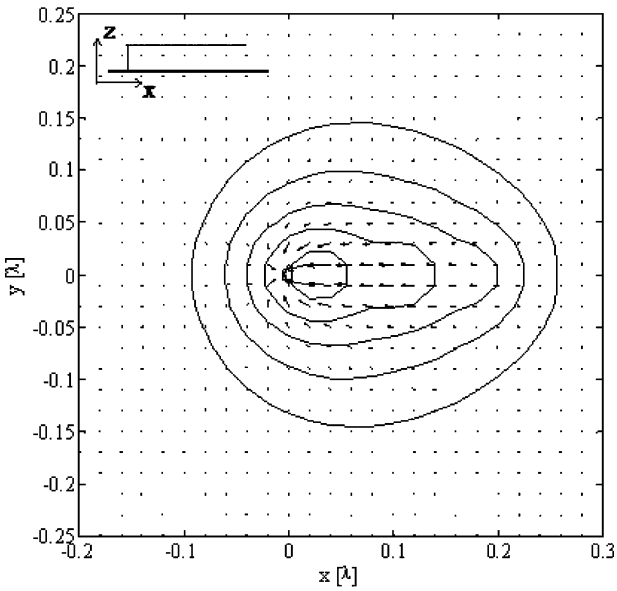

Fig. 1. Flat inverted-L antenna and the surface current distribution it generates. The intensity contours represent half-values.

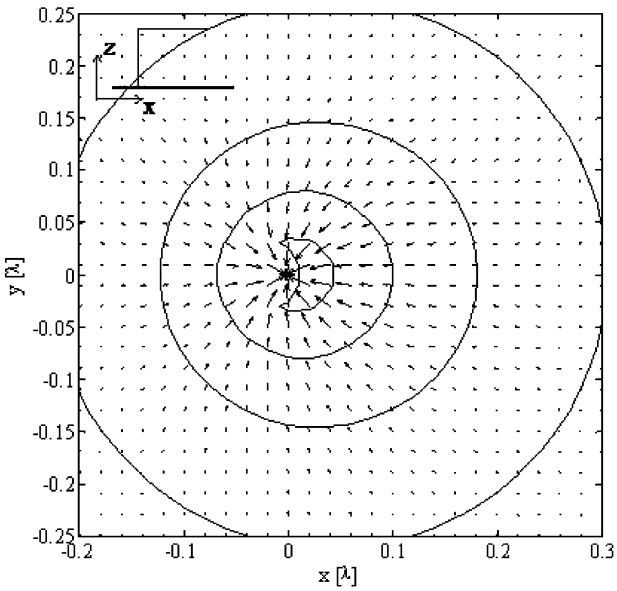

Fig. 2. High-profile version of the inverted-L antenna and its surface current distribution. The same intensity contours are displayed as in Fig. 1.

IV. Conclusion

Antennas backed with a groundplane can be divided into a set of horizontal and vertical current elements. It has been demonstrated in this paper that such elements generate different kinds of surface current patterns, and that the rates of decay of these current densities are disparate. A formula was derived by means of which the surface current pattern induced by an antenna in front of a groundplane can be constructed. Knowledge of the surface current pattern is essential when one tries to reduce

the size of the groundplane without compromising the antenna performance.

REFERENCES

[1] M.-C. Huynh and W. Stutzman, "Ground plane effects on planar inverted-F antenna (PIFA) performance," *Proc. Inst. Elect. Eng.—Microw. Antennas Propag.*, vol. 150, no. 4, pp. 209–213, Aug. 2003.

[2] S. Noghanian and L. Shafai, "Control of microstrip antenna radiation characteristics by ground plane size and shape," *Proc. Inst. Elect. Eng.—Microw. Antennas Propag.*, vol. 145, no. 3, pp. 207–212, Jun. 1998.

[3] A. K. Bhattacharyya, "Effects of ground plane truncation on the impedance of a patch antenna," *Proc. Inst. Elect. Eng.—Microw. Antennas Propag.*, vol. 138, no. 6, pp. 560–564, Dec. 1991.

[4] P. Salonen, "Effects of finite-sized groundplane on radiation pattern deformation, impedance bandwidth, and radiation efficiency of U-PIFA," *Microw. Opt. Tech. Lett.*, vol. 36, no. 6, pp. 491–496, Mar. 20, 2003.

[5] J. A. Kong, *Electromagnetic Wave Theory*. New York: Wiley, 1986.

PUBLICATION 6

Planar inverted-F antenna for radio frequency identification

In: Electronics Letters 2004.
Vol. 40, No. 14, pp. 848–850.
Reprinted with permission from the publisher.

Planar inverted-F antenna for radio frequency identification

M. Hirvonen, P. Pursula, K. Jaakkola and K. Laukkanen

A small and low-cost antenna solution for radio frequency identification (RFID) tags is presented. The impedance of the antenna is designed to match directly to the impedance of the RFID microchip. Also, the impedance of the antenna is immune to the platform. Thus, the antenna is applicable in many different environments. The design and measurement results are reported and discussed.

Introduction: Radio frequency identification has lately gained much interest in several service industries. Inductively coupled short-range RFID is already widely used, but demand is growing in the field of long-range identification, where electromagnetic waves and an antenna are used for coupling [1]. However, many challenging features are required from the antenna intended to be used in long-range RFID tags. First, the antenna has to be really small, preferably low-profile, in order to be usable. Secondly, the fabrication has to be inexpensive, since RFID tags are generally designed to be disposable. In passive systems the signal power received by the antenna supplies the microchip. Thus, a perfect impedance match between the antenna and the RFID microchip is essential in order to sustain the power supply of the chip. The impedance level of the chip usually differs from the common 50 Ω case, and the matching has to be direct, since matching networks cannot be used because of the cost and size limitations. More importantly, the matching has to hold in any environment. Since in RFID applications tags are attached directly to different kinds of objects, the impedance tolerance to the platform is a key issue.

Printed dipole antennas may be used in RFID tags, but their performance is highly platform dependent. Conversely, microstrip patch antennas are more tolerant to the effects of the platform, but are very large in size. By using a planar inverted-F antenna (PIFA) structure smaller size may be achieved, but generally at the cost of reduced tolerance to the environment [2]. To meet the challenging demands of long-range RFID, a platform-tolerant design of PIFA is presented in this Letter.

Antenna design: The geometry of the developed antenna is presented in Fig. 1. At the operation frequency of 869 MHz the antenna is only 3 mm (0.013λ) high and the patch is 45 mm (0.19λ) wide. The patch and the ground plane are square in shape. The antenna is filled with Teflon in the area under the patch. According to preliminary experiments cheaper polyethylene may also be used.

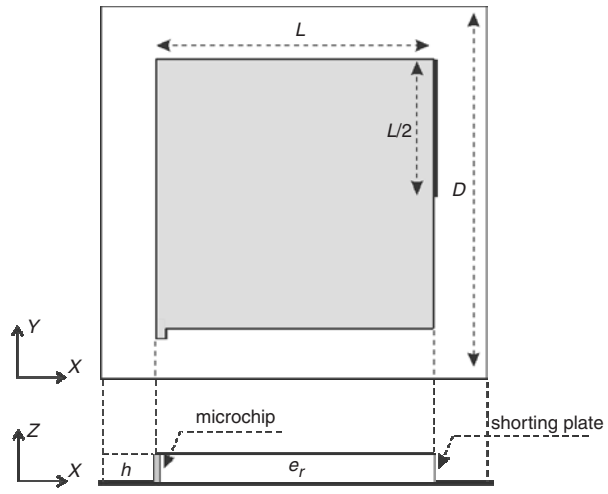

Fig. 1 *Antenna design*

The microchip feed is placed on one corner and the shorting plate is half the width of the patch edge. In this case the impedance of the antenna is matched to $(7-j170)$ Ω. With this design it is possible to achieve immunity to different platforms. The ground plane is optimised to be as small as possible (59 mm or 0.25λ), while still providing the impedance tolerance to the platform. However, the antenna is rather narrowband and the radiation is almost omnidirectional. Usually these features lead to platform-sensitive impedance behaviour, but in this case also the right radiation mode plays an important role. The main current flow is directed diagonally from the shorting plate to the feed. The patch is not in resonance and there is no dual-resonance with the ground plane near 869 MHz. In addition, it was discovered that with the presented design the radiation from the shorting plate is reduced, leading to better tolerance to different platforms.

Experimental results: The antenna performance was verified with a scattering measurement technique. A microchip with an input impedance of $(7-j170)$ Ω was attached as a feed of the antenna. The chip contains a 200 kHz oscillator which modulates the input reactance of the chip, causing a phase modulation of the backscattered signal. The modulation starts if the chip is fed at least with 10 μW of input RF power. As the limiting power is known, the transmitted power P_{tx} needed to wake up the chip is measured against the frequency to determine the antenna bandwidth, and against the antenna alignment to determine the antenna radiation pattern, i.e. the effective antenna aperture including mismatch is measured. Both the input impedance and the required power level of the chip are similar to that of the RFID chip in the passive long distance multiple access UHF RFID (PALOMAR) system [3].

The performance of the antenna has been studied with different platforms. The results of the bandwidth measurements are presented in Fig. 2 and in Table 1. In Fig. 2 all the peaks have been scaled to 0 dB. The bandwidth is defined as the half-power bandwidth of the antenna aperture, which is equivalent to +3 dB in required transmitted power P_{tx}. As seen from Fig. 2 and Table 1, the centre frequency varies only ±1 MHz around the operation frequency of 869 MHz. Also, the bandwidth varies only from 15 to 17 MHz. It is clear that the impedance and bandwidth variance against different platforms is minimal, indicating very good tolerance to different platforms.

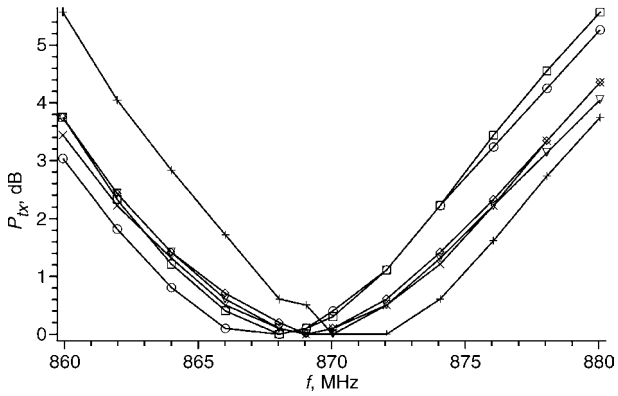

Fig. 2 *Results of bandwidth measurement*
—+— free-space
—◇— metal 150 × 150 mm
—▽— metal 600 × 600 mm
—○— wood
—□— PVC plastic
—×— water canister

Table 1: Measured centre frequencies and bandwidths

Platform	Centre frequency [MHz]	Half-power bandwidth [MHz]
Free-space	870	15
Metal 150 × 150 mm	869	17
Metal 600 × 600 mm	869	17
Wood	868	16
PVC plastic	868	15
Water canister	869	17

The co- and cross-polarisation radiation patterns measured with the scattering technique are presented in Fig. 3. It is evident that the antenna is rather omnidirectional with a simulated directivity of only 1.5 dBi. Also, the antenna has a rather high cross-polarisation level, which has to be considered in developing the reader device. Otherwise the orientation of the tag may have a major impact on the reading

reliability. Also, the three-dimensional radiation patterns were measured with a traditional far-field measurement system. From these results the radiation efficiency could be calculated exploiting the spherical wave expansion. The radiation efficiency of the antenna varied between 50 and 60% depending on the platform.

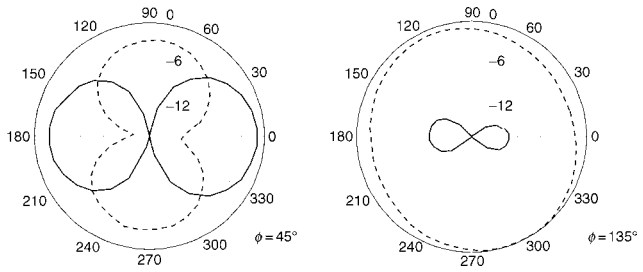

Fig. 3 *Measured radiation patterns*

—— E_ϕ
- - - - E_θ

Table 2: Maximum reading distances

Platform	Maximum reading distance, m
Free-space	2.0
Metal 150 × 150 mm	5.1
Metal 600 × 600 mm	4.3
Wood	3.9
PVC plastic	3.2
Water canister	2.0

The maximum reading distances were studied with the PALOMAR system, using the maximum allowed transmission power of 0.5 W ERP. The reading distances of the antenna on different platforms are presented in Table 2. Because of different directivity values on different platforms, the reading distances vary between 2 and 5 m. It is clear that the antenna operates satisfactorily on every tested platform, but the best performance is achieved on metal.

Conclusions: A compact and low-cost antenna applicable to RFID tags has been developed. By using a certain design an RFID microchip may be directly matched to the antenna. More importantly, a platform-independent impedance behaviour can be achieved. Also, the antenna has adequate bandwidth and radiation characteristics. Because of these features, the antenna is applicable in several RFID environments, e.g. on metal, wood and plastic surfaces or even on a water canister.

Acknowledgment: This work has been supported by Tekes, The National Technology Agency of Finland.

© IEE 2004
27 April 2004
Electronics Letters online no: 20045156
doi: 10.1049/el:20045156

M. Hirvonen, P. Pursula, K. Jaakkola and K. Laukkanen (*VTT Information Technology, PO Box 1202, FIN-02044 VTT, Finland*)

E-mail: mervi.hirvonen@vtt.fi

References

1 Finkenzeller, K.: 'RFID handbook' (John Wiley & Sons, Chichester, UK, 2003)
2 Huynh, M.C., and Stutzman, W.: 'Ground plane effects on planar inverted-F antenna (PIFA) performance', *IEE Proc., Microw. Antennas Propag.*, 2003, **140**, (4), pp. 209–213
3 The Palomar project: 'Passive long distance multiple access UHF RFID system', European Commission, Public Report, Project Number IST1999-10339, November 2002

PUBLICATION 7

Dual-band platform tolerant antennas for radio-frequency identification

In: IEEE Transactions on Antennas and Propagation 2006.
Vol. 54, No. 9, pp. 2632–2637.
© 2006 IEEE.
Reprinted with permission from the publisher.

This material is posted here with permission of the IEEE. Such permission of the IEEE does not in any way imply IEEE endorsement of any of the VTT Technical Research Centre of Finland's products or services. Internal or personal use of this material is permitted. However, permission to reprint/republish this material for advertising or promotional purposes or for creating new collective works for resale or redistribution must be obtained from the IEEE by writing to pubs-permissions@ieee.org.

Dual-Band Platform Tolerant Antennas for Radio-Frequency Identification

Mervi Hirvonen, Kaarle Jaakkola, Pekka Pursula, and Jussi Säily

***Abstract*—A technique for tuning a single-element planar inverted F-antenna (PIFA) to provide a dual-band operation is introduced. The tuning is possible due to the particular impedance level typical to radio-frequency identification microchips. As the desired impedance level resides near the outer rim of the Smith chart, a single impedance locus may be arranged to pass the input impedance twice resulting in dual-band operation. The tuning of the impedance locus is based on the feed inductance and capacitive coupling at the open end of the patch. In this paper, also a discussion about the principles of platform tolerance of small antennas is provided. A design, circuit model, simulations, and measurement results of dual-band platform tolerant PIFAs are reported and discussed.**

***Index Terms*—Dual-band, energy scavenging, planar inverted F-antenna (PIFA), platform tolerance, radio-frequency identification (RFID).**

I. Introduction

RADIO-frequency identification (RFID) has gained much interest in several service industries recently. However, for RFID tag antennas, many challenging features are required. For example, small size, low profile, direct impedance matching to the microchip, and suitability to low-cost mass production are crucial issues. Also, platform tolerance of the antenna is necessary in order to gain usability in different environments and applications. In addition, currently different frequencies are allocated for RFID use in Europe (867 MHz), North America (915 MHz), and Japan (953 MHz). Also, in RFID sensor applications, it would be beneficial to scavenge energy from radio networks in order to sustain constant sensor activity in passive systems or charge the battery in active systems. Suitable energy scavenging bands would be, for instance, the transmit frequencies allocated to GSM base stations. Thus, a multiband operation of the RFID tag antennas is preferred.

Multiband operation is traditionally achieved in antennas by using several resonant elements or exploiting the harmonics [1]. Placing several resonant elements for example in PIFA structures leads to large size. Also, coupling between the elements may degrade the performance of the antenna severely. On the other hand, by exploiting the harmonic frequencies, only multiples of the base frequency may be generated. In most cases, also different platforms tend to affect the characteristics of the antenna [2]–[6]. In this paper, the technique for tuning a single-element platform-tolerant PIFA for dual-band operation at arbitrary frequency bands is introduced.

Manuscript received September 8, 2005; revised April 5, 2006. This work was supported by Tekes (The National Technology Agency of Finland) and UPM Rafsec.

The authors are with the VTT Technical Research Centre of Finland, FI-02044 VTT, Finland (e-mail: Mervi.Hirvonen@vtt.fi).

Digital Object Identifier 10.1109/TAP.2006.880726

II. Platform Tolerance

For many antennas, the radiation pattern, bandwidth, and input impedance are typically highly platform dependent. However, in RFID applications the same antenna type may be attached directly on top of different kinds of objects. Especially stable impedance behavior is essential, since the power supply of the RFID microchip depends greatly on matching. Traditionally, the effects of the platform to antenna impedance are decreased by using large ground planes in the antenna structure. For example, according to [2]–[4], a ground plane of wavelengths in size is needed to stabilize the input impedance of a vertical monopole. Also, results concerning circular microstrip antennas have been reported in [5]. The study shows that a ground plane radius beyond 1.3 times the patch radius is enough to stabilize the input impedance. A similar study concerning a PIFA structure has been reported in [6], where the ground plane of only less than 0.2λ in size had an impact on the input impedance. Still, the exact size of the ground plane needed to stabilize the input impedance of the antenna depends also on the impedance bandwidth. Broad bandwidth is thus another technique to minimize the platform effects. However, in small antenna structures like PIFAs, broad bandwidth usually means large size and more importantly, high profile. For example, the PIFA introduced in [6] is 0.065λ high, which is unacceptable in RFID applications.

Regardless of the antenna bandwidth, platform-tolerant impedance behavior may also be achieved with a certain current distribution. It has been presented that surface currents induced by horizontal point sources above the ground plane decay more rapidly than those induced by vertical sources [7]. In other words, e.g., PIFA structures with dominating horizontal current distribution tend to be more platform tolerant than those with dominating vertical sources. Of course, the proximity of the ground plane for dominating horizontal current leads to very narrow bandwidth behavior, but in RFID applications only a narrow operation band is required. Dominating vertical current distribution is typical to many PIFA structures, since a vertical short tends to attract the current. However, by widening the short, i.e., reducing the inductance of the vertical part and lowering the height of the antenna, a dominating horizontal current distribution is achievable [8].

III. Dual-Band Operation

In RFID applications, the antenna is connected to a microchip. In order to maximize the power supply of the chip,

0018-926X/$20.00 © 2006 IEEE

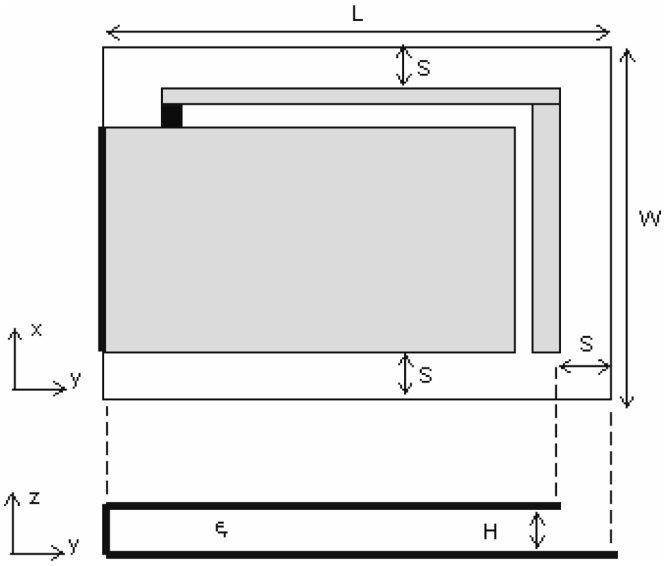

Fig. 1. Dual-band PIFA design.

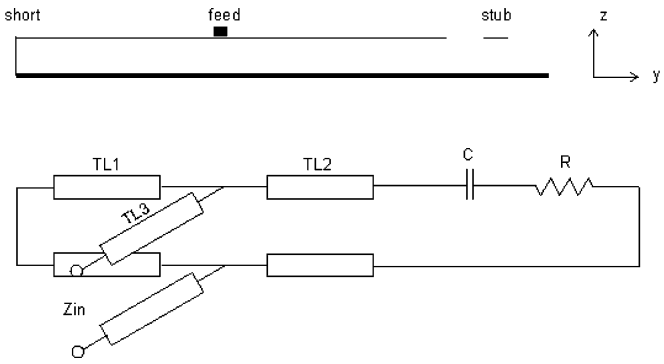

Fig. 2. Equivalent circuit of the proposed PIFA structure.

the RFID antennas are directly conjugately matched to the microchip terminal impedance. The impedance of the RFID microchips usually behaves as a series RC-circuit. In practice, this means a large reactive part of the impedance [9]. On the other hand, the real part of the impedance is quite low. The required input impedance of the RFID antenna is thus typically between (5-30)+j(130-250) Ω.

Like microstrip antennas, PIFA structures are typically modeled as parallel resonant circuits [10], [11]. However, in these cases, the PIFA structures are fed by 50 Ω coaxial probes. In RFID applications, the feed of the antenna is a microchip. The ground of the microchip may be arranged by via or, more importantly, by an open-ended stub as presented in Fig. 1. The use of an open-ended stub instead of a ground via is often preferred in RFID PIFA structures because of the manufacturing issues.

As the open-ended stub may be bent near the radiating edge of the patch, a series capacitance is formed instead of a parallel one. The equivalent circuit for this kind of PIFA structure is presented in Fig. 2. Transmission line 1 (TL1) defines the distance from the feed point to the short and transmission line 2 (TL2) the distance from the feed point to the open end of the patch. Transmission line 3 (TL3) represents the feed inductance relating to the length and width of the open-ended stub.

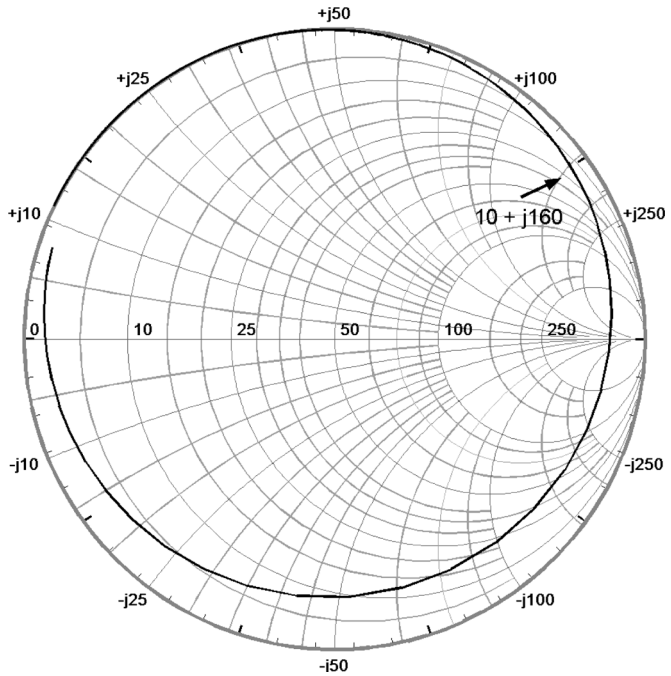

Fig. 3. Typical impedance behavior in the probe or microchip with a via fed PIFA.

In the typical case, where the antenna is fed by a probe or the ground of the microchip is arranged with a via, the feed inductance caused by TL3 is not easily tuned. In other words, the location of the impedance locus on the Smith chart is somewhat fixed. Hence, the desired input impedance may be achieved only by tuning the location of the feed (TL1 and TL2). In practice, reaching the low real impedance and highly inductive reactance usually means rather large locus, and the feed of the antenna has to be far away from the short and near the open end of the patch ($\mathrm{TL1} \gg \mathrm{TL2}$). The typical matching case is illustrated in Fig. 3. The frequency range is from 500 to 1500 MHz. As can be seen from Fig. 3, the locus passes the example input impedance 10+j160 typical to RFID only once, indicating single-band operation.

On the other hand, in the case of an open-ended stub, the length and width of the stub relate to the feed inductance TL3 and move the locus towards the load as presented in Fig. 4. In this case, the desired input impedance may be achieved with an arbitrary size impedance locus, which is moved suitably towards the load. As in RFID, the desired input impedance resides near the outer rim of the Smith chart, the impedance locus may be placed such that it passes near the desired impedance point twice, as illustrated in Fig. 4 case 3TL3. Thus, a dual-band operation may be achieved with only one resonant element. Series capacitance relates to the size of the locus as presented in Fig. 5. As the capacitance increases, a narrower frequency range forms the locus. In other words, the vicinity of the two frequency bands may be tuned by altering the coupling between the open-ended stub and the radiating edge of the patch. In practice, tuning the parameters affects the overall current distribution of the antenna. Thus, the circuit model only gives reasoning behind the dual-band tuning technique but is not suited for exact calculation.

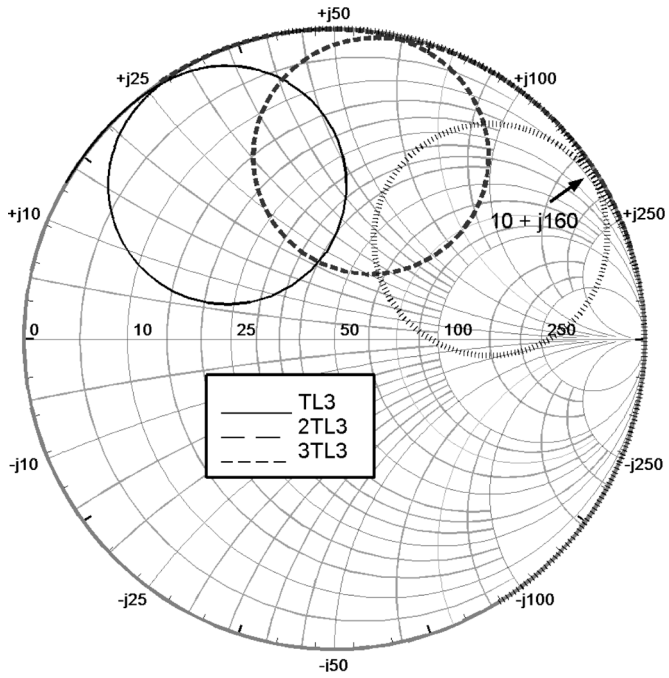

Fig. 4. Impedance behavior as a function of the length of the open-ended stub.

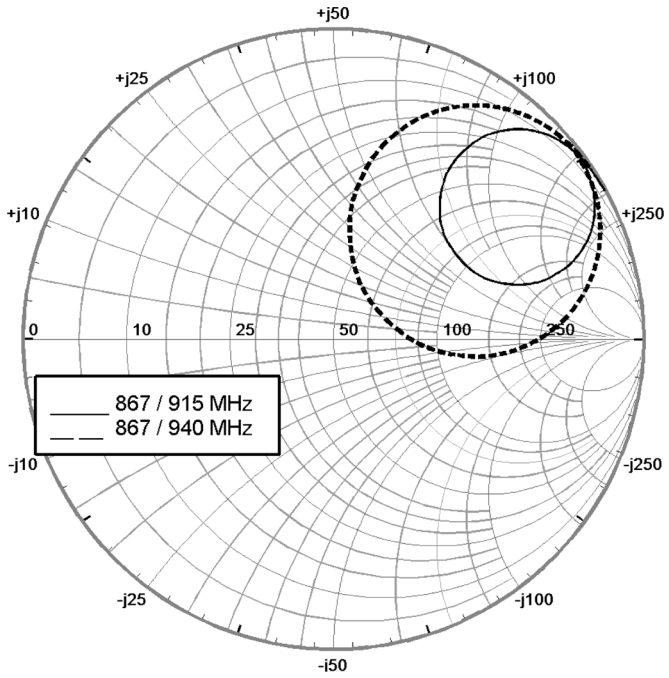

Fig. 6. Simulated input impedance.

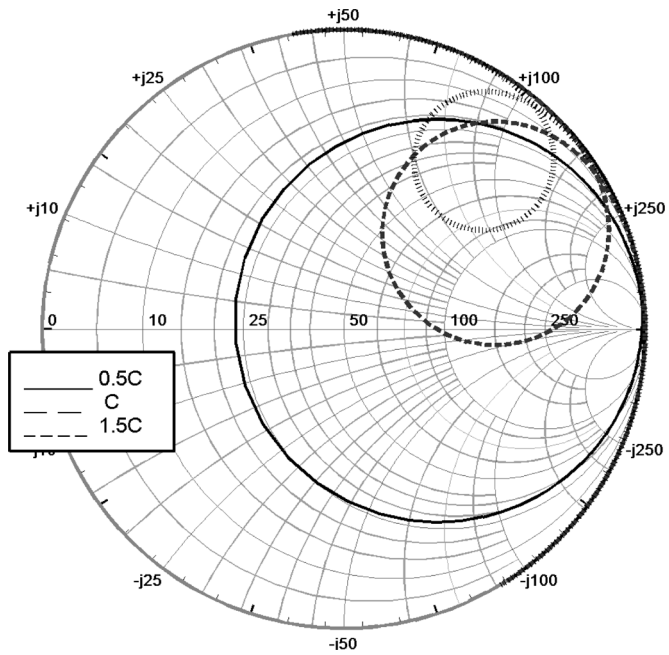

Fig. 5. Impedance behavior as a function of the series capacitance.

IV. Simulations and Measurements

The geometry of a dual-band platform-tolerant planar inverted F-antenna is presented in Fig. 1. As discussed in Section II, for achieving platform tolerance, the short is as wide as the patch edge and the antenna is really low in profile. More importantly, no ground plane is needed behind the short in order to achieve platform tolerance, which is a great asset in manufacturing. The ground of the microchip is arranged with an open ended stub in order to achieve dual-band operation as discussed in Section III.

The proposed antenna may be tuned to provide a dual-band operation for any frequency combination related to RFID. In this paper, two example cases are introduced: RFID use in Europe and in North America (867/915 MHz) and RFID use and energy scavenging in Europe (867/940 MHz). With a polyethylene substrate, $\varepsilon_{\rm r} = 2.35$, $\tan\delta = 0.002$, the length L of the antenna is 62.0 mm and width W is 51.3 mm including the ground plane. The metallization is 18-μm-thick copper. The height H of the antenna is only 3.0 mm, and 5.0 mm of ground plane frame S is needed to achieve the platform tolerance. The dimensions of the upper patch are 53.0×38.5 mm^2. In the case of a 867/915 MHz antenna, the gap between the stub and the edge of the patch is 1.0 mm, which is 0.9 mm narrower compared to the 867/940 MHz antenna, providing larger capacitance and thus more adjacent operating bands.

The simulated impedance behaviors between 850–955 MHz of the antennas are presented in Figs. 6 and 7. The simulations were conducted with Zeland IE3D software based on method of moments (MoM). The impedance of the RFID microchip in question behaves as a series RC-circuit with input impedances of (10−j160) Ω at 867 MHz, (10−j150) at 915 MHz and (10−j145) at 940 MHz. As can be seen from Fig. 6, the impedance loci pass near the desired impedance level twice providing dual-band operation. The impedance mismatch η is presented in Fig. 7.

The simulated radiation patterns are presented in Fig. 8. The patterns are the same at 867 MHz for both example antennas. As can be seen from Fig. 8, the patterns look quite similar for all the studied frequencies. The radiation is almost omnidirectional, including a strong backlobe. Also, the radiation is highly linearly polarized, resembling the radiation of a loop or magnetic dipole due to the dominating horizontal current distribution.

The impedance matchings of the antennas were verified with a scattering measurement technique [12]. A test microchip was

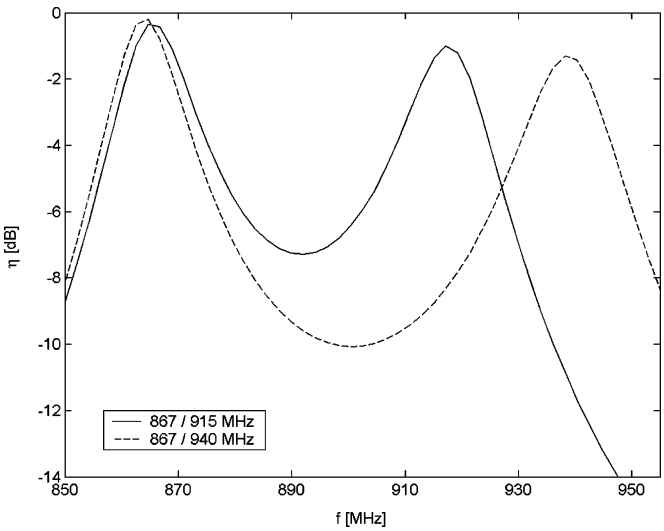

Fig. 7. Simulated impedance mismatch.

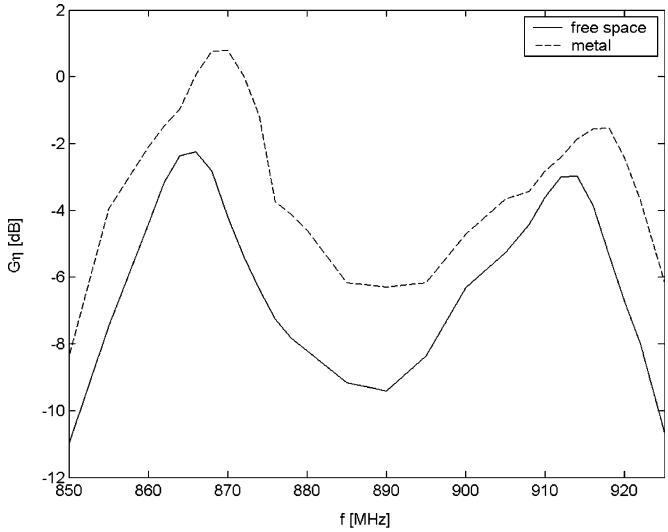

Fig. 9. Measured gain including mismatch of the 867/915 MHz antenna.

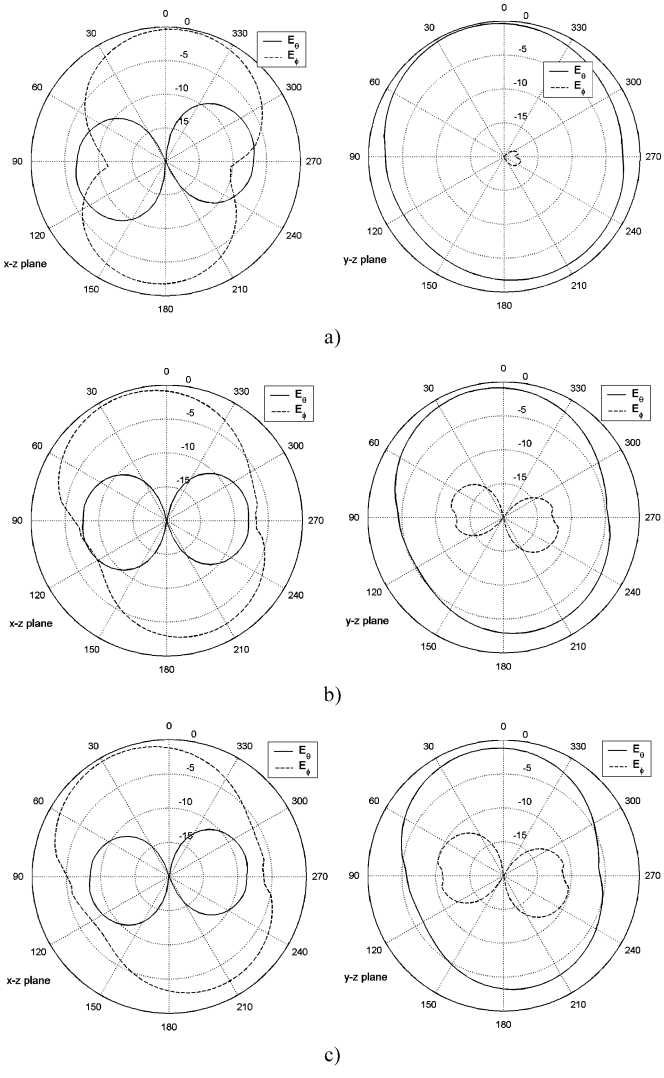

Fig. 8. Simulated radiation patterns at (a) 867 MHz, (b) 915 MHz, and (c) 940 MHz.

connected as a load to the antenna. The chip contains an oscillator that drives a varactor at the input of the chip, causing a phase modulation of the backscattered signal. The modulation starts if the chip is fed at least with $P_{req} = 16\ \mu$W of input RF power. Because this limiting power is constant, the transmit power P_{tx} needed to wake up the modulation describes the power transfer between the antenna and the chip. The lower the required transmit power P_{tx}, the better the matching between the antenna and the chip. In fact, the effective antenna aperture A_e including the mismatch η between the antenna and the load is inversely proportional to the required transmit power P_{tx}

$$A_e\eta = \frac{\lambda^2 G}{4\pi}\eta = \frac{P_{req}}{S} = \frac{4\pi r^2 P_{req}}{G_{tx}P_{tx}} \tag{1}$$

where S describes the power density of the transmitted field at a distance r. Measuring the required transmit power as a function of the frequency gives information of the antenna bandwidth with the microchip as its load. The oscillator chip has the same input impedance as the RFID chip, with which the antenna will be used. Thus, the measurement describes the antenna in the actual application.

The results of the scattering measurements, in other words, gain including the impedance mismatch between the antenna and the chip, are presented in Figs. 9 and 10. Polarization mismatch is neglected. As can be seen from Fig. 9, two separate bands are detected at 867 and 915 MHz, and the bandwidths are around 14 MHz. The bandwidth is defined as a half-power bandwidth of the antenna gain. The results for the 867/940 MHz antenna are quite similar. Two distinct bands are detected with bandwidths around 13 MHz. As can be seen from both cases, the center frequencies of the bands are about the same for the measurements done in free space and for the measurement, where the antennas were placed directly on top of a 46×46 cm^2 metal plate. The results indicate very good tolerance to platform. The gain levels are higher for the results on metal as expected because of the increased directivity.

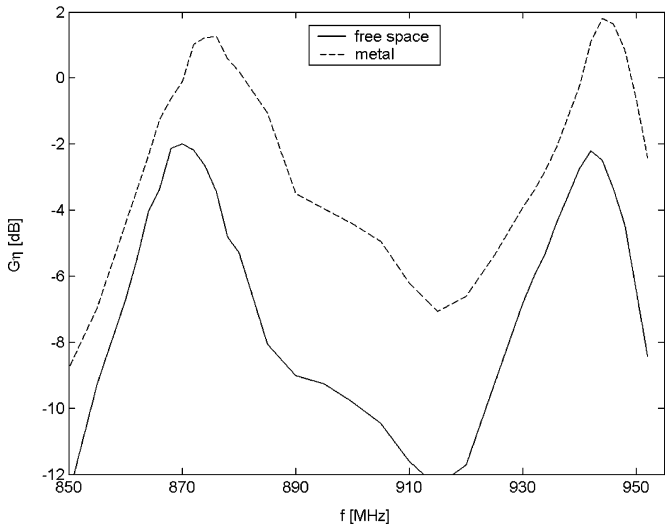

Fig. 10. Measured gain including mismatch of the 867/940 MHz antenna.

TABLE I
RADIATION CHARACTERISTICS

	867 MHz	915 MHz	940 MHz
D_{sim} [dB]	2.3	2.7	2.8
$\eta_{eff,\ sim}$	0.36	0.32	0.31
G_{sim} [dB]	-2.1	-2.2	-2.3
$G\eta_{mes}$ [dB]	-2.2	-2.9	-2.2

TABLE II
CALCULATED AND MEASURED READ-RANGES

	867 MHz	869 MHz	915 MHz
$r_{cal,\ free\ space}$ [m]	9.7	4.8	9.3
$r_{mes,\ free\ space}$ [m]	7.0	3.5	N/A
$r_{cal,\ metal}$ [m]	13.7	6.8	13.2
$r_{mes,\ metal}$ [m]	10.9	5.6	N/A

The radiation characteristics of the antennas in free space are presented in Table I. The values are about the same for both antennas at 867 MHz. According to the simulation results, the directivity and radiation efficiency are low. Simulated and measured gain values correspond well, even though these parameters are not fully comparable, since impedance mismatch is included in the measurement results.

The calculated and measured read-ranges of the developed antennas are presented in Table II. The calculated read-ranges at 867 MHz (ETSI 2 W ERP), 869 MHz (ETSI 0.5 W ERP), and 915 MHz (FCC 4 W EIRP) are based on measured gain values $G\eta$ and calculation on (1). The read-range measurements were conducted with a Deister UDL 500 reader device at the entrance hall of a block of offices. In other words, the measured values correspond to a reliable and reproducible maximum reading distance in a real application environment. The measurements were conducted only with the two European bands, since frequency allocation issues prevented the measurements in the 915 MHz band. As expected, the measured ranges are shorter than the calculated ones because of multipath propagation.

V. CONCLUSIONS

In this paper, a dual-band platform-tolerant single element PIFA structure has been introduced. Platform tolerance of the structure is achieved by utilizing dominating horizontal current distribution. The dual-band operation at frequencies related to RFID is achieved by exploiting the particular impedance level typical to RFID microchips. The tunable feed inductance and the series capacitance at the radiating edge of the patch play the key roles in the dual-band operation. Simulations and measurements are presented for two example antennas, showing good correlation. Also, the presence of metal is demonstrated not to have any significant effect on antenna matching performance. Thus, the structure is expected to be useful in many different RFID applications and on several continents.

REFERENCES

[1] K.-L. Wong, *Planar Antennas for Wireless Communications*. New York: Wiley, 2003.
[2] A. S. Meier and W. P. Summers, "Measured impedance of vertical antennas over finite ground planes," *Proc. IEEE*, vol. 37, pp. 609–616, Jun. 1949.
[3] K. H. Awadalla and T. S. M. Maclean, "Input impedance of a monopole antenna at the center of a finite ground plane," *IEEE Trans. Antennas Propag.*, vol. AP-26, pp. 244–248, Mar. 1978.
[4] J. H. Richmond, "Monopole antenna on circular disk," *IEEE Trans. Antennas Propag.*, vol. AP-32, pp. 1282–1287, Dec. 1984.
[5] K. Antoszkiewicz and L. Shafai, "Impedance characteristics of circular microstrip patches," *IEEE Trans. Antennas Propag.*, vol. AP-38, pp. 942–946, Jun. 1990.
[6] M.-C. Huynh and W. Stutzman, "Ground plane effects on planar inverted-F antenna (PIFA) performance," *Proc. Inst. Elect. Eng. Microw. Antennas Propag.*, vol. 150, no. 4, pp. 209–213, Aug. 2003.
[7] J. C.-E. Sten and M. Hirvonen, "Decay of groundplane currents of small antenna elements," *IEEE Antennas Wireless Propag. Lett.*, vol. 4, pp. 82–84, 2005.
[8] M. Hirvonen, P. Pursula, K. Jaakkola, and K. Laukkanen, "Planar inverted F-antenna for radio frequency identification," *Electron. Lett.*, vol. 40, no. 14, pp. 848–850, Jul. 2004.
[9] U. Karthaus and M. Fischer, "Fully integrated passive UHF RFID transponder IC with 16.7-μW minimum RF input power," *IEEE J. Solid-State Circuits*, vol. 38, pp. 1602–1608, Oct. 2003.
[10] K. Hirasawa and M. Haneishi, *Analysis, Design, and Measurement of Small and Low-Profile Antennas*. Norwood, MA: Artech House, 1992.
[11] J. Ollikainen, "Design and implementation techniques of wideband mobile communications antennas" Ph.D. dissertation, Helsinki Univ. of Technology, Espoo, Nov. 2004 [Online]. Available: http://www.lib.tkk.fi/Diss/2004/isbn9512273810
[12] P. Pursula, T. Varpula, K. Jaakkola, and M. Hirvonen, "Antenna radiation characterization by backscattering modulation," in *URSI/IEEE XXIX Nat. Conv. Radio Science, VTT Symp. 235*, Nov. 2004 [Online]. Available: http://www.vtt.fi/inf/pdf/symposiums/2004/S235.pdf

Mervi Hirvonen was born in Espoo, Finland, in 1980. She received the master of science (Tech.) degree in electrical engineering from Helsinki University of Technology (TKK), Espoo, Finland, in 2004.

Since 2002, she has been with the VTT Technical Research Centre of Finland, initially as a Research Trainee and, since 2004, as a Research Scientist. Her current research interests include antennas and electromagnetics related to wireless sensors, RFID systems, and mobile communications.

Kaarle Jaakkola was born in Helsinki, Finland, in 1976. He received the master of science (Tech.) degree in electrical engineering from Helsinki University of Technology (TKK), Espoo, Finland, in 2003.

Since 2000, he has been with the VTT Technical Research Centre of Finland, first as a Research Trainee and, since 2003, as a Research Scientist. In 2000–2002, he participated in the Palomar (EC IST) project developing RF parts for a new RFID system. His current research interests include RFID systems, wireless and applied sensors, antennas, electromagnetic modelling, and RF electronics.

Pekka Pursula was born in Vantaa, Finland, in 1978. He received the master of science (Tech.) degree (with distinction) in technical physics from Helsinki University of Technology (TKK), Espoo, Finland, in 2002.

In 2002, he was with Philips Medical Systems Finland developing RF systems in magnetic resonance imaging. Since 2003, he has been with the VTT Technical Research Centre of Finland. His present research interests include RFID systems and wireless sensors.

Mr. Pursula received the Young Scientist Award at the URSI/IEEE XXIX Convention on Radio Science, Espoo, Finland, in November 2004.

Jussi Säily was born in Rantsila, Finland, in 1974. He received the master of science (Tech.), licentiate of science (Tech.), and doctor of science (Tech.) degrees in electrical engineering from Helsinki University of Technology (TKK), Espoo, Finland, in 1997, 2000, and 2003, respectively.

In 1996, he was a Research Trainee with the Automation/Measurement Technology Laboratory, VTT Technical Research Centre Finland, where he studied microelectromechanical sensors. From 1997 to 2003, he was a Research Engineer with the Radio Laboratory, TKK, where he studied, e.g., phase-locked millimeter- and submillimeter-wave signal sources and receivers for antenna measurements. Since 2004, he has been with the Circuits and Antennas Knowledge Centre (formerly the Antennas and Electromagnetics Research Group), VTT, where he is currently a Senior Research Scientist. His current research interests include beam-steerable millimeter-wave antenna arrays for short-range communications, smart base-station antenna arrays for telecommunications, RFID antennas, and low-noise signal sources for instrumentation.

PUBLICATION 8

Antenna effective aperture measurement with backscattering modulation

In: IEEE Transactions on Antennas and Propagation 2007.
Vol. 55, No. 10, pp. 2836–2843.
© 2007 IEEE.
Reprinted with permission from the publisher.

This material is posted here with permission of the IEEE. Such permission of the IEEE does not in any way imply IEEE endorsement of any of the VTT Technical Research Centre of Finland's products or services. Internal or personal use of this material is permitted. However, permission to reprint/republish this material for advertising or promotional purposes or for creating new collective works for resale or redistribution must be obtained from the IEEE by writing to pubs-permissions@ieee.org.

Antenna Effective Aperture Measurement With Backscattering Modulation

Pekka Pursula, Mervi Hirvonen, Kaarle Jaakkola, and Timo Varpula

***Abstract*—A scattering measurement method for antenna characterization is described. The antenna backscattering is modulated by an oscillator circuit. The modulation begins, when a known RF power is transferred to the oscillator circuit from the antenna. This enables the measurement of the effective aperture of the antenna, from which the antenna bandwidth and radiation pattern are obtained. A theory for antenna aperture measurement is developed using a simple circuit model for the antenna—oscillator system. A dipole and a PIFA with a reactive input impedance at the application frequency were measured. The antenna aperture was measured to an accuracy of 9%, and the measurements complied with simulated and measured references. The method provides simple and accurate bandwidth and radiation pattern measurements with the reactive load the antenna is designed to work with.**

***Index Terms*—Antenna measurements, apertures, radar cross sections, scattering.**

I. Introduction

SINCE the pioneering work of King in 1949 [1], the study of antenna backscattering has developed into a very diverse field of study. The methods have developed far beyond the measurement of the radar cross section (RCS) of the antenna. Several authors have demonstrated backscattering-based methods for measuring the antenna gain (e.g., [2] and [3]) and the antenna input impedance (e.g., [3] and [4]). In most methods, the antenna under test is connected to known passive loads, but also negative resistance devices have been used [5]. Because the methods require the measurement of the power level of the scattered signal, environmental reflections limit the signal-to-noise ratio and accuracy of the measurement [4].

In this paper, a new approach to backscatter measurement is taken. The antenna under test is connected to an oscillator, which modulates the backscattered signal. This enables measuring the effective antenna aperture (also antenna aperture, or aperture, in this paper) and radar cross section associated with the modulated backscattering.

The oscillator circuit drives a small varactor in the input of the oscillator chip. The oscillator wakes up, when the antenna under test supplies it with enough power. If the RF power required by the oscillator chip is known, the effective antenna aperture can be measured. The method enables a fast and robust way to measure the center frequency, bandwidth and radiation pattern of the antenna under test as was shown, to some extent, in [6].

Manuscript received June 1, 2005; revised April 26, 2007. This work was supported by Tekes, The National Technology Agency of Finland.

The authors are with the VTT Technical Research Centre Finland, Espoo FI-02044, Finland (e-mail: pekka.pursula@vtt.fi).

Digital Object Identifier 10.1109/TAP.2007.905821

The method has been inspired by the need to characterize small radio frequency identification (RFID) antennas. In RFID applications, the antenna is usually directly matched to a capacitive IC chip. Hence the input impedance of the antenna is inductive, which makes it difficult to measure with conventional transmission techniques. The oscillator IC that is used in the measurements has same input impedance than the RFID chip, which the antenna will actually be used with. This is very important, because high mismatch in the antenna input can affect the current modes in an antenna.

In this paper, measurement results of a dipole and a small PIFA antenna at UHF frequencies are presented. The dipole, with well-known characteristics, is measured, even though its input impedance is nearly real at the application band. To demonstrate the method with a reactive antenna, a PIFA with direct matching to the oscillator chip is measured. The radiation pattern and frequency behavior of the both antennas are measured.

The scattering methods are commonly agreed to give better measurement results than the transmission measurements in the case of small antennas, because there is no feed line to disturb the near fields of the antenna, as is the case with transmission measurements. This is often referred to as a fact, but the effect is rarely demonstrated. The PIFA is designed to be mounted on metal surfaces. The disturbing effect of the feed line can be clearly seen, when the PIFA is measured on different sizes of metal platforms.

This paper proceeds as follows. In the Section II a theoretical model for the antenna—load system is developed and an expression for the effective antenna aperture is derived. The Section II also describes the basic idea of the measurements and considers the effect of different error sources. In Section III measurement results, as well as simulation and reference measurement results are presented.

II. Measurement Method

A. Theoretical Construction

To study the scattering effects on a loaded antenna, the model presented in Fig. 1 was used. The antenna and the load are described as impedances $Z_A = R_A + jX_A$ and $Z_L = R_L + jX_L$, respectively. The antenna resistance consists of the radiation resistance R_R and the dissipations in the antenna R_D, i.e., $R_A = R_R + R_D$. The voltage V is the equivalent voltage generated by the incident wave. This model assumes a reciprocal antenna: the current distributions, and thus antenna characteristics, should be identical for transmission and receiving.

Following the reasoning in [7] and [8] expressions for the effective aperture A_e and the radar cross section σ of the antenna

0018-926X/$25.00 © 2007 IEEE

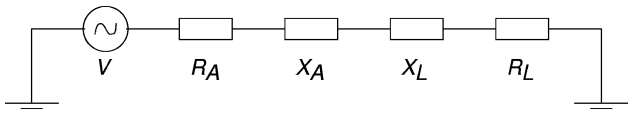

Fig. 1. Series model of a loaded antenna.

can be derived. The RF current I in the circuit can be calculated as

$$I = \frac{V}{Z} = \frac{V}{(R_A + R_L) + j(X_A + X_L)} \tag{1}$$

where Z is the impedance of the circuit. The effective aperture A_e is defined as the ratio of the power dissipated in the load resistance R_L and the power density S of the incident wave, i.e.

$$A_e = \frac{R_L I_{\rm rms}^2}{S} \tag{2}$$

where $I_{\rm rms}$ is the effective RF-current in the circuit. Similarly the radar cross section σ is defined as the power the antenna radiates, i.e., power dissipated in the radiation resistance R_R times the directivity D of the antenna, divided by the power density S

$$\begin{aligned}\sigma &= \frac{DR_R I_{\rm rms}^2}{S} = \frac{\eta D R_A I_{\rm rms}^2}{S} \\ &= \frac{G_A R_A I_{\rm rms}^2}{S}.\end{aligned} \tag{3}$$

Here, η is the radiation efficiency and G_A is the gain of the antenna.

Assuming conjugate matching between the antenna and the load, where $Z_A = Z_L^\dagger$, the maximum power $P_{\rm max}$ transferred from the antenna to the load can be expressed as

$$P_{\rm max} = \frac{V_{\rm rms}^2}{4R_A}. \tag{4}$$

The power $P_{\rm max}$ can be identified with the transferred power of the Friis transmission equation

$$P_{\rm max} = \frac{G_A \lambda^2}{4\pi} S. \tag{5}$$

Combining (1)–(5), expressions for the effective aperture A_e and the radar cross section σ become

$$\begin{aligned}A_e &= \frac{G_A \lambda^2}{4\pi} \frac{4R_A R_L}{(R_A + R_L)^2 + (X_A + X_L)^2} \\ \sigma &= \frac{G_A^2 \lambda^2}{4\pi} \frac{4R_A^2}{(R_A + R_L)^2 + (X_A + X_L)^2}.\end{aligned} \tag{6}$$

The equations consist of a maximum aperture (first fraction) and a second fraction describing the mismatch between the antenna and the load. Equation (6) can be also expressed with a reflection coefficient

$$\begin{aligned}A_e &= \frac{G_A \lambda^2}{4\pi} \left(1 - |\Gamma|^2\right) \\ \sigma &= \frac{G_A^2 \lambda^2}{4\pi} |1 - \Gamma|^2\end{aligned} \tag{7}$$

where the reflection coefficient is defined as

$$\Gamma = \frac{Z_L - Z_A^\dagger}{Z_L + Z_A} \tag{8}$$

and † stands for a complex conjugate.

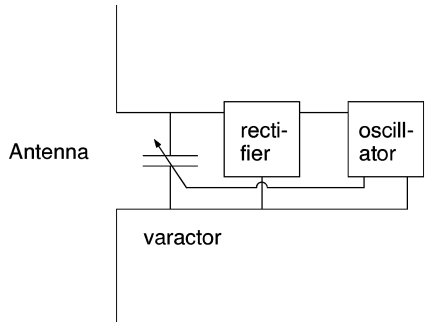

Fig. 2. Block diagram of the antenna—chip system.

In previous studies, the measurement methods have been based on measuring the radar cross section. The antenna can also be characterized by measuring the antenna aperture. To do this, the antenna is connected to an oscillator chip, whose input impedance is known. The chip includes a rectifier, a low-frequency oscillator and a varactor, as sketched in Fig. 2. The chip has no battery, but it extracts all the power it needs from the RF power transmitted by an illuminating antenna. The critical RF power $P_{rf,0}$ the chip requires for the modulation to start, is known.

In this study, two kinds of resonator chips were used, which are described in [8] and [9]. The input impedance of the chips is about $(7 - \mathrm{j}180)\ \Omega$.

When the oscillator drives the varactor at the input of the chip, the input reactance X_L of the chip varies a small amount of ΔX. As seen from (1), a change in chip input reactance modulates the phase of the current in the antenna—chip system. Thus the field scattered from the antenna—chip system is also phase modulated, which is seen as sidebands in the scattered signal. The scattered power is not measured, but only used to indicate the power transferred to the load. Only the transmitted power is measured. This simplifies the measurement apparatus considerably, and enables the center frequency, bandwidth and normalized radiation pattern measurements even in normal laboratory conditions.

Even though it is not necessary to measure the backscattered power, it is interesting to calculate also the radar cross section of the first sideband of the antenna.

B. Effects of Modulation

The analysis in Section II-A was based on the assumption that the input impedance of the oscillator chip is constant. Actually the reactance of the chip is modulated by an amount ΔX. What is the effective impedance of the chip, that is actually seen in the measurements?

If the varactor was in the same state all the time, one would measure the antenna aperture given in (6). If the varactor was switched to the other state, one would measure a similar aperture curve, which was shifted to a new center frequency. At a certain frequency, one of the varactor states induces more mismatch to the antenna—chip boundary than the other state. In the higher mismatch state, less RF power is transferred into the chip than in the other varactor state. The oscillator has to get enough DC power to function in the both states of the varactor, for the modulation to function properly.

Without DC capacitors, the chip has to get enough RF power for the oscillator to function in the higher mismatch state of the varactor. In this case, the limiting power $P_{rf,0}$ would refer to different states of the varactor, and hence to different input impedances of the chip, on different sides of the aperture peak.

But, because the chip has relatively big DC capacitors, the energy charged in the capacitors can be used to drive the oscillator over the higher mismatch state of the varactor. Of course, in the lower mismatch state the chip has to get some extra RF power to charge the capacitors. This averaging behavior leads to a situation, where the critical power $P_{\mathrm{rf},0}$ refers to neither of the varactor states, but to a state, which corresponds to the rms-current in the antenna—chip system.

To calculate the rms-current the modulation has to be fixed. For a square wave modulation, the impedance of the antenna—chip system is

$$Z(t) = \begin{cases} R + j(X + \Delta X) & -T/2 < t < 0 \\ R + j(X - \Delta X) & 0 < t < T/2 \end{cases} \tag{9}$$

where $R = (R_A + R_L)$, $X = (X_A + X_L)$ and T is the period of the modulation. Now the effective current can be expressed as an integral

$$\begin{aligned} I_{\mathrm{rms}}^2 &= \frac{V^2}{T} \int_{-T/2}^{T/2} \frac{\sin^2(\omega_0 t)}{|Z(t)|^2} dt \\ &= \frac{V_{\mathrm{rms}}^2}{2} \left(\frac{1}{R^2 + (X + \Delta X)^2} \right. \\ &\qquad \left. + \frac{1}{R^2 + (X - \Delta X)^2} \right) \end{aligned} \tag{10}$$

where $\omega_0 \gg 1/T$ is the RF frequency. Now the aperture becomes

$$A_e = \frac{\lambda^2 G_A}{4\pi} \left(\frac{2R_A R_L}{R^2 + (X + \Delta X)^2} + \frac{2R_A R_L}{R^2 + (X - \Delta X)^2} \right). \tag{11}$$

Especially interesting are the two limits of the mismatch reactance X

$$A_e = \begin{cases} \frac{\lambda^2 G_A}{4\pi} \frac{4R_A R_L}{R^2 + \Delta X^2} & X \ll \Delta X \\ \frac{\lambda^2 G_A}{4\pi} \frac{4R_A R_L}{R^2 + X^2} & X \gg \Delta X. \end{cases} \tag{12}$$

At the sides of the peak, where $|X|$ is big, the modulation does not affect the aperture. But in the middle of the peak, where $X = 0$, the aperture is reduced due to the modulation. In other words, the modulation flattens the aperture peak.

Measuring the aperture requires only the measurement of the critical transmit power $P_{tx,0}$, but it is interesting to study the scattered power also. To derive a theoretical expression for the power in the sidebands, the baseband current in the antenna—chip system is expressed as a Fourier series $I = 1/2 I_0 + \Sigma_n (I_{n,\sin} \sin(n\omega_m t) + I_{n,\cos} \cos(n\omega_m t))$, where ω_m is the modulation frequency. The Fourier coefficients are

$$\begin{aligned} I_0 &= \frac{2V}{T} \int_{-T/2}^{T/2} \frac{dt}{Z(t)} \\ &= 4V \frac{R + jX}{(R + jX)^2 + \Delta X^2} \\ I_{n,\sin} &= \frac{2V}{T} \int_{-T/2}^{T/2} \frac{\sin(n\omega_m t)}{Z(t)} dt \\ &= \begin{cases} \frac{4V}{n\pi} \frac{j\Delta X}{(R + jX)^2 + \Delta X^2} & n \text{ odd} \\ 0 & n \text{ even} \end{cases} \\ I_{n,\cos} &= \frac{2V}{T} \int_{-T/2}^{T/2} \frac{\cos(n\omega_m t)}{Z(t)} dt \\ &= 0. \end{aligned} \tag{13}$$

The effective RF current corresponding to one of the first sidebands is $I_{\mathrm{rms}}^2 = 1/8 I_{1,\sin}^2$. Two factors of 1/2 arise because of baseband and RF "root-mean-squaring." The third factor discards power in the other of the first sidebands. Thus the effective current describes power in only one of the symmetric first sidebands. The power in the sideband can also be described by a radar cross section σ_1, which can be calculated from the effective current using (3)–(5)

$$\sigma_1 = \frac{\lambda^2 G_A^2}{4\pi} \frac{16}{\pi^2} \frac{R_A^2 \Delta X^2}{\left(R^2 + X^2 + \Delta X^2\right)^2 + 4R^2 X^2}. \tag{14}$$

C. Measurement Procedure

The measurement setup is shown in Fig. 3. It consists of a continuous wave transmitter and a receiver with a spectrum analyzer. The oscillator IC chip is connected to the antenna under test (AUT), which is attached to a rotating mount.

The loaded antenna is illuminated with the transmitter, which creates a power intensity S at the antenna under test. In each

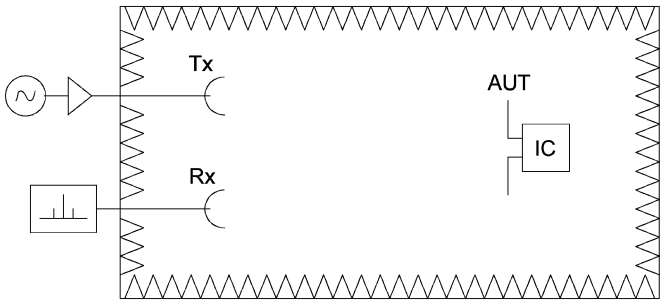

Fig. 3. Measurement setup.

measurement point, the transmitted power P_{tx} is increased until the modulation wakes up, i.e., the sidebands are detected at the receiver. At this critical transmission power $P_{tx,0}$, the IC chip gets just enough power to function, i.e., the rf power P_{rf} coupled to the oscillator chip is the known critical power $P_{\mathrm{rf},0}$, which the chip needs to function. The critical transmission power $P_{tx,0}$ is recorded to calculate the antenna aperture. The received power at the sideband frequency $P_{rx,1}$ was recorded to test (14).

The effective aperture A_e and the radar cross section of the first sideband σ_1 are defined as

$$A_e = \frac{P_{\mathrm{rf}}}{S}$$
$$\sigma_1 = \frac{P_{\mathrm{sc},1}}{S} \tag{15}$$

where $P_{\mathrm{sc},1}$ is the power scattered from the antenna at sideband frequency.

Because the power intensity S is proportional to the transmitted power P_{tx}, it can be measured at a single reference power level $P_{tx,\mathrm{ref}}$, and then scaled

$$S = \frac{P_{tx}}{P_{tx,\mathrm{ref}}} S_{\mathrm{ref}} \tag{16}$$

where $S_{\mathrm{ref}} = S(P_{tx,\mathrm{ref}})$. The transmitted power is increased until the modulation wakes up. At this power level, the IC chip gets just enough power to function. In other words $P_{\mathrm{tx}} = P_{tx,0}$ and $P_{\mathrm{rf}} = P_{\mathrm{rf},0}$. Now the antenna aperture and the radar cross section can be expressed as

$$A_e = \frac{P_{\mathrm{rf},0}}{S_{\mathrm{ref}}} \frac{P_{tx,\mathrm{ref}}}{P_{tx,0}}$$
$$\sigma_1 = \frac{(4\pi d)^2}{\lambda^2 G_{rx}} \frac{P_{rx,1}}{S_{\mathrm{ref}}} \frac{P_{tx,\mathrm{ref}}}{P_{tx,0}} \tag{17}$$

where d is the distance between antenna under test and receiver antenna. The power propagation from the antenna under test to the receiver has been calculated with Friis equation. The reference power intensity S_{ref} can be measured to quite a high accuracy with the same equipment used in the actual measurement.

D. Error Analysis

Most antenna scattering measurement methods require the power level measurement of the scattered field. Usually the antenna is connected to a passive load and the scattered field is at the same frequency than the transmitted field. In this kind of a measurements, the transmitted field connects through environment or directly to the receiver, which severely impairs the receiver sensitivity. Thus complicated decoupling and background cancellation systems (e.g., [3]) has been used. In the aperture method described here, the power level of the scattered field is not measured, but only the transmission power, which is much easier to do with high accuracy.

Even if one measures the scattered power, direct coupling is not a problem, because the scattered signal is transferred to sidebands.

On the other hand, the aperture method requires exact knowledge of the required RF power of the oscillator chip. This is not trivial to measure with high accuracy due to the reactive input impedance of the chip. There is also some hysteresis in the rectifier as a function of incoming power. Thus care has to be taken in the measurements, to sweep the transmission power always in the same direction.

Another common error source is the repositioning error in scattering methods, that require antenna under test to be measured with different loads (for example, [3] and [4]). In the aperture method, only one load is used, but the measurement of the reference power intensity at AUT is required. This introduces some repositioning error. But repositioning error gives rise much faster to phase than power level errors [4]. Because in aperture method only power level is measured, repositioning error is not a major problem.

The aperture measurement suffer of course from environmental reflections, which effect the power intensity at antenna under test. But this is taken care of by the reference power intensity measurement.

A quantitative analysis in measurement error can be calculated by using a total differential of the antenna aperture in (17). This yields a relative error of the form

$$\frac{\Delta A_e}{A_e} = \frac{\Delta P_{\mathrm{rf},0}}{P_{\mathrm{rf},0}} + \frac{\Delta P_{tx,\mathrm{ref}}}{P_{tx,\mathrm{ref}}} + \frac{\Delta P_{tx,0}}{P_{tx,0}} + \frac{\Delta S_{\mathrm{ref}}}{S_{\mathrm{ref}}} \tag{18}$$

where prefix Δ refers to the uncertainty of the quantity.

The power levels can be measured to an accuracy of 0.1 dB with basic measurement equipment, except the required RF power $P_{\mathrm{rf},0}$. This was measured to an accuracy of 6%. Adding up the terms, a relative error of 9% is acquired.

Similar error analysis can be carried out for the radar cross section of the first sideband in (17). Now there are more error sources, but they can be measured to an accuracy on 0.1 dB, or 1% quite easily, for required RF power $P_{\mathrm{rf},0}$ is not included. Thus, the estimated error is 7%.

III. Measurement Results

In this section measurements of two antennas are described. First, a dipole antenna is measured due to its well-known characteristics. The oscillator chip used in the measurements has a capacitive input impedance, and thus an external matching circuit is needed. The dipole was measured in an ordinary laboratory environment, to demonstrate the robustness of the measurement system.

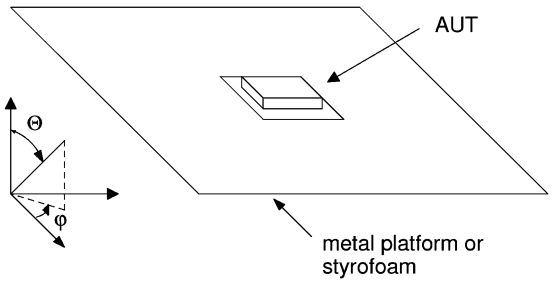

Fig. 4. PIFA (AUT) attached to platform.

The measurement method is well suited for measuring antennas with reactive input impedance. Thus a modified planar inverted antenna (PIFA), with direct impedance matching to the oscillator chip, is measured. The antenna under test is a PIFA that has been designed for RFID applications at 869 MHz band [10]. The antenna is designed to be attached on metal platforms. Hence the measurements were carried out on metal platforms of different sizes, and on a styrofoam support, to simulate the free space condition. The PIFA on an platform is presented in Fig. 4. The PIFA measurements were carried out in an anechoic chamber.

Two kinds of measurements were carried out. In bandwidth measurement, the critical transmitted power $P_{tx,0}$ was measured at different frequencies. In radiation pattern measurement, the critical power was measured as a function of antenna alignment. First the radiation pattern measurement is considered.

A. Radiation Pattern Measurements

To measure the normalized power radiation pattern P_n, one does not have know the reference power intensity S_{ref} or the critical rf power $P_{\mathrm{rf},0}$ in (17). If the measurement setup is stable, these quantities remains constant through the measurement. Because the antenna aperture is the measure of the power transfer between the antenna and the load, the radiation pattern can be calculated as

$$P_n(\varphi,\Theta) = \frac{A_e(\varphi,\Theta)}{A_{e,\max}} = \frac{P_{tx,0,\min}}{P_{tx,0}(\varphi,\Theta)} \tag{19}$$

where the $A_{e,\max} = \max(A_e(\varphi,\Theta))$ is the maximum aperture, which corresponds to the minimum critical transmitted power $P_{tx,0,\min} = \min(P_{tx,0}(\varphi,\Theta))$. Note that (19) holds exactly only, if the frequency remains constant, as is the case when measuring the radiation pattern.

The error analysis is quite straightforward taking total differential of (19). The uncertainty in the measured power levels was 0.1 dB, which leads approximately to an overall error $\Delta P_n = 0.2\ \mathrm{dB}$.

The dipole antenna is 15 cm in length, and resonating at about 870 MHz as such. The antenna is a little shorter than a $\lambda/2$-dipole, as real implementations of the dipole antenna tend to be. The dipole antenna was connected to the oscillator chip with a Π-type LC matching circuit. The matching was best at 850 MHz, at which frequency the radiation pattern was measured. The measured radiation pattern of the dipole is presented in Fig. 5, as well as theoretical radiation pattern of a $\lambda/2$ -dipole from [7]. As can be seen from the figure, the patterns are almost identical.

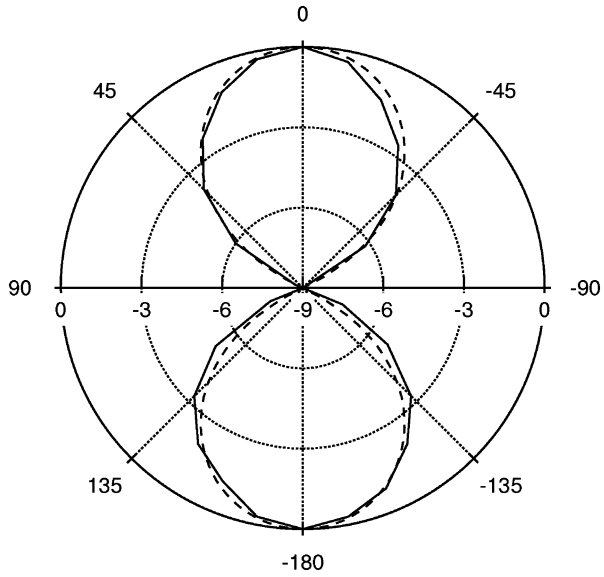

Fig. 5. Measured (—) and theoretical (- -) radiation patterns in decibels of the dipole antenna.

The measured radiation patterns of both polarizations in a main plane ($\phi = 135°$) of the PIFA are presented in Fig. 6. Both polarizations are scaled to main polarization main beam value. These results can be compared to simulated radiation patterns in Fig. 7 and transmission measurement results in Fig. 8. In the transmission measurements the AUT was fitted to a 50 Ω feed line with a strip line fitting network. To reduce the amount of metallic feed line near the antenna, the fitting network was connected to other measurement apparatus through an optical link. The antenna mounting, including the platform, was identical to the aperture measurement. The antenna was fed through the metal platform.

The results of the transmission measurements differ from the other results significantly, especially in free space, where there is no metal plane to screen the feed line from the antenna. As the radiation patterns become more similar when the size of the metal platform grows, it seems that the feed line and the fitting network disturb the antenna radiation. Thus the transmission measurement results cannot be used as a absolute reference for the aperture method.

The simulated and aperture method radiation patterns are almost identical. Only on the biggest metal platform a difference is seen. The biggest measured metal platform was only $(600\ \mathrm{mm})^2$ in area, but simulations were performed on an infinite platform, which explains the difference.

B. Bandwidth Measurements

The critical power was measured as a function of frequency with a step of a few MHz. The measurements were carried out for the dipole antenna and for the PIFA on different platforms. The antenna aperture was calculated using (17) and the relative error was approximated in Section II-C to be about 10%, mainly from the uncertainty in $P_{\mathrm{rf},0}$.

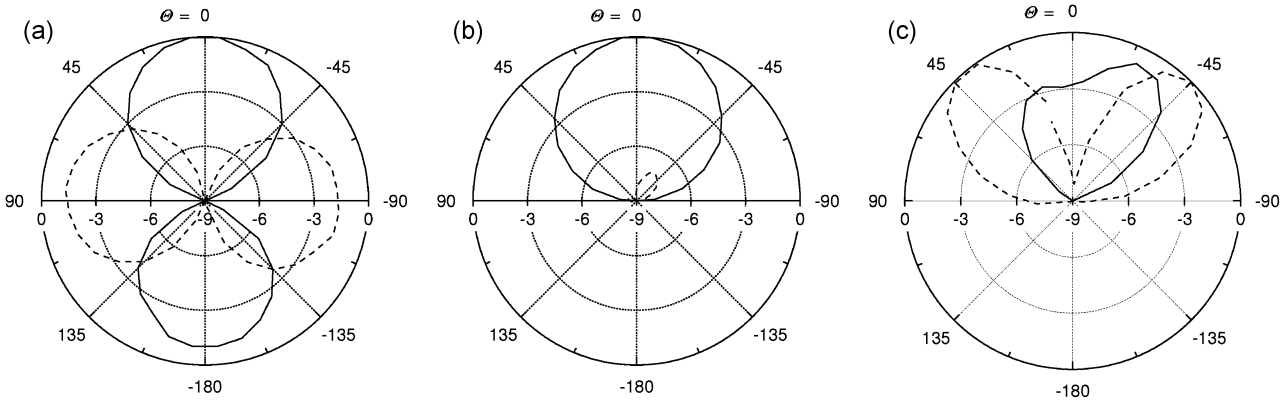

Fig. 6. Radiation patterns in decibels of the PIFA measured with the aperture method: (a) in free space, (b) on $(150\ \mathrm{mm})^2$ metal, and (c) on $(600\ \mathrm{mm})^2$ metal. Solid line (—) present the co-polarization and dashed line (- -) the cross-polarization radiation pattern.

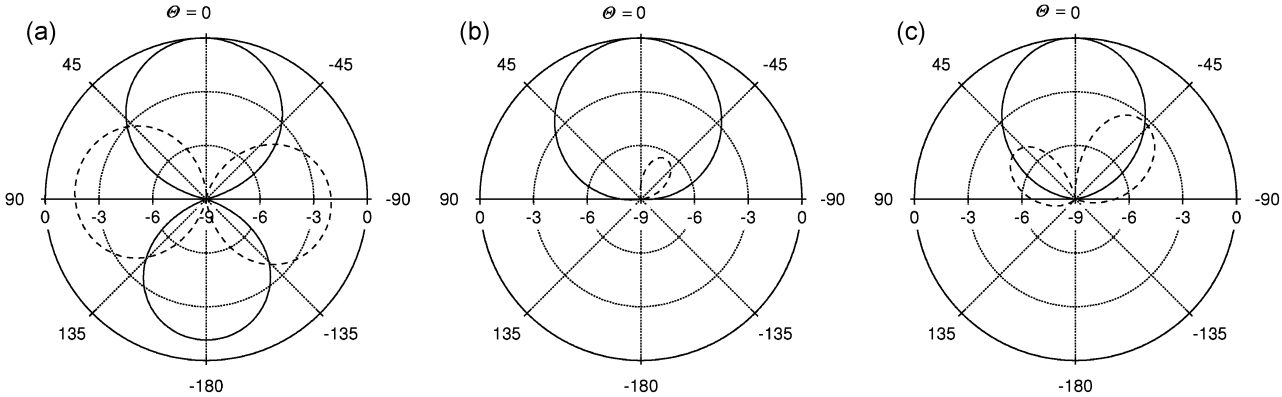

Fig. 7. Radiation patterns in decibels of the PIFA simulated with HFSS: (a) in free space, (b) on $(150\ \mathrm{mm})^2$ metal, and (c) on infinite metal. Solid line (—) present the co-polarization and dashed line (- -) the cross-polarization radiation pattern.

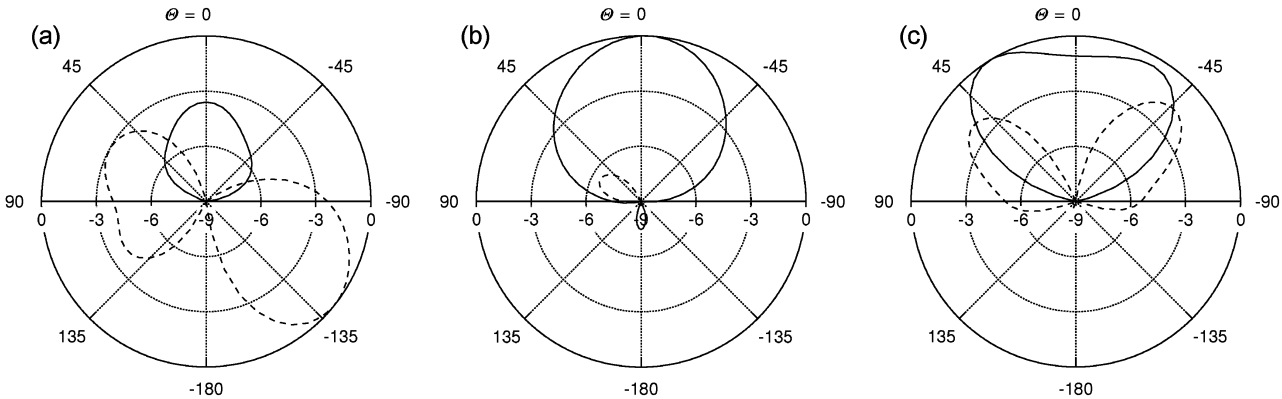

Fig. 8. Radiation patterns in decibels of the PIFA measured with the transmission method: (a) in free space, (b) on $(150\ \mathrm{mm})^2$ metal, and (c) on $(600\ \mathrm{mm})^2$ metal. Solid line (—) present the co-polarization and dashed line (- -) the cross-polarization radiation pattern.

To calculate the absolute value of the aperture, the RF power required by the chip has to be known. The required RF power was measured in a test fixture with a network analyzer (VNA). The required power of the oscillator chip used in PIFA measurements was measured to be $P_{\mathrm{rf},0} = (16 \pm 1)\ \mu\mathrm{W}$. This is in line with [8], which describes the chip used.

In the case of the dipole, the oscillator was connected to the VNA with the LC matching circuit used with the antenna. The required power of the chip connected to the matching circuit was measured to be $P_{\mathrm{rf},0} = (25 \pm 1)\ \mu\mathrm{W}$. The input impedance $Z_{\mathrm{in,osc}}$ of the oscillator chip connected to the matching circuit was measured to calculate a reference. The dipole input impedance $Z_{\mathrm{in,dip}}$ is well known, and can be calculated for example from a circuit model presented in [11]. Now the antenna aperture of the dipole can be calculated with (7) and theoretical dipole gain. The measured antenna aperture of the dipole and the calculated reference are presented in Fig. 9.

The matching circuit has a strong effect to the measured peak shape: The matching was designed for an average state of the chip, but the reference does not take into account the modulation. Nevertheless, the curves are almost identical in magnitude and in shape for about −3 dB from the aperture maximum. When comparing the curves, one must remember that the relative error in the circuit model is 6%, which is almost enough

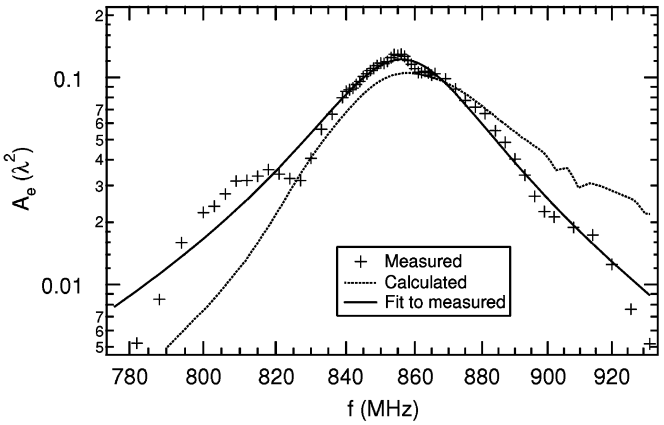

Fig. 9. Measured aperture of the dipole and a calculated reference.

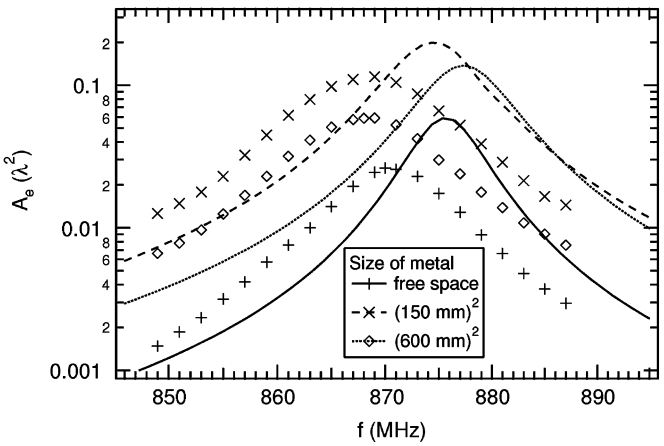

Fig. 10. Measured (markers) and calculated (lines) apertures of the PIFA on different platforms as a function of frequency.

to explain the difference in the curves. The measured maximum aperture at 854 MHz is $0.13\lambda^2$, which is almost exactly the theoretical maximum [$\Gamma = 0$ in (6)].

For the PIFA, a reference was calculated in similar way. Values for antenna gain and impedance were simulated with HFSS and measured values of the oscillator chip input impedance were used. The measured and calculated apertures for the PIFA is presented in Fig. 10.

The calculated and measured curves are similar in shape, but shifted in frequency. This can be either a simulator or a measurement error. The simulated peaks are narrower, and about 3 dB higher than measured ones. This is due to the flattening effect of the modulation, as seen from (12). As the chip reactance is modulated by $\Delta X \approx R_L$, a flattening of about 3 dB is only to be expected.

Also the radar cross section of the first sideband was measured. In Fig. 11 the measured aperture and radar cross section of the PIFA in free space are presented. The uncertainty was estimated in Section II-C, giving $\Delta\sigma_1/\sigma_1 = 7\%$.

The figure illustrates the fact that the effect of mismatch at the antenna—chip interface has a stronger effect to the radar cross section than the aperture. This is also seen in the expressions of A_e and σ_1 [(11) and (14)]: the aperture $A_e \propto X^{-2}$, but the radar cross section $\sigma_1 \propto X^{-4}$.

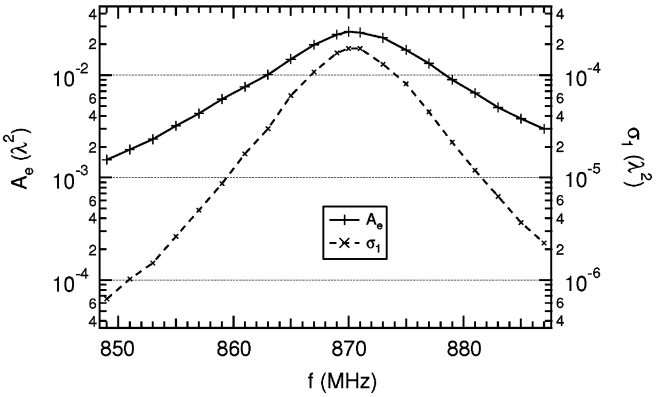

Fig. 11. Measured aperture A_e and radar cross section σ_1 of the PIFA in free space.

IV. Summary and Conclusion

A new method utilizing backscatter data to characterize antenna was presented. The method is based on backscattering modulation, which is achieved by connecting the antenna to a IC chip that consists of an oscillator driven modulator. The method enables the measurement of the antenna aperture and radar cross section of the modulated signal. Because carrier signal coupling from transmitter to receiver does not disturb the measurement, the measurement apparatus is very simple and quite accurate results can be acquired even in normal laboratory conditions.

The method was justified theoretically, and expressions for the antenna aperture and the radar cross section were derived with and without backscattering modulation. It was shown, that the modulator in the antenna load flattens the measured antenna aperture peak.

Radiation pattern and bandwidth measurements are simple and accurate with the introduced method. One reference measurement for the power intensity S is required for determining the absolute value of the antenna aperture, which essentially describes the antenna gain including mismatch at antenna input. From bandwidth measurements, the center frequency and bandwidth can be accurately determined.

A dipole antenna was measured near 869 MHz with the aperture method to demonstrate the method with a well known antenna. The measured radiation pattern was almost identical to the theoretical dipole radiation pattern. The measured frequency behavior was compared to a calculated frequency behavior. In the middle of the peak the curves differed less than 10% in value, and were of identical shape.

Because the method is well suited for measuring also antennas with reactive input impedance, a reactive RFID antenna with direct impedance matching was measured. The radiation pattern measurement results were similar to simulations and traditional transmission method measurement results, except that the disturbing effect of the feed line when measuring small antennas with transmission measurement technique was clearly seen. The measured center frequency of the PIFA differed from simulated values about 5 MHz. The simulated peaks were narrower and higher, which was only to be expected, because of the load modulation.

In general, the introduced method complied very well with the calculated and measured references.

ACKNOWLEDGMENT

The authors would like to thank Mr. O. Jaakkola for his contribution to the concept of the study. The IC chips were manufactured by Atmel Germany GmbH.

REFERENCES

[1] D. D. King, "Measurement and interpretation of antenna scattering," *Proc. IRE*, vol. 37, pp. 770–777, Jul. 1949.
[2] W. Wiesbeck and E. Heidrich, "Wide-band multiport antenna characterization by polarimetric RCS measurements," *IEEE Trans. Antennas Propag.*, vol. 46, pp. 341–350, Mar. 1998.
[3] J. Appel-Hansen, "Accurate determination of gain and radiation patterns by radar cross-section measurements," *IEEE Trans. Antennas Propag.*, vol. AP-27, pp. 640–646, Sep. 1979.
[4] J. T. Mayhan, A. R. Dion, and A. J. Simmons, "A technique for measuring antenna drive port impedance using backscatter data," *IEEE Trans. Antennas Propag.*, vol. 42, pp. 526–532, Apr. 1994.
[5] R. F. Harrington, "Field measurements using active scatterers," *IEEE Trans. Microw. Theory Tech.*, vol. MTT-11, p. 454, Sep. 1963.
[6] P. Pursula, T. Varpula, K. Jaakkola, and M. Hirvonen, "Antenna radiation characterization by backscattering modulation," in *Proc. URSI/IEEE XXIX Nat. Convention on Radio Science, VTT Symp. 235*, Nov. 2004, pp. 115–118 [Online]. Available: http://www.vtt.fi/inf/pdf/symposiums/2004/S235.pdf
[7] J. D. Kraus, *Antennas*. New York: McCraw-Hill, 1950, pp. 41–56.
[8] U. Karthaus and M. Fischer, "Fully integrated passive UHF RFID transponder IC with 16.7- μW minimum RF input power," *IEEE J. Solid-State Circuits*, vol. 38, pp. 1602–1608, Oct. 2003.
[9] Application note, ATA5590 Tag Antenna Matching [Online]. Available: http://www.atmel.com/dyn/resources/prod_documents/doc4843.pdf cited Sep. 4, 2006
[10] M. Hirvonen, P. Pursula, K. Jaakkola, and K. Laukkanen, "Planar inverted-F antenna for radio frequency identification," *Electron. Lett.*, vol. 40, pp. 848–850, Jul. 2004.
[11] T. G. Tang, Q. M. Tieng, and M. W. Gunn, "Equivalent circuit of a dipole antenna using frequency-independent lumped elements," *IEEE Trans. Antennas Propag.*, vol. 41, pp. 100–103, Jan. 1993.

Pekka Pursula was born in Vantaa, Finland, in 1978. He received the Master of Science (Tech.) degree (with distinction) in technical physics from Helsinki University of Technology (TKK), Espoo, Finland, in 2002.

In 2002, he was with Philips Medical Systems Finland developing RF systems in magnetic resonance imaging. Since 2003, he has been with the VTT Technical Research Centre of Finland, Espoo. His present research interests include RFID systems and wireless sensors.

Mr. Pursula received the Young Scientist Award at the URSI/IEEE XXIX Convention on Radio Science, Espoo, Finland, in November 2004.

Mervi Hirvonen received the Master of Science (Tech.) and Licentiate of Science (Tech.) degrees in electrical engineering from Helsinki University of Technology (TKK), Espoo, Finland, in 2004 and 2006, respectively.

Since 2002, she has been with the VTT Technical Research Centre of Finland, Espoo, initially as a Research Trainee and, since 2004, as a Research Scientist. Her current research interests include antennas and electromagnetics related to wireless sensors, RFID systems and mobile communications.

Kaarle Jaakkola was born in Helsinki, Finland, in 1976. He received the Master of Science (Tech.) degree in electrical engineering from Helsinki University of Technology (TKK), Espoo, Finland, in 2003.

Since 2000, he has been working with the VTT Technical Research Centre of Finland, Espoo, first as a Research Trainee and, since 2003, as a Research Scientist. From 2000 to 2002, he participated in the Palomar (EC IST) project developing RF parts for a new RFID system. His current research interests include RFID systems, wireless and applied sensors, antennas, electromagnetic modelling, and RF electronics.

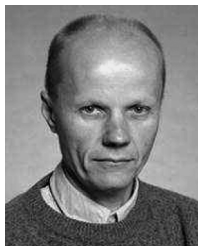

Timo Varpula was born in Seinjoki, Finland, in 1954. He received the Doctor degree from Helsinki University of Technology (TKK), Espoo, Finland, in 1982.

At TKK, he conducted research on weak magnetic fields produced by the human brain, eye, and heart. He also developed superconducting magnetometers and data analysis for biomagnetic signals. From 1983 to 1986, he worked as a Project Manager at Instrumentarium Corporation, Ltd., where he developed whole-body nuclear magnetic resonance imaging systems. After joining the VTT Technical Research Centre of Finland, Espoo, he was Section Leader from 1986 to 1994 and conducted research on measurement devices for metrological and industrial purposes. In 1994 to 2004, he worked as a Group Manager at VTT Automation and VTT Information Technology. In 2004 to 2006, he was the Research Manager at VTT Microsensing. He is presently Technology Manager at VTT Sensors. His research interests include radiofrequency identification, RF, microwave, and wireless sensors for scientific and industrial applications. He has coauthored 32 scientific publications and holds seven patents.

Series title, number and
report code of publication

VTT Publications 688
VTT-PUBS-688

Author(s)
Hirvonen, Mervi

Title

Performance enhancement of small antennas and applications in RFID

Abstract

The focus of this thesis is on the performance enhancement of small antennas and design and verification of antennas for radio frequency identification (RFID) and wireless sensors. The work is presented in eight scientific papers and in a summary, which introduces relevant fundamental concepts and previous work done in the field of small antennas.

Previously, several performance enhancement methods have been proposed to improve the antenna performance especially in mobile communication applications. However, solutions for the fundamental small antenna problem, high reactive energy and low radiation resistance, which in practice lead to narrowband and low efficiency operation, are rarely provided. In this thesis, alternative methods to alleviate the high reactive energy and low radiation resistance like material loading, non-Foster tuning and multi-port loading are discussed.

Also, lately antennas for RFID and wireless sensor applications have gained growing interest. However, several characteristic design features exist for these antennas. Especially, the concept of platform insensitivity is essential and discussed in detail. Also, antenna designs and dual-band tuning technique applicable to RFID antennas are presented. In addition, wireless measurement techniques for RFID antenna verification are reported.

ISBN
978-951-38-7108-6 (soft back ed.)
978-951-38-7109-3 (URL: http://www.vtt.fi/publications/index.jsp)

Series title and ISSN	Project number
VTT Publications 1235-0621 (soft back ed.) 1455-0849 (URL: http://www.vtt.fi/publications/index.jsp)	

Date	Language	Pages
September 2008	English, Finnish abstr.	45 p. + app. 57 p.

Name of project	Commissioned by
	TES Finnish Foundation for Technology Promotion, VTT Technical Research Centre of Finland

Keywords	Publisher
small antennas, RFID, wireless sensors, quality factor, near-zero permittivity, non-Foster tuning, multi-port antennas, platform insensitivity, dual-band, backscattering measurement	VTT Technical Research Centre of Finland P.O. Box 1000, FI-02044 VTT, Finland Phone internat. +358 20 722 4520 Fax +358 20 722 4374

Julkaisun sarja, numero ja raporttikoodi

VTT Publications 688
VTT-PUBS-688

Tekijä(t)
Hirvonen, Mervi

Nimeke

Pienten antennien suorituskyvyn parantaminen sekä sovelluksia etälukuun

Tiivistelmä

Väitöskirjatyö käsittelee pienten antennien suorituskyvyn parantamista sekä etälukuun (RFID) ja langattomiin antureihin soveltuvien antennien suunnittelua ja mittausta. Työ koostuu kahdeksasta tieteellisestä julkaisusta sekä yhteenvedosta, jossa on esitetty pienten antennien peruskäsitteitä sekä alan aikaisempia tutkimustuloksia.

Aikaisemmin pienten antennien suorituskykyä on pyritty parantamaan mm. matkaviestinlaitteissa. Kuitenkin ratkaisuja pienten antennien perusongelmaan, korkeaan reaktiiviseen energiatasoon sekä matalaan säteilyresistanssiin, jotka tekevät antennista käytännössä kapeakaistaisen ja hyötysuhteeltaan huonon, on harvemmin esitetty. Tässä työssä on analysoitu eri menetelmiä korkean energiatason ja matalan säteilyresistanssin lieventämiseen, kuten materiaalikuormitusta, non-Foster-viritystä sekä usean portin kuormitusta.

Viime aikoina etälukuun ja langattomiin antureihin soveltuvat antennit ovat herättäneet kasvavaa kiinnostusta. Näissä sovelluksissa antenneihin liittyy kuitenkin useita erityisiä ominaisuuksia. Erityisesti antennien alustaepäherkkyys on tärkeää, ja sitä on käsitelty työssä yksityiskohtaisesti. Lisäksi tässä työssä on esitetty RFID-antennimalleja sekä niihin sopiva kaksitaajuusviritystekniikka. Myös RFID-antenneille soveltuvia langattomia mittaustekniikoita on esitetty.

ISBN
978-951-38-7108-6 (nid.)
978-951-38-7109-3 (URL: http://www.vtt.fi/publications/index.jsp)

Avainnimeke ja ISSN	Projektinumero
VTT Publications 1235-0621 (nid.) 1455-0849 (URL: http://www.vtt.fi/publications/index.jsp)	

Julkaisuaika	Kieli	Sivuja
Syyskuu 2008	Englanti, suom. tiiv.	45 s. + liitt. 57 s.

Projektin nimi	Toimeksiantaja(t)
	Tekniikan edistämissäätiö, VTT

Avainsanat	Julkaisija
small antennas, RFID, wireless sensors, quality factor, near-zero permittivity, non-Foster tuning, multi-port antennas, platform insensitivity, dual-band, backscattering measurement	VTT PL 1000, 02044 VTT Puh. 020 722 4520 Faksi 020 722 4374

VTT PUBLICATIONS

673 Alkio, Martti. Purification of pharmaceuticals and nutraceutical compounds by sub- and supercritical chromatography and extraction. 2008. 84 p. + app. 42 p.

674 Mäkelä, Tapio. Towards printed electronic devices. Large-scale processing methods for conducting polyaniline. 2008. 61 p. + app. 28 p.

675 Amundsen, Lotta K. Use of non-specific and specific interactions in the analysis of testosterone and related compounds by capillary electromigration techniques. 2008. 109 p. + app. 56 p.

676 Häkkinen, Kai. Managerial approach to subcontract manufacture co-operation in the metal industry. Common Agenda as a management tool between parties. 2008. 131 s. + liitt. 14 s.

677 Hanhijärvi, Antti & Kevarinmäki, Ari. Timber failure mechanisms in high-capacity dowelled connections of timber to steel. Experimental results and design. 2008. 53 p. + app. 37 p.

678 FUSION Yearbook. Association Euratom-Tekes. Annual Report 2007. Eds. by Seppo Karttunen & Markus Nora. 2008. 136 p. + app. 14 p.

679 Salusjärvi, Laura. Transcriptome and proteome analysis of xylose-metabolising *Saccharomyces cerevisiae*. 2008. 103 p. + app. 164 p.

680 Sivonen, Sanna. Domain-specific modelling language and code generator for developing repository-based Eclipse plug-ins. 2008. 89 p.

681 Kallio, Katri. Tutkimusorganisaation oppiminen kehittävän vaikuttavuusarvioinnin prosessissa. Osallistujien, johdon ja menetelmän kehittäjän käsityksiä prosessin aikaansaamasta oppimisesta. 2008. 149 s. + liitt. 8 s.

682 Kurkela, Esa, Simell, Pekka, McKeough, Paterson & Kurkela, Minna. Synteesikaasun ja puhtaan polttokaasun valmistus. 2008. 54 s. + liitt. 5 s.

683 Hostikka, Simo. Development of fire simulation models for radiative heat transfer and probabilistic risk assessment. 2008. 103 p. + app. 82 p.

684 Hiltunen, Jussi. Microstructure and superlattice effects on the optical properties of ferroelectric thin films. 2008. 82 p. + app. 42 p.

685 Miettinen, Tuukka. Resource monitoring and visualization of OSGi-based software components. 2008. 107 p. + app. 3 p.

686 Hanhijärvi, Antti & Ranta-Maunus, Alpo. Development of strength grading of timber using combined measurement techniques. Report of the Combigrade-project – phase 2. 2008. 55 p.

687 Mirianon, Florian, Fortino, Stefania & Toratti, Tomi. A method to model wood by using ABAQUS finite element software. Part 1. Constitutive model and computational details. 2008. 51 p.

688 Hirvonen, Mervi. Performance enhancement of small antennas and applications in RFID. 2008. 45 p. + app. 57 p.

689 Setälä, Harri. Regio- and stereoselectivity of oxidative coupling reactions of phenols. Spirodienones as construction units in lignin. 104 p. + app. 38 p.

Julkaisu on saatavana	Publikationen distribueras av	This publication is available from
VTT PL 1000 02044 VTT Puh. 020 722 4520 http://www.vtt.fi	VTT PB 1000 02044 VTT Tel. 020 722 4520 http://www.vtt.fi	VTT P.O. Box 1000 FI-02044 VTT, Finland Phone internat. + 358 20 722 4520 http://www.vtt.fi

ISBN 978-951-38-7108-6 (soft back ed.)
ISSN 1235-0621 (soft back ed.)

ISBN 978-951-38-7109-3 (URL: http://www.vtt.fi/publications/index.jsp)
ISSN 1455-0849 (URL: http://www.vtt.fi/publications/index.jsp)